AD_____

Award Number: W81XWH-08-1-0394

TITLE: Interplay of CREB and ATF2 in Ionizing Radiation-Induced Neuroendocrine Differentiation of Prostate Cancer Cells

PRINCIPAL INVESTIGATOR: Chang-Deng Hu

CONTRACTING ORGANIZATION: Purdue University
West Lafayette, IN 47907

REPORT DATE: June 2012

TYPE OF REPORT: Final

PREPARED FOR: U.S. Army Medical Research and Materiel Command
Fort Detrick, Maryland 21702-5012

REPORT DOCUMENTATION PAGE

Form Approved
OMB No. 0704-0188

1. REPORT DATE	2. REPORT TYPE	3. DATES COVERED
06/1/2012	Final	1 June 2008 - 31 May 2012

4. TITLE AND SUBTITLE
Interplay of CREB and ATF2 in Ionizing Radiation-Induced Neuroendocrine Differentiation of Prostate Cancer Cells

5a. CONTRACT NUMBER

5b. GRANT NUMBER
W81XWH-08-1-0394

5c. PROGRAM ELEMENT NUMBER

6. AUTHOR(S)
Chang-Deng Hu
Xuehong Deng
Chih-chao Hsu
Christopher Suarez

5d. PROJECT NUMBER

5e. TASK NUMBER

5f. WORK UNIT NUMBER

7. PERFORMING ORGANIZATION NAME(S) AND ADDRESS(ES)
Purdue University
West Lafayette, IN 47907-2040

8. PERFORMING ORGANIZATION REPORT NUMBER

9. SPONSORING / MONITORING AGENCY NAME(S) AND ADDRESS(ES)
U.S. Army Medical Research and Material Commend
Fort Detrick, Maryland 21702-5012

10. SPONSOR/MONITOR'S ACRONYM(S)

11. SPONSOR/MONITOR'S REPORT NUMBER(S)

12. DISTRIBUTION / AVAILABILITY STATEMENT
Approved for Public Release; Distribution Unlimited

13. SUPPLEMENTARY NOTES

14. ABSTRACT

Radiation therapy is a first line treatment for prostate cancer patients and the patient's response is generally good. However, approximately 10% of low-risk and up to 60% of high-risk prostate cancer patients will experience biochemical recurrence within five years after radiotherapy. We have found that following a clinical radiation therapy protocol (2 Gy/day, 5 days/week), ionizing radiation (IR) induced the LNCaP prostate cancer cells to transdifferentiate into neuroendocrine-like (NE-like) cells, a process also known as neuroendocrine differentiation (NED) that is associated with disease progression and the acquisition of androgen-independent growth. Once differentiated, the NE-like cells are highly resistant to radiation and survive the treatment without any obvious cell death. Furthermore, we have demonstrated that two transcription factors, CREB and ATF2 oppose each other to regulate IR-induced NED. Significantly, we also found that IR-induced NE-like cells are reversible and dedifferentiated cells are cross-resistant to treatments. We have also extended our findings in LNCaP cells to two other prostate cancer cell lines and demonstrated that targeting CREB signaling can increase IR-induced cell death. We also demonstrated that IR induces NED in xenograft nude mouse models and in human prostate cancer patients. Preliminary screening has identified CaMKII and PRMT5 as important regulators of CREB involved in IR-induced NED. These findings suggest that radiation-induced NED may represent a novel pathway by which prostate cancer cells survive the treatment and contribute to recurrence.

15. SUBJECT TERMS
LNCaP, prostate cancer, ionizing radiation, neuroendocrine differentiation, ATF2, CREB

16. SECURITY CLASSIFICATION OF:			17. LIMITATION OF ABSTRACT	18. NUMBER OF PAGES	19a. NAME OF RESPONSIBLE PERSON
a. REPORT	b. ABSTRACT	c. THIS PAGE			19b. TELEPHONE NUMBER *(include area code)*
U	U	U	UU	85	USAMRMC

Standard Form 298 (Rev. 8-98)
Prescribed by ANSI Std. Z39.18

Table of Contents

Introduction

The neuroendocrine (NE) cells are one of the three types of epithelial cells in the human prostate, and are present in almost all cases of prostatic adenocarcinoma [1, 2]. Although the physiological role of NE cells in the normal prostate remains unclear, increased number of NE-like cells is found in advanced prostate cancer. Accumulated evidence suggests that NE-like cells produce a number of growth factors and peptide hormones that facilitate the growth of surrounding tumor cells in a paracrine manner, and that NE-like cells are clinically associated with androgen-independent growth of prostate cancer, currently called as castration resistant prostate cancer (CRPC) [1-4]. Consistent with this, androgen ablation can also induce NE differentiation (NED) of prostate cancer *in vitro* and *in vivo* [4-10]. Hence, the number of NE-like cells appears to be an indicator of prostate cancer progression. In addition to androgen ablation, IL-6 [11-16] and agents that elevate the intracellular level of cAMP also induce NED [12, 17-20]. Our preliminary results showed that ionizing radiation (IR) also induced NED *in vitro*. Interestingly, irradiated cells showed increased cytoplasmic localization of activating transcription factor 2 (ATF2) and an increase in the phosphorylated form of cAMP response element binding (CREB) protein. ATF2 and CREB both belong to the basic region leucine zipper (bZIP) family of transcription factors and bind the same cAMP response element (CRE) as a homodimer or a heterodimer to regulate gene transcription [21]. While some target genes can be activated by CREB and ATF2 equally or cooperatively [22-24], differential regulation of other target genes by CREB and ATF2 has also been observed [25-29]. Importantly, CREB is implicated in prostate cancer growth [30], acquisition of androgen independent growth [31], cAMP-induced NED [18, 32], and transcription of prostate-specific antigen [33] and chromogranin A (CgA), a protein secreted by NE and NE-like cells [32]. Based on these preliminary findings, we hypothesized that ATF2 may function as a transcriptional repressor and CREB acts as a transcription activator of NED. Hence, IR induces NED by sequestering ATF2 in the cytoplasm and activating CREB in the nucleus. To determine how ATF2 and CREB regulate NED at the transcriptional level, we proposed three specific aims in the applications: **(1)** determine functional relationship between CREB and ATF2 in IR-induced NED; (**2**) elucidate molecular mechanisms underlying regulation of IR-induced NED by pCREB and ATF2; **(3)** identify cytoplasmic signals responsible for the cytoplasmic sequestration of ATF2 and nuclear accumulation of pCREB. Given that NE-like cell is an indicator of cancer progression and that NE-like cells are highly resistant to radiation- and other agents-induced apoptosis, our novel observation that IR can induce NED in prostate cancer cells uncovers a novel pathway by which cancer cells may develop radioresistance. Successful completion of this project will allow for the development of novel radiosensitization approaches by targeting NED at the transcriptional regulation level.

Body

Completion of Approved Statement of Work

Task 1. Aim 1: Determine the functional relationship between CREB and ATF2 in IR-induced NED (Months 1-18)

a. We will first use LNCaP cells to establish stable cell lines expressing tetracycline repressor (Months 1-3)
b. Subclone our current two siRNA constructs for both CREB and ATF2 into pRNATin-H1.2/Neo vector and stably transfect them into repressor-expressing cell lines to isolate stably integrated clones (Months 2-6).
c. Subclone cDNAs encoding different CREB and ATF2 mutants into pcDNA4/TO vector (Months 4-6).
d. Establish stable cell lines expressing siRNA and different mutant CREB and ATF2 proteins (Months 6-12).
e. Optimize expression conditions (Months 7-10).
f. Examine knockdown effect of CREB and ATF2 on IR-induced NED (Months 7-18).
g. Examine the effect of overexpressed constitutively cytoplasmic- and nuclear-localized pCREB or ATF2 on IR-induced NED (Months 7-18).

We have completed all experiments proposed in Aim 1. Stable and tetracycline-inducible LNCaP cell lines to express tetracycline repressor were established and screened. Screening of these stable cell lines identified one that showed high expression of the tetracycline repressor. This cell line was used to establish several stable cell lines [pcDNA4/TO, pcDNA4/TO-CREB(S133A), pcDNA4/TO-nATF2, pRNATin-H1.2/Neo-ATF2shRNA, pRNATin-H1.2/Neo-CREBshRNA)]. Three stable cell lines expressing the dominant negative mutant CREB (CREB-S133A) and the constitutively nuclear-localized ATF2 (nATF) were used to assess their role in IR-induced NED. We found that induction of CREB-S133A or nATF2 inhibited IR-induced NED. The results are presented in our Cancer Research paper [34]. Results are presented in Figure 4 (page 9667) and methods are presented on page 9664.

We have also demonstrated that overexpression of a constitutively cytoplasmic-localized ATF2 induced NED. This is due to the sequestration of endogenous ATF2 in the cytoplasm by cATF2. This result is similar to NED induced by ATF2 knockdown in transient transfection. These results are presented in Figure 3 (page 9666) and Supplemental Figures 2 and 3.

Because CREB can be phosphorylated and activated by multiple phosphorylation at multiple sites [35], we reasoned that targeting of CREB using dominant negative mutants would allow elucidation of the critical role of CREB in IR-induced NED. For this purpose, we have developed tetracycline-inducible stable cell lines expressing ACREB (Fig. 1A). ACREB is a bZIP domain only in which the basic region was replaced with acidic residues, which prevents the binding to DNA while retaining he ability to dimerize with CREB or other partners. ACREB has been used as a potent dominant negative mutant to evaluate the role of CREB in cellular processes [36, 37].

With these stable cell lines in hands, we have demonstrated that overexpression of ACREB can sensitize LNCaP cells to IR (Fig. 1B, 1C). Because IR-induced NED constitutes two distinct phases: acquisition of radioresistance during the first two weeks (weeks 1-2) and NED during the second two weeks (weeks 3-4) (Fig. 2A). We have specifically examined whether knockdown of CREB can inhibit IR-induced NED during the second phase. As shown in Fig. 2B and 2C, induction of CREB shRNAs by doxycycline during weeks 3 and 4 inhibited IR-induced neurite outgrowth and increased IR-induced cell death. These results provide strong evidence that inhibition of IR-induced NED per se is sufficient to sensitize prostate cancer cells to radiation.

Task 2. Aim 2: Elucidate molecular mechanisms underlying the promotion of NED by pCREB and the repression by ATF2 (Months 12-24)

a. Make reporter gene constructs or obtain from other labs and optimize ChIP conditions (Months 12-16).
b. Determine the effect of pCREB and ATF2 on CgA-Luc activation (Months 12-16).
c. Perform ChIP assays to determine the kinetic changes in the binding of pCREB, CREB, ATF2 and other possible AP-1 proteins on the CRE site in the CgA promoter and NSE promoter in response to IR (Months 16-24).
d. Determine the role of ATF2 in prostate cancer cell growth and cell death (Months 16-24).

We have completed all experiments proposed in Aim 2. (1) We performed EMSA assays and confirmed that CREB and ATF2 both can bind the conserved CRE site in the CgA promoter (Fig. 3). (2)We made CgA and NSE luciferase reporter gene constructs and examined the effect of CREB and ATF2 on these reporter genes. We indeed observed that IR can activate the CgA reporter gene and its activity can be inhibited by ATF2 (Fig. 4). (3) We also performed ChIP assay and found that IR increased pCREB binding to the CgA promoter (Fig. 5). However, the binding of ATF2 to the CgA promoter did not change in non-irradiated or irradiated cells. (4) We observed that knockdown of ATF2 also induced neurite extension and cell death and these results are presented in the Cancer Research paper [34].

Task 3. Aim 3: Determine how IR induces cytoplasmic sequestration of ATF2 and identify cytoplasmic signals that may regulate subcellular localization of pCREB and ATF2 (Months 24-36)

a. Examine whether IR increases ATF2 homodimerization in the cytoplasm (Months 24-28).
b. Examine whether IR stabilizes the intramolecular interaction of ATF2 (Months 24- 28).
c. Examine the effect of AKT on the subcellular localizations of ATF2 and pCREB (Months 24-36).
d. Screen for other possible cytoplasmic signal that may be involved in regulating the subcellular localizations of ATF2 and pCREB (Months 24-36).
e. Identify cytoplasmic interacting proteins of pCREB and ATF2 using mass

spectrometry and functionally determine the roles of candidate interacting proteins in regulating the subcellular localizations of pCREB and ATF2 and in regulating IR-induced NED (Months 24-36)

We have completed all experiments proposed in Aim 3. We have screened several other protein kinases including AKT using specific inhibitors to determine whether any of these protein kinases might be involved in radiation-induced CREB phosphorylation. We identified PKA as a potential protein kinase responsible for IR-induced CREB phosphorylation during the first week treatment (Fig. 6). We also collaborated with Dr. Andy Tao to identify cytoplasmic interacting proteins of ATF2 and CREB using mass spectrometry. We identified some candidate proteins and demonstrated that CaMKII is a cytoplasmic interacting protein of pCREB (Fig. 7A). We also found that CaMKII interacted pCREB in the cytoplasm (Fig. 7B). In addition, inhibition of CaMKII activity by its specific inhibitor KN-93 did result in inhibition of neurite extension and increased IR-induced cell death (Fig. 7C, left panel) and inhibited IR-induced CREB phosphorylation (Fig. 7C, right panel). We also characterized the role of protein arginine methyltransferase 5 (PRMT5) in IR-induced NED and radioresistance, another protein identified from the CREB mass spectrometry analsysis. PRMT5 belongs to a family of PRMTs, which are important epigenetic regulators and involved in regulation of many cellular processes [38]. PRMT5 has recently been reported to regulate DNA damage response by dimethylating arginine residues in histones (e.g. H4R3, H3R8) and non-histone substrates (e.g. CBP, p53, Rad9) [39-43]. First, we performed co-immunoprecipitation to confirm the interaction between CREB and PRMT5 (Fig. 8A). Second, we verified that PRMT5 interacts with CREB primarily in the cytoplasm using our BiFC assay (Fig. 8B). Third, we confirmed that PRMT5 does regulate IR-induced CREB activation as knockdown of PRMT5 inhibited IR-induced phosphorylation of CREB (Fig. 8C). These results suggest that PRMT5 may play an important role in regulating IR-induced NED. Because the mechanism of radiotherapy is the induction of double stranded breaks, we were very interested in the potential role of PRMT5 in regulating IR-induced NED. To functionally and systematically characterize the role of PRMT5 in regulating the response of prostate cancer cells to radiation, we examined whether IR alters the expression level of PRMT5. As shown in Fig. 9A, IR increased the expression of PRMT5 in a dose-dependent manner not only in LNCaP cells but also in DU-145 and PC-3 prostate cancer cells. Importantly, we verified that IR also induced PRMT5 overexpression LNCaP xenograft tumors (Fig. 9B). Furthermore, radiation-induced PRMT5 overexpression was observed in the isolated dedifferentiated LNCaP sublines (Fig. 10A) and in clinically recurrent prostate cancer tissues from prostate cancer patients after radiotherapy failure (Fig. 10B). Importantly, knockdown of PRMT5 or inhibition of PRMT5 by a small molecule inhibitor (provided by collaborator Dr. Chenglong Li at Ohio State University) increased IR-induced cell death and sensitized cells to IR (Fig. 11). Taken together, these preliminary results strongly suggest that IR-induced PRMT5 overexpression may confer the resistance to radiotherapy and contribute to tumor recurrence. These exciting preliminary data have enabled us to successfully secure a second DOD grant (Idea Development Award) starting from July 1, 2012.

We also performed an ATF2 mass spectrometry analysis. Unfortunately, there is no interesting candidate protein in the list (Table 1) and we did not characterize them

further. We failed to observe any increased homodimerization of ATF2 using our BiFC assay. We have used a variety of assays (BiFC, Co-IP, GST pulldown, *in vitro* binding) to prove a previously reported intramolecular interaction of ATF2. Unfortunately, we failed to demonstrate it. Instead, we identified a novel NES in the most N-terminal end of ATF2, which is required for ATF2 nuclear localization and transcriptional activity. This work has been published in the Journal of Biological Chemistry (see Attached PDF) [44]. As reviewers pointed out, the proposed Aim 3 was overambitious. Nevertheless, we have conducted all proposed experiments and identified some interesting regulators of CREB and discovered a novel regulatory mechanism of ATF2 subcellular localization. We will continue the characterization of these regulators, in particular PRMT5, under the support of our new DOD grant.

Additional accomplishments beyond the Approved SOW

(1) We have also demonstrated that IR-induced NED is reversible. Importantly, we have isolated three dedifferentiated clones and found that these dedifferentiated cells have acquired the ability to be cross-resistant to radiation, androgen ablation, and chemotherapeutic agent docetaxel. Also, these dedifferentiated clones respond poorly to IR- or androgen ablation-induced NED. These findings strongly suggest that IR-induced NED may represent a novel pathway by which prostate cancer cells survive the treatment and contribute to recurrence. These results are presented in Figures 5 and 6 (page 9668) and Supplementary Figures 4 and 5 in the Cancer Research paper [34].

(2) We have extended our finding in LNCaP cells to two other prostate cancer cell lines (DU-145 and PC-3). We observed that IR induced neurite extension and the expression of CgA and NSE to a lesser extent when compared with LNCaP cells. We also confirmed that IR induced cytoplasmic sequestration of ATF2 and CREB phosphorylation in a subset of cells in DU-145 and PC-3. These results are now included in the attached publication (Am J Cancer Res) [45].

(3) We have also initiated the collaboration with Dr. Tim Ratliff, Dr. Ben Elzey, Dr. Jean Poulson and Dr. Wally Morrison at Purdue to confirm that IR also induced NED in LNCaP xenograft tumors. More importantly, we found that IR elevated the plasma CgA level by 2-4 fold after 20 and 40 Gy of irradiation when compared with the plasma CgA level before radiation. This finding is very exciting given that CgA has been used to diagnose neuroendocrine tumors clinically. We hypothesized that monitoring plasma CgA will allow for evaluation of radiotherapy-induced NED and this may allow for the establishment of a clinical correlation between radiation-induced NED and clinical outcomes. Since we noticed that plasma CgA levels are affected by the tumor volume (no of tumor cells), we have recently measured plasma PSA levels and normalized CgA levels to PSA levels. In all irradiated tumor-bearing mice, we observed an average of 5-fold increase. This result along with the immunohistochemical results are all included in the Am J Cancer Res [45].

(4) Our exciting finding from *in vivo* studies prompted us to explore whether radiotherapy can induce NED in prostate cancer patients. For this purpose, we have collaborated with Dr. Song-Chu Ko at Indiana University School of

Medicine to perform a pilot study. We enrolled 9 prostate cancer patients, and collected their blood samples before, in the middle of, and immediately after radiotherapy. We then measured serum CgA levels and PSA levels. Two patients showed elevation of serum CgA levels after radiotherapy. When normalized to serum PSA levels, 4 out of 9 patients (44%) showed 1.5-2.2 fold increase in serum CgA. This finding, along with our *in vitro* and *in vivo* studies, strongly suggests that radiotherapy can indeed induce NED in a subset of prostate cancer patients. Further detailed analysis of radiotherapy-induced NED in prostate cancer patients in a large scale study will likely provide new insight into the role of NED in the therapeutic responses and prognosis in prostate cancer patients. These results are also included in the Am J Cancer Res paper [45].

Key Research Accomplishments

- Demonstrated that 40 Gy of irradiation is sufficient to induce neurite extension in LNCaP cells
- Demonstrated that 40 Gy of irradiation can induce expression of two NE markers chromagranin A (CgA) and neuron specific enolase (NSE)
- Demonstrated that IR-induced NE-like cells show increased cytoplasmic localization of ATF2 and increased pCREB in the nucleus
- Demonstrated that 10 Gy of irradiation is enough to induce cytoplasmic sequestration of ATF2 and nuclear accumulation of pCREB
- Demonstrated that knockdown of ATF2 or overexpression of a constitutively cytoplasmic-localized ATF2 induces NED
- Demonstrated that overexpression of VP16-bCREB induces NED and its induction of NED can be attenuated by a constitutively nuclear-localized ATF2 (nATF2)
- Demonstrated that overexpression of nATF2 or CREB-S133A (dominant negative mutant of CREB) can inhibit IR-induced neurite outgrowth. However, only nATF2, but not CREB-S133A, inhibits IR-induced CgA and NSE expression.
- Demonstrated that IR-induced NED is reversible and dedifferentiated cells are cross-resistant to the treatments with radiation, androgen ablation and chemotherapeutic agent docetaxel.
- Demonstrated that CREB can activate the CgA reporter gene.
- Demonstrated that IR induced pCREB binding to CgA.
- Demonstrated that IR also induced neurite extension in DU-145, PC-3 and VCaP cells and the expression of CgA and NSE to certain extent.
- Demonstrated that IR induced CgA expression in LNCaP xenograft tumors.
- Demonstrated that IR increased plasma CgA levels in LNCaP xenograft tumor-bearing nude mice.
- Identified PKA as a potential protein kinase responsible for IR-induced CREB activation
- Identified CaMKII as a potential upstream protein kinase of CREB involved in IR-induced NED.
- Identified PRMT5 as a potential regulator of CREB involved in radiation-induced NED
- Demonstrated that radiation-induced PRMT5 overexpression may confer the resistance to radiotherapy and contribute to tumor recurrence.
- Demonstrated that A-CREB expression can sensitize LNCaP cells to IR.
- Showed that radiotherapy in prostate cancer patients can induce NED in 44% of patients.

Reportable Outcomes

1. Publications of research results relevant to the DOD grant
   (1) Deng, X., Liu, H., Huang, J., Cheng, L., Keller, E, Parsons, S.J. and **Hu, C.D.** Ionizing radiation induces prostate cancer cell neuroendocrine differentiation through interplay of CREB and ATF2: Implications for disease progression. *Cancer Res.* **68**:9663-9670 (2008)
   (2) Deng, X., Elzey, B.D, Poulson, J.M., Morrison, W.B., Ko, S.C., Hahn, N.M., Ratliff, T.L., and **Hu, C.D.** Ionizing radiation induces neuroendocrine differentiation in vitro, in vivo and in human prostate cancer patients. *Am. J. Cancer. Res.* 1:834:844 (2011)
   (3) Hsu, C. and **Hu, C.D**. Critical role of an N-terminal end nuclear export signal in regulation of ATF2 subcellular localization and transcriptional activity. *J. Biol. Chem*. 287:8621-8632 (2012)

2. Manuscript in preparation
   Suarez C., Deng, X. and **Hu, C.D**. CREB signaling is critical for radiation-induced neuroendocrine differentiation: implication for prostate cancer radiotherapy

3. Meeting attendance
   The interplay of CREB and ATF2 in regulating ionizing radiation-induced neuroendocrine differentiation in prostate cancer cells
   Authors: Xuehong Deng, Han Liu, Jiaoti Huang, Liang Cheng, Evan T. Keller, Sarah J. Parsons, and Chang-Deng Hu
   Meeting: Mechanisms and Models of Cancer
   Place and Date: Cold Spring Harbor, August 13-17, 2008

   Radiation induces neuroendocrine differentiation of prostate cancer cell lines in vitro and in vivo
   Authors: Chang-Deng Hu, Bennett Elzey, Jean Poulson, Wallace Morrison, Xuehong Deng, Sandra Torregrosa-Allen, Timothy Ratliff
   Meeting: 2010 AUA Meeting and SBUR meeting
   Place and Date: San Francisco, May 28-June 3, 2010

   Radiation induces neuroendocrine differentiation of prostate cancer cells *in vitro* and *in vivo:* Implications for prostate cancer radiotherapy
   Authors: Chang-Deng Hu, Xuehong Deng, Christopher Suarez, Bennett D. Elzey, Jean M. Poulson, Wallace B. Morrison, Sandra Torregrosa-Allen, Jiaoti Huang, Liang Cheng, Evan T. Keller, Sarah J. Parsons, Timothy L. Ratliff
   Meeting: 2011 IMPaCT
   Place and Date: Orlando, March 9-12, 2011

   Targeting radiation-induced neuroendocrine differentiation as a novel radiosensitization approach for prostate cancer radiotherapy
   Authors: Chang-Deng Hu, Xuehong Deng, Christopher Suarez, Bennett D. Elzey, Jean M. Poulson, Wallace B. Morrison, Song-chu Ko, Noah Hahn, Timothy L. Ratliff

Meeting: 2011 SBUR
Place and Data: Las Vegas, November 10-13, 2011

4. Invited Seminars (prostate cancer related only)
   (1) Ionizing radiation-induced neuroendocrine differentiation: implication in prostate cancer therapy
   Place: University of Virginia Cancer Center
   Date: December 18, 2008
   (2) Ionizing radiation-induced neuroendocrine differentiation: implication in prostate cancer therapy
   Place: Indiana University Medical School, Department of Bioehcmistry
   Date: February 2, 2009
   (3) Mechanisms and targeting of therapy-resistant prostate cancer
   Place: Beijing University Cancer Hospital
   Date: September 13, 2010
   (4) Mechanisms and targeting of therapy-resistant prostate cancer
   Place: Wannan Medical College
   Date: September 25, 2010
   (5) Mechanisms and targeting of therapy-resistant prostate cancer
   Place: Tulane University
   Date: February 8, 2010
   (6) Mechanisms and targeting of therapy-resistant prostate cancer
   Place: Sun-Yat-sun University Medical School
   Date: July 10, 2011
   (7) Mechanisms and targeting of therapy-induced neuroendocrine differentiation for prostate cancer treatment
   Place: Mayo Clinic
   Date: March 13, 2012
   (8) Radiotherapy-induced neuroendocrine differentiation: Implications in prostate cancer progression and treatment
   Place: University of Western Ontario Cancer Center
   Date: April 25, 2012
   (9) Recent advances in prostate cancer diagnosis and treatment
   Place: Tongling Traditional Chinese Medicine Hospital
   Date: May 31, 2012
   (10) Mechanisms and targeting of radiotherapy-induced neuroendocrine differentiation for prostate cancer treatment
   Place: Jiangshu University School of Medical Technology and Laboratory Medicine
   Date: June 6, 2012

5. Development of cell lines
   We have isolated three radiation resistant clones LNCaP-IRR1, LNCaP-IRR2 and LNCaP-IRR3 from dedifferentiated cells. These clones will be useful for molecular mechanism study and for development of novel therapeutics. We have also recently isolated several sublines from DU-145 after 40 and 70 Gy of irradiation.

6. Degrees awarded
   Chih-chao Hsu: Thesis defense has been scheduled for August and Ph.D. degree will be awarded in December, 2012.
   Christopher Suarez: Thesis defense will take place in December of 2012 and Ph.D. degree will be awarded.

7. Funding applied and funded
   Title: Targeting of prostate cancer transdifferentiation and proliferation via a novel DNA nanotube-based nucleic acid delivery
   Agency: Lilly Seed Grant (School of Pharmacy and Pharmaceutical Sciences, Purdue)
   PI: Chang-Deng Hu
   Total Cost: $100,000
   Period: Jan 2009 – Dec 2010

   Title: Radiation-induced prostate cancer transdifferentiation *in vivo*
   Agency: Purdue University Center for Cancer Research
   PI: Chang-Deng Hu
   Grant Period: 01/01/09-12/31/10
   Total Cost: $23,400 (milestone-based funding for a total of $50,000)
   Goals: The goal of this project is to use xenograft nude mice prostate cancer cell models to investigate whether CREB and ATF2 contribute to radiation-induced neuroendocrine differentiation *in vivo* and to determine whether radiation induces changes of pCREB and ATF2 subcellular localization.

   Title: Chromogranin A: a biomarker to monitor radiotherapy-induced neuroendocrine differentiation and to predict prognosis
   Agency: Indiana Translational Science Institute
   PI: Chang-Deng Hu
   Grant Period: 07/01/2010-06/30/2011
   Total Cost: $8,000
   Goals: The goal of this pilot study is to measure serum CgA before, during and after radiotherapy from 20 prostate cancer patients. We will use the preliminary results to do power calculation for a large scale analysis. We have already obtained results from 9 patients and found that 4 out of 9 patients showed serum CgA elevation. This is sufficient for our purpose.

   Title: Targeting PRMT5 as a novel radiosensitization approach for primary and recurrent prostate cancer treatment
   Agency: DoD PCRP
   PI: Chang-Deng Hu
   Grant Period: 07/01/2012-06/30/2015
   Total cost: $559,269
   Goals: The goal of this Idea Development Award will test whether targeting PRMT5 can radiosensitize prostate cancer cells. *In vitro* and *in vivo* model systems developed

through current DoD support will be used to assess the role of radiation-induced PRMT5 overexpression in radioresistance and tumor recurrence.

List of people who have been supported (pay received)

Chang-Deng Hu (PI)
Xuehong Deng (Technician)
Christopher Suarez (Graduate student)
Chih-chao Hsu (Graduate Student)

Conclusion

Under the support of this prostate cancer idea development award, we have demonstrated that IR can induce neuroendocrine differentiation (NED) in the prostate cancer cells LNCaP, DU-145 and PC-3. Furthermore, we have also shown that radiation also induces NED in LNCaP xenografted tumors in nude mice and increases plasma chromogranin A levels. We have shown that two CRE-binding transcription factors ATF2 and CREB plays an opposite role in regulation of NED and that IR induces NED by impairing ATF2 nuclear import and increasing nuclear-localized phosphorylated CREB (pCREB). Importantly, we have also shown that IR-induced NED is reversible and three radiation resistant clones derived from dedifferentiated cells are cross-resistant to radiation, androgen depletion and docetaxel treatments. Further evidence comes from the finding that IR increases the CgA reporter gene activity and induces pCREB binding to the CgA promoter. All of these together strongly support the idea that CREB plays a critical role in IR-induced NED. We have provided evidence that targeting of CREB by a dominant negative CREB, A-CREB, or CREB knockdown can sensitize LNCaP cells to IR and inhibit IR-induced NED. These findings suggest that IR-induced NED may represent a novel pathway by which prostate cancer cells survive treatment and contribute to recurrence. Mass spectrometry analysis of CREB interacting proteins have enabled us to identify CaMKII as a potential upstream protein kinase of CREB involved in IR-induced NED. Importantly, we have identified PRMT5 as a novel regulator of CREB in prostate cancer cells. Significantly, IR also induces PRMT5 overexpression and confers the resistance to radiation. We will continue to elucidate the role of PRMT5 in regulating the response of prostate cancer cells to radiation under the support of our new DOD grant. In addition, we have extended beyond the proposed experiments in the original submission and found that IR induces NED in two other prostate cancer cell lines and in LNCaP xenograft tumors in nude mice. Interestingly, we have also observed that irradiation of LNCaP xenograft tumors in nude mice also increases the serum CgA level in mice. This finding suggests that serum CgA levels can be used as a biomarker to monitor radiotherapy-induced NED in prostate cancer patients. In fact, our pilot study with 9 prostate cancer patients has shown that 4 out of 9 patients show serum CgA elevation after radiotherapy. Therefore, we are seeking additional funding to conduct a large scale study to confirm this pilot study.

References

[1] Daneshmand S, Quek ML and Pinski J. Neuroendocrine differentiation in prostate cancer. Cancer Therapy 2005;3:383-396.

[2] Nelson EC, Cambio AJ, Yang JC, Ok JH, Lara PN, Jr. and Evans CP. Clinical implications of neuroendocrine differentiation in prostate cancer. Prostate Cancer Prostatic Dis 2007;10:6-14.

[3] Amorino GP and Parsons SJ. Neuroendocrine cells in prostate cancer. Crit Rev Eukaryot Gene Expr 2004;14:287-300.

[4] Yuan TC, Veeramani S and Lin MF. Neuroendocrine-like prostate cancer cells: neuroendocrine transdifferentiation of prostate adenocarcinoma cells. Endocr Relat Cancer 2007;14:531-47.

[5] Yuan TC, Veeramani S, Lin FF, Kondrikou D, Zelivianski S, Igawa T, Karan D, Batra SK and Lin MF. Androgen deprivation induces human prostate epithelial neuroendocrine differentiation of androgen-sensitive LNCaP cells. Endocr Relat Cancer 2006;13:151-67.

[6] Ismail AH, Landry F, Aprikian AG and Chevalier S. Androgen ablation promotes neuroendocrine cell differentiation in dog and human prostate. Prostate 2002;51:117-25.

[7] Wright ME, Tsai MJ and Aebersold R. Androgen receptor represses the neuroendocrine transdifferentiation process in prostate cancer cells. Mol Endocrinol 2003;17:1726-37.

[8] Jin RJ, Wang Y, Masumori N, Ishii K, Tsukamoto T, Shappell SB, Hayward SW, Kasper S and Matusik RJ. NE-10 neuroendocrine cancer promotes the LNCaP xenograft growth in castrated mice. Cancer Res 2004;64:5489-95.

[9] Jiborn T, Bjartell A and Abrahamsson PA. Neuroendocrine differentiation in prostatic carcinoma during hormonal treatment. Urology 1998;51:585-9.

[10] Zhang XQ, Kondrikov D, Yuan TC, Lin FF, Hansen J and Lin MF. Receptor protein tyrosine phosphatase alpha signaling is involved in androgen depletion-induced neuroendocrine differentiation of androgen-sensitive LNCaP human prostate cancer cells. Oncogene 2003;22:6704-16.

[11] Lee SO, Chun JY, Nadiminty N, Lou W and Gao AC. Interleukin-6 undergoes transition from growth inhibitor associated with neuroendocrine differentiation to stimulator accompanied by androgen receptor activation during LNCaP prostate cancer cell progression. Prostate 2007;67:764-73.

[12] Deeble PD, Murphy DJ, Parsons SJ and Cox ME. Interleukin-6- and cyclic AMP-mediated signaling potentiates neuroendocrine differentiation of LNCaP prostate tumor cells. Mol Cell Biol 2001;21:8471-82.

[13] Wang Q, Horiatis D and Pinski J. Interleukin-6 inhibits the growth of prostate cancer xenografts in mice by the process of neuroendocrine differentiation. Int J Cancer 2004;111:508-13.

[14] Xie S, Lin HK, Ni J, Yang L, Wang L, di Sant'Agnese PA and Chang C. Regulation of interleukin-6-mediated PI3K activation and neuroendocrine differentiation by androgen signaling in prostate cancer LNCaP cells. Prostate 2004;60:61-7.

[15] Spiotto MT and Chung TD. STAT3 mediates IL-6-induced neuroendocrine differentiation in prostate cancer cells. Prostate 2000;42:186-95.

[16] Qiu Y, Robinson D, Pretlow TG and Kung HJ. Etk/Bmx, a tyrosine kinase with a pleckstrin-homology domain, is an effector of phosphatidylinositol 3'-kinase and is involved in

interleukin 6-induced neuroendocrine differentiation of prostate cancer cells. Proc Natl Acad Sci U S A 1998;95:3644-9.
[17] Cox ME, Deeble PD, Lakhani S and Parsons SJ. Acquisition of neuroendocrine characteristics by prostate tumor cells is reversible: implications for prostate cancer progression. Cancer Res 1999;59:3821-30.
[18] Farini D, Puglianiello A, Mammi C, Siracusa G and Moretti C. Dual effect of pituitary adenylate cyclase activating polypeptide on prostate tumor LNCaP cells: short- and long-term exposure affect proliferation and neuroendocrine differentiation. Endocrinology 2003;144:1631-43.
[19] Zelivianski S, Verni M, Moore C, Kondrikov D, Taylor R and Lin MF. Multipathways for transdifferentiation of human prostate cancer cells into neuroendocrine-like phenotype. Biochim Biophys Acta 2001;1539:28-43.
[20] Bang YJ, Pirnia F, Fang WG, Kang WK, Sartor O, Whitesell L, Ha MJ, Tsokos M, Sheahan MD, Nguyen P and et al. Terminal neuroendocrine differentiation of human prostate carcinoma cells in response to increased intracellular cyclic AMP. Proc Natl Acad Sci U S A 1994;91:5330-4.
[21] Vinson C, Myakishev M, Acharya A, Mir AA, Moll JR and Bonovich M. Classification of human B-ZIP proteins based on dimerization properties. Molecular & Cellular Biology 2002;22:6321-35.
[22] Ma Q, Li X, Vale-Cruz D, Brown ML, Beier F and Luvalle P. Activating transcription factor 2 controls Bcl-2 promoter activity in growth plate chondrocytes. J Cell Biochem 2007;101:477-87.
[23] Sangerman J, Lee MS, Yao X, Oteng E, Hsiao CH, Li W, Zein S, Ofori-Acquah SF and Pace BS. Mechanism for fetal hemoglobin induction by histone deacetylase inhibitors involves gamma-globin activation by CREB1 and ATF-2. Blood 2006;108:3590-9.
[24] Gueorguiev VD, Cheng SY and Sabban EL. Prolonged activation of cAMP-response element-binding protein and ATF-2 needed for nicotine-triggered elevation of tyrosine hydroxylase gene transcription in PC12 cells. J Biol Chem 2006;281:10188-95.
[25] Ionescu AM, Drissi H, Schwarz EM, Kato M, Puzas JE, McCance DJ, Rosier RN, Zuscik MJ and O'Keefe RJ. CREB Cooperates with BMP-stimulated Smad signaling to enhance transcription of the Smad6 promoter. J Cell Physiol 2004;198:428-40.
[26] Ionescu AM, Schwarz EM, Zuscik MJ, Drissi H, Puzas JE, Rosier RN and O'Keefe RJ. ATF-2 cooperates with Smad3 to mediate TGF-beta effects on chondrocyte maturation. Exp Cell Res 2003;288:198-207.
[27] Niwano K, Arai M, Koitabashi N, Hara S, Watanabe A, Sekiguchi K, Tanaka T, Iso T and Kurabayashi M. Competitive binding of CREB and ATF2 to cAMP/ATF responsive element regulates eNOS gene expression in endothelial cells. Arterioscler Thromb Vasc Biol 2006;26:1036-42.
[28] Flint KJ and Jones NC. Differential regulation of three members of the ATF/CREB family of DNA-binding proteins. Oncogene 1991;6:2019-26.
[29] Hay CW, Ferguson LA and Docherty K. ATF-2 stimulates the human insulin promoter through the conserved CRE2 sequence. Biochim Biophys Acta 2007;1769:79-91.
[30] Garcia GE, Nicole A, Bhaskaran S, Gupta A, Kyprianou N and Kumar AP. Akt-and CREB-mediated prostate cancer cell proliferation inhibition by Nexrutine, a Phellodendron amurense extract. Neoplasia 2006;8:523-33.

[31] Unni E, Sun S, Nan B, McPhaul MJ, Cheskis B, Mancini MA and Marcelli M. Changes in androgen receptor nongenotropic signaling correlate with transition of LNCaP cells to androgen independence. Cancer Res 2004;64:7156-68.
[32] Canaff L, Bevan S, Wheeler DG, Mouland AJ, Rehfuss RP, White JH and Hendy GN. Analysis of molecular mechanisms controlling neuroendocrine cell specific transcription of the chromogranin A gene. Endocrinology 1998;139:1184-96.
[33] Kim J, Jia L, Stallcup MR and Coetzee GA. The role of protein kinase A pathway and cAMP responsive element-binding protein in androgen receptor-mediated transcription at the prostate-specific antigen locus. J Mol Endocrinol 2005;34:107-18.
[34] Deng X, Liu H, Huang J, Cheng L, Keller ET, Parsons SJ and Hu CD. Ionizing radiation induces prostate cancer neuroendocrine differentiation through interplay of CREB and ATF2: Implications for disease progression. Cancer Res. 2008;68:9663-9670.
[35] Johannessen M and Moens U. Multisite phosphorylation of the cAMP response element-binding protein (CREB) by a diversity of protein kinases. Front Biosci 2007;12:1814-32.
[36] Ahn S, Olive M, Aggarwal S, Krylov D, Ginty DD and Vinson C. A dominant-negative inhibitor of CREB reveals that it is a general mediator of stimulus-dependent transcription of c-fos. Mol Cell Biol 1998;18:967-77.
[37] Impey S, McCorkle SR, Cha-Molstad H, Dwyer JM, Yochum GS, Boss JM, McWeeney S, Dunn JJ, Mandel G and Goodman RH. Defining the CREB regulon: a genome-wide analysis of transcription factor regulatory regions. Cell 2004;119:1041-54.
[38] Krause CD, Yang ZH, Kim YS, Lee JH, Cook JR and Pestka S. Protein arginine methyltransferases: evolution and assessment of their pharmacological and therapeutic potential. Pharmacol Ther 2007;113:50-87.
[39] Jansson M, Durant ST, Cho EC, Sheahan S, Edelmann M, Kessler B and La Thangue NB. Arginine methylation regulates the p53 response. Nat Cell Biol 2008;10:1431-9.
[40] Scoumanne A, Zhang J and Chen X. PRMT5 is required for cell-cycle progression and p53 tumor suppressor function. Nucleic Acids Res 2009;37:4965-76.
[41] Xu X, Hoang S, Mayo MW and Bekiranov S. Application of machine learning methods to histone methylation ChIP-Seq data reveals H4R3me2 globally represses gene expression. BMC Bioinformatics 2010;11:396.
[42] Yang M, Sun J, Sun X, Shen Q, Gao Z and Yang C. Caenorhabditis elegans protein arginine methyltransferase PRMT-5 negatively regulates DNA damage-induced apoptosis. PLoS Genet 2009;5:e1000514.
[43] He W, Ma X, Yang X, Zhao Y, Qiu J and Hang H. A role for the arginine methylation of Rad9 in checkpoint control and cellular sensitivity to DNA damage. Nucleic Acids Res 2011; 39:4719-4727.
[44] Hsu CC and Hu CD. Critical role of N-terminal end-localized nuclear export signal in regulation of activating transcription factor 2 (ATF2) subcellular localization and transcriptional activity. J Biol Chem 2012;287:8621-32.
[45] Deng X, Elzey BD, Poulson JM, Morrison WB, Ko SC, Hahn NM, Ratliff TL and Hu CD. Ionizing radiation induces neuroendocrine differentiation of prostate cancer cells in vitro, in vivo and in prostate cancer patients. Am J Cancer Res 2011;1:834-844.

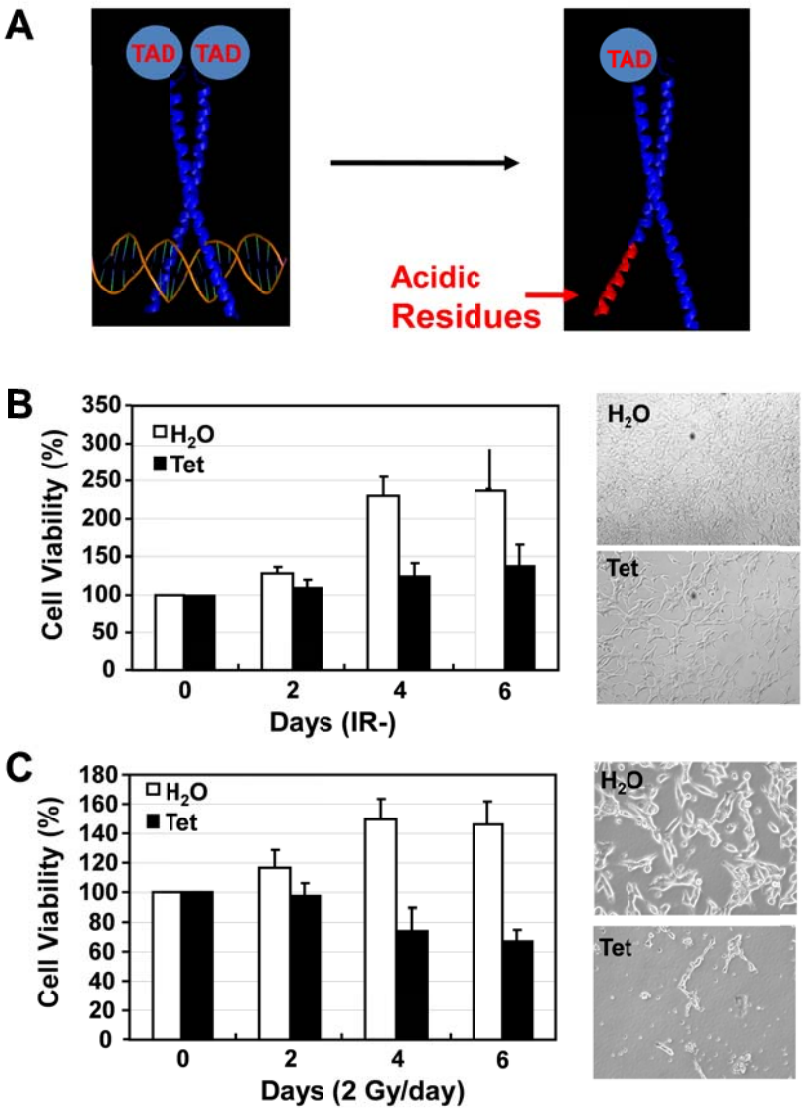

Figure 1. ACREB overexpression increased IR-induced cell death. **A**. Shown are the model of CREB dimer bound on DNA (the model on left). TAD refers to transcriptional activation domain, which is required for transcriptional activity. ACREB is the bZIP domain only without the TAD domain and has its basic region (required for DNA binding) replaced with acidic residues (the model on right). However, ACREB retains its ability to dimerize with CREB or other partners without DNA binding, thus acting as a dominant negative mutant. **B**. Effect of ACREB induction on cell growth in the absence of fractionated IR. LNCaP cells cultured in RPMI1640 supplemented with antibiotics and 10% FBS were treated with tetracycline (1 mg/ ml) or water control for the indicated days and harvested for cell viability analysis using MTT assay. **C**. Similar experiments were performed as B except that cells were subjected fractionated IR (2 Gy/day). Images shown in B and C were representative images acquired after 6 days of treatment.

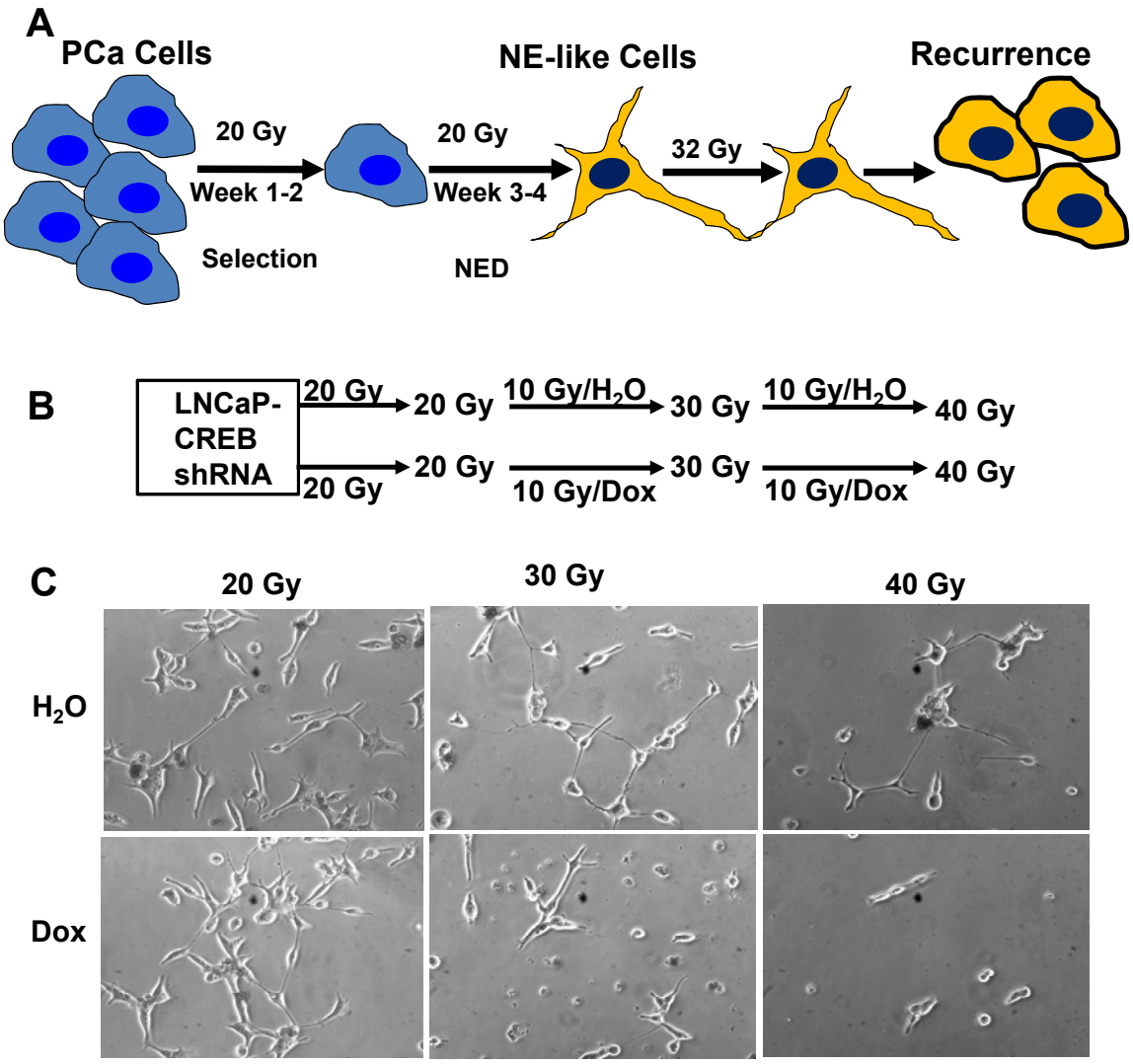

Figure 2. CREB is critical for radiation-induced NED. **A.** Based on our *in vitro* and *in vivo* data, we hypothesize that radiation-induced NED involves at least two phases. The first two weeks is the acquisition of radioresistance phase, in which the majority of cells die and a fraction of cells is selectively survived. The second phase is the differentiation process in which survived cells reprogram to differentiate into NE-like cells. **B**. Shown is the scheme of treatments of LNCaP stable cell lines that can inducibly express CREB shRNA. Cells were first irradiated for two weeks (20 Gy) without the induction of CREB shRNA by doxycline (Dox). Beginning the third week, cells were treated with Dox to induce CREB shRNA expression. The control group was treated with H_2O only. Cells were continued irradiated and treatment for the third (30 Gy) and fourth week (40 Gy). **C.** Shown are representative images of cells that were irradiated for 20 Gy, 30 Gy and 40 Gy with or without the induction of CREB shRNA during the third and fourth week treatment.

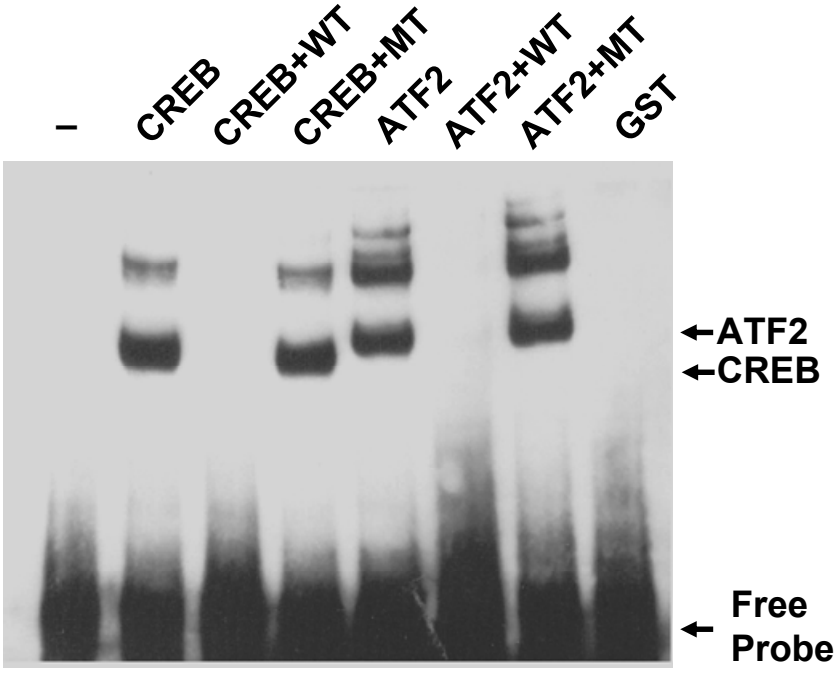

Figure 3. DNA binding of ATF2 and CREB to CgA. The bZIP regions of CREB and ATF2 were expressed in *E. coli* and purified as GST-tagged fusion proteins. Approximately 2 pmol of indicated purified fusion proteins were incubated with 50 ng of biotin-labeled CRE consensus sequences derived from the CgA promoter in the absence or presence of 100x unlabeled wild-type (WT) or mutant (MT) probes. The protein-DNA complexes were resolved on a 4% polyacrylamide gel, transferred and crosslinked to Nylon membrane. The detection of protein-DNA complexes was performed by incubating the membrane with Streptavidin-HRP followed by ECL. The arrows indicate the positions of DNA-protein complexes composed of CREB homodimers or ATF2 homodimers. Note that one slower mobility shift band for both ATF2 and CREB likely represents oligomers bound to DNA, which are often seen with other bZIP proteins.

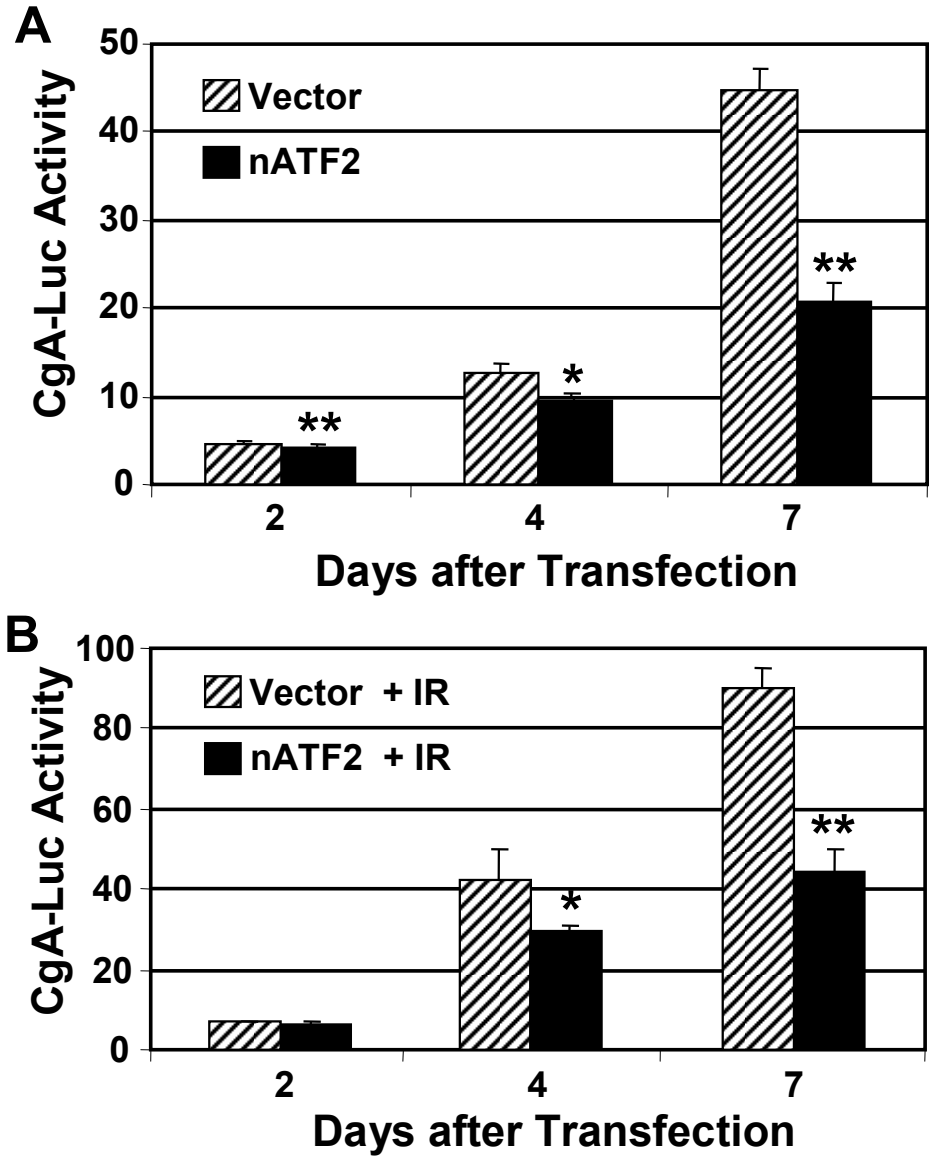

Figure 4: Inhibition of CgA-Luc reporter gene activity by nATF2 in LNCaP cells. LNCaP cells cultured in 12-well plates were co-transfected with 0.5 μg of the reporter plasmid pGL4.10-CgA-Luc and 50 ng of pRL-TK with 0.5 μg of the vector control (vector) or the plasmid encoding the constitutively nuclear-localized ATF2 (nATF2) using FuGENE HD. The transfected cells were left untreated (**A**) or irradiated every day (2 Gy/day) (**B**), and harvested at the indicated time posttransfection. Five μg of total protein was used for the measurement of luciferase activity using the Dual-Luciferasce Assay kit (Promega). *$p<0.05$ when compared with the respective vector control. **$p<0.01$ when compared with the respective vector control.

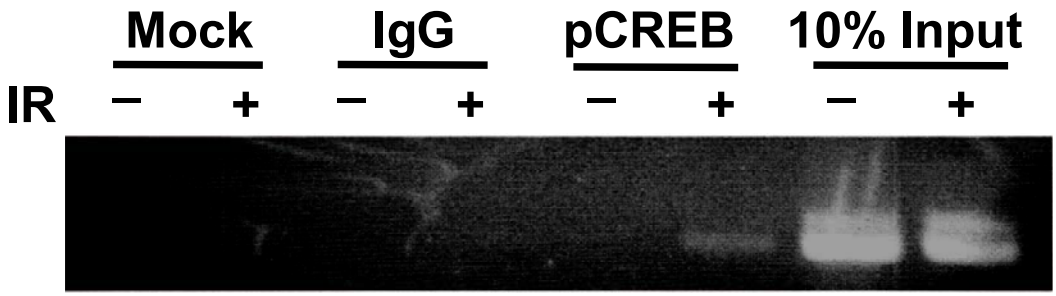

Figure 5. ChIP analysis of pCREB binding to the CgA promoter in LNCaP cells. DNA-protein complexes in non-irradaited (IR-) or irradiated for five times (IR+) LNCaP cells were crosslinked in whole cells using formaldehyde. Following nuclei isolation and lysis, the chromatin was sonicated to an average length of ~600 bp prior to immunoprecipitation with the antibody against phospho-CREB and mouse IgG (IgG) or without antibody (Mock). The proteins in the immunoprecipitates were digested by Protease K and the DNA was directly extracted using Chelex beads. The DNA eluted from the beads was used for PCR amplification of the CgA promoter containing the CRE binding site. The right two lanes show the PCR product amplified with 10% of the total DNA-protein complexes used for immunoprecipitation.

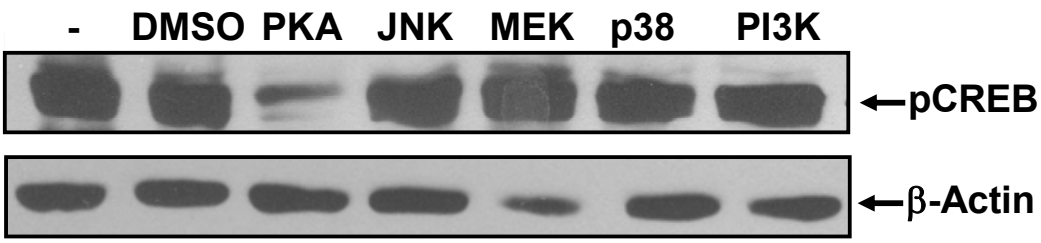

Figure 6. PKA mediates IR-induced CREB phosphorylation. LNCaP cells cultured in 10-cm dishes were irradiated (2 Gy/day) for five days in the absence (DMSO) or presence of the indicated protein kinase inhibitors at the commonly used concentrations. Total cell lysate was prepared after the treatment and subjected to immunoblotting analysis of pCREB. The lack of effect of an AKT inhibitor on IR-induced CREB phosphorylation was performed in a different experiment and was not included here.

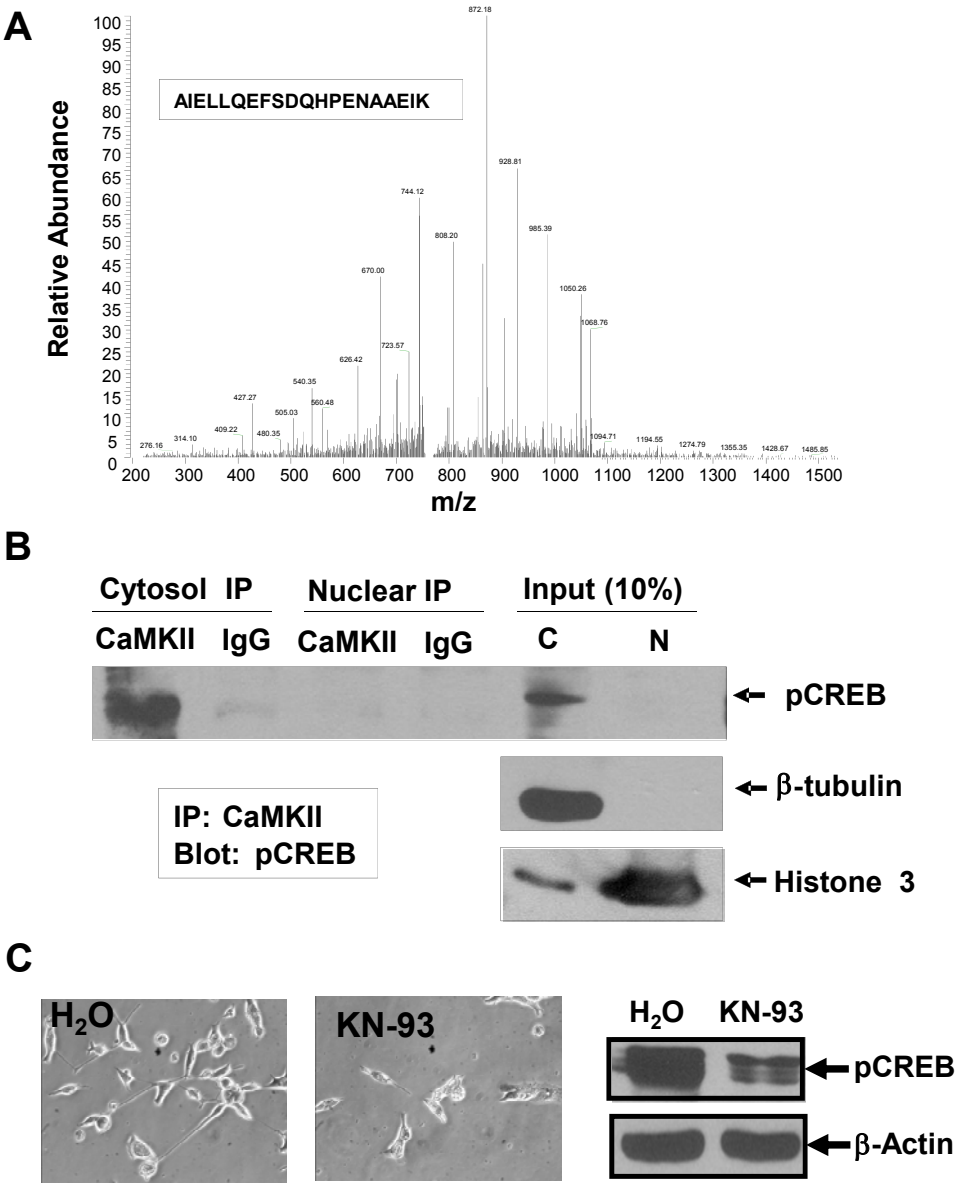

Figure 7. CaMKII interacts with pCREB in LNCaP cells. A. LNCaP cells were cultured to confluence and cytosolic extract was prepared. Approximately 1 mg of cytosolic extract was used to immunoprecipitate CREB with anti-CREB antibody and the immunoprecipitate was processed for mass spectrometry analysis. Shown is the spectrum for one of the peptides indentified. The insert shows the peptide sequence. **B**. Cytosolic extract (1 mg) and equal portion of nuclear extract from non-irradiated cells were used to immunoprecipitate CaMKII and blotted for pCREB. The input (10%) for both cytosolic (C) and nuclear (N) fractions was loaded on the last two lanes. Histone 3 and β-tubulin immunoblotting shown below were used as evidence of a successful fractionation. **C**. LNCaP cells were irradiated with fractionated ionization radiation for 40 Gy (2 Gy/day, 5 days/week) in the presence of the CaMKII inhibitor KN-93 (10 μM) or H_2O control. Shown are representative images acquired after the completion of 40 Gy irradiation (left panel). The right panel shows the inhibition of pCREB by KN93 assayed by Western blotting using the cell lysates from the experiments after the completion of 40 Gy of irradiation.

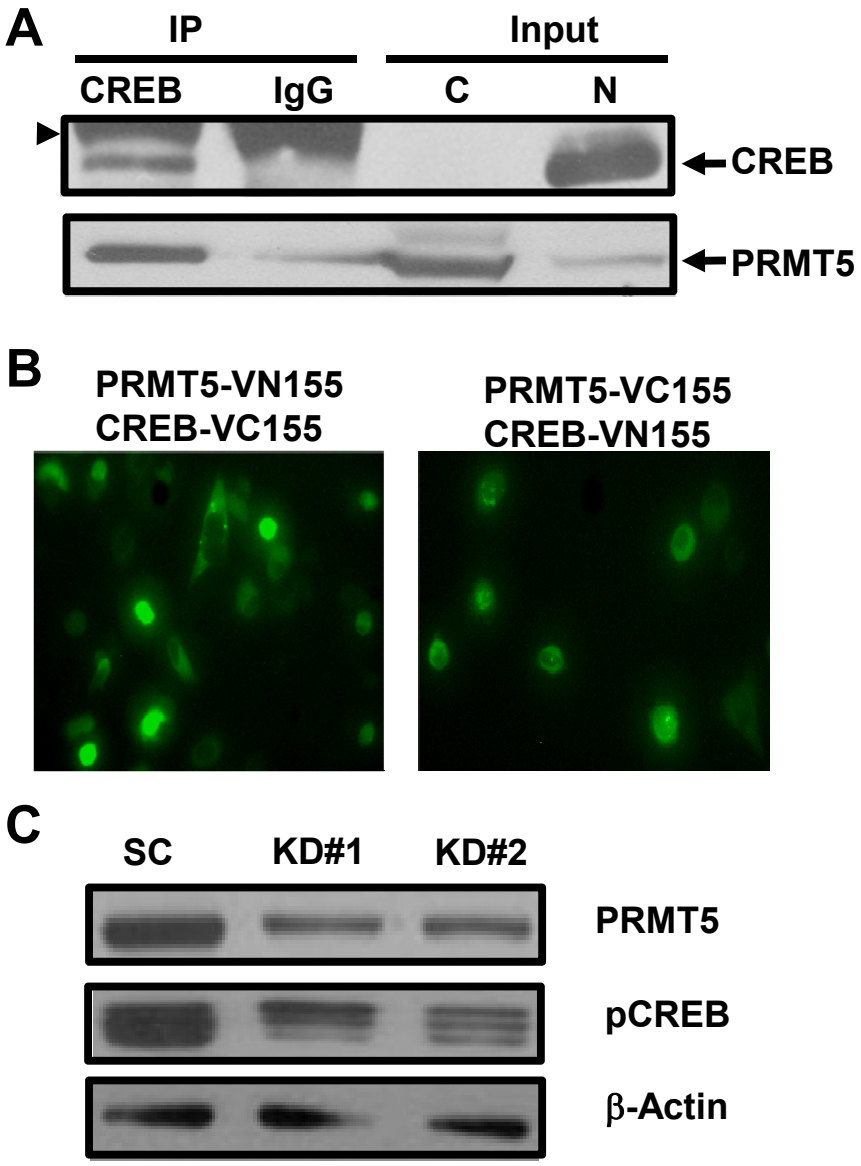

Figure 8. Identification of PRMT5 as a novel regulator of CREB. **A**. Co-immunoprecipitation of PRMT5 with CREB. Total cell lysate (~ 200 μg) of LNCaP cells was immunprepicitated with anti-CREB antibody and co-immunoprecipitated PRMT5 was detected by immunoblotting. **B**. BiFC analysis of PRMT5-CREB interaction in prostate cancer cells. PC-3 cells were co-transfected with the indicated plasmids (0.25 μg for each) using FuGENE6 and the representative images were acquired 24 h after transfection. The results indicate that PRMT5 and CREB primarily interact in the cytoplasm. **C**. PRMT5 regulates IR-induced CREB activation. LNCaP cells were first transfected with plasmids encoding a scrambled control (SC) or the plasmid encoding PRMT5 shRNAs (KD#1 or KD#2) for 24 h and then subjected to fractionated IR of 10 Gy (2 Gy/day). Total cell lysate (~40 μg) was used for immunoblotting analysis of PRMT5 and phosphorylated CREB (pCREB). β-actin was used as a loading control.

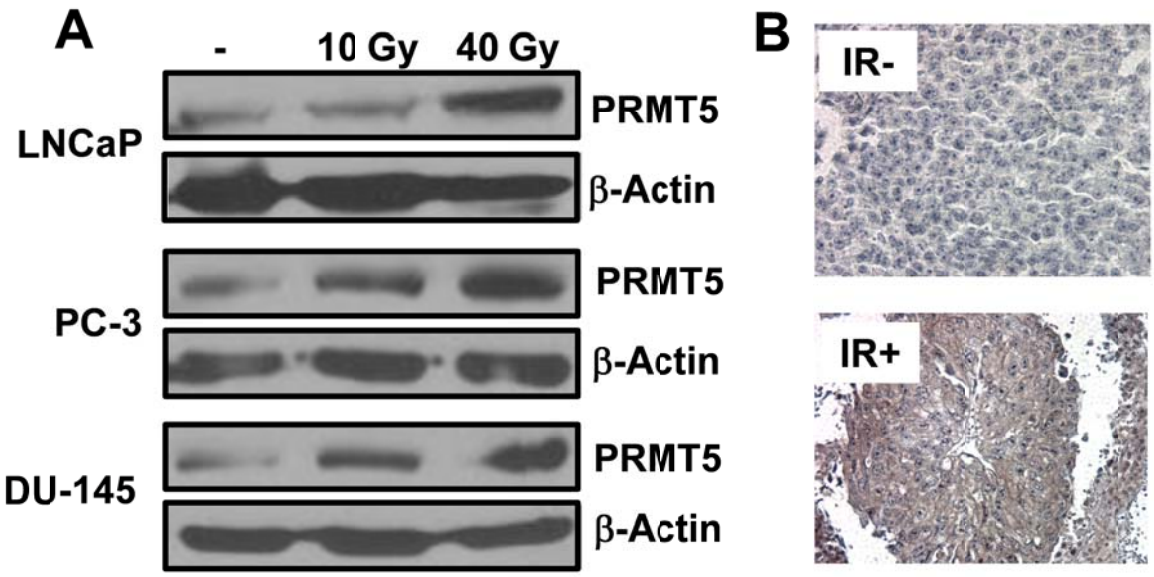

Figure 9. Ionizing radiation induces PRMT5 expression in prostate cancer cells *in vitro and in vivo.* **A**. The indicated prostate cancer cells were irradiated with the indicated fractionated dose (2 Gy/day, 5 days/week), and harvested for Western blotting analysis of PRMT5. **B**. Immunohistochemical analysis of PRMT5 expression in LNCaP xenograft tumors in nude mice without (IR-) or with 40 Gy of fractionated IR (IR+).

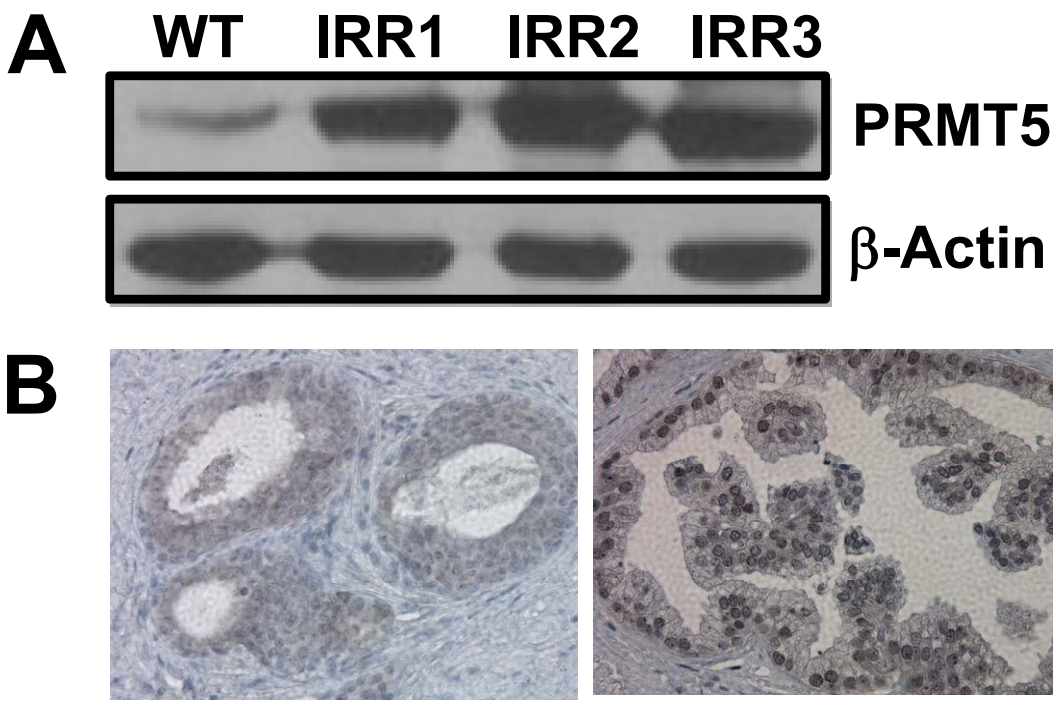

Figure 10 Higher expression of PRMT5 in recurrent radiation-resistant LNCaP sublines and in recurrent human prostate cancer tissues. A. Expression of PRMT5 in parental LNCaP (WT) and its derived sublines regrown from survived cells after 40 Gy of fractionated ionizing radiation. **B**. Expression of PRMT5 in recurrent prostate cancer tissues after radiotherapy failure.

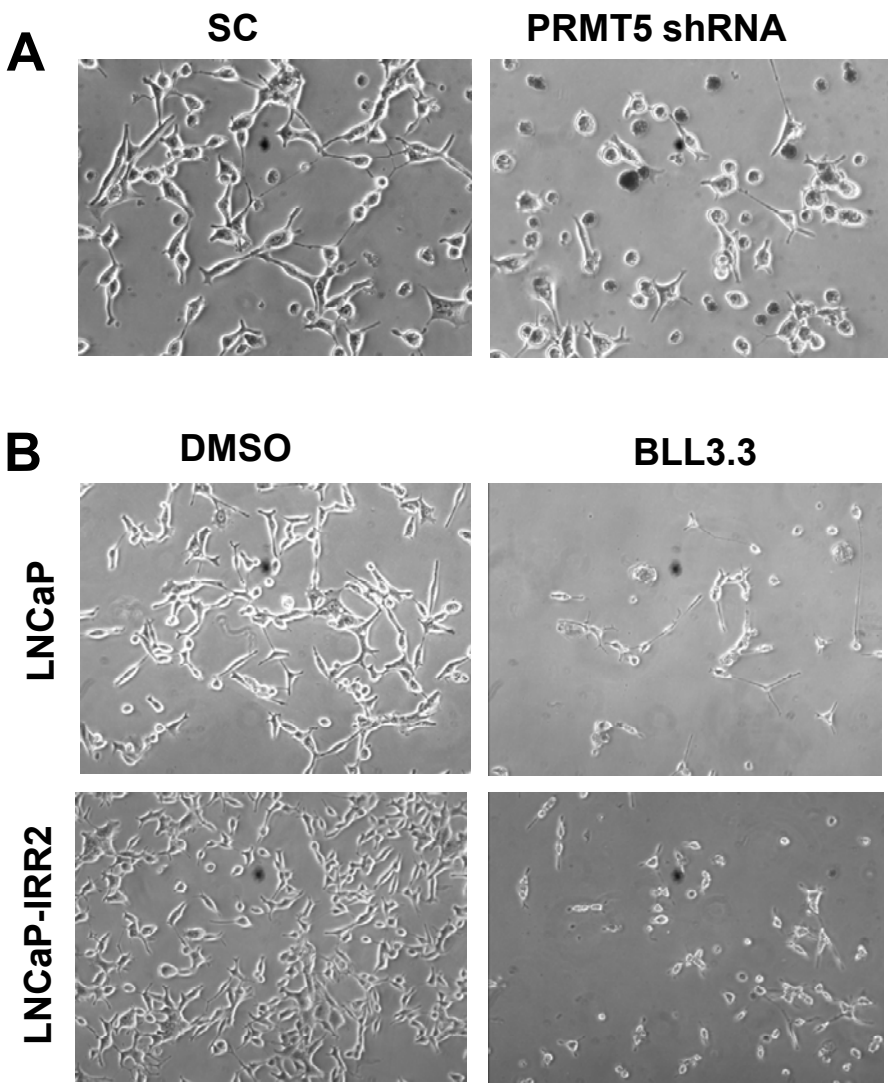

Figure 11. Knockdown or inhibition of PRM T5 increases IR-induced cell death. **A**. LNCaP cells were first transfected with the scrambled control (SC) or PRMT5 shRNA constructs for one day, a nd then subjected to 10 Gy of fractionated I R (2 Gy/day). Shown are the representative images acquired aft er 10 Gy o f IR. **B.** LNCaP or its derived radiation-resistant subline IRR2 were treated similarly fractionated with 10 Gy of IR in the presence of DMSO or a PRMT5 sp ecific inhibitor BLL3.3 (10 μM). Similar results were obtained with IRR1 and IRR3 radiation-resistant sublines.

Table 1. ATF2 Interacting Proteins Identified by Mass Spectrometry

Accession	List of ATF2 Interacting Proteins Identified by MS	Score	Coverage
IPI00021338.2	Dihydrolipoyllysine-residue acetyltransferase component of pyruva	46.77	27.67
IPI00798351.1	35 kDa protein	39.79	41.01
IPI00001639.2	Importin subunit beta-1	34.37	13.47
IPI00220327.4	Keratin, type II cytoskeletal 1	30.51	17.39
IPI00306301.2	Mitochondrial PDHA1	30.41	35.75
IPI00909140.6	Tubulin beta chain	29.00	22.97
IPI00292059.2	Nuclear pore complex protein Nup153	25.83	8.20
IPI00009865.4	Keratin, type I cytoskeletal 10	22.01	12.50
IPI00922178.1	Isoform 5 of Shootin-1	17.02	13.49
IPI00002214.1	Importin subunit alpha-2	16.70	14.56
IPI00913991.1	pyruvate dehydrogenase complex, component X isoform 2	15.47	12.55
IPI00793930.1	TUBA1B protein	15.23	17.91
IPI00220834.8	ATP-dependent DNA helicase 2 subunit 2	13.91	12.84
IPI00170581.1	nucleoporin 50kDa isoform a	13.82	10.68
IPI00554711.3	Junction plakoglobin	11.91	8.86
IPI00384697.2	Isoform 2 of Serum albumin	11.69	8.87
IPI00795303.2	cDNA FLJ50996, highly similar to 60S ribosomal protein L4	11.58	11.11
IPI00288941.1	Nuclear receptor coactivator 5	11.42	10.54
IPI00945454.1	21 kDa protein	11.28	29.61
IPI00384575.1	cDNA FLJ25836 fis, clone TST08317	10.22	16.55
IPI00655812.1	Rhabdomyosarcoma antigen MU-RMS-40.12	10.05	7.39
IPI00893179.1	X-ray repair complementing defective repair in Chinese hamster ce	9.68	3.95
IPI00153051.5	Isoform 1 of Poly(A) RNA polymerase, mitochondrial	9.03	6.70
IPI00216730.3	Histone H2A type 2-B	8.76	23.08
IPI00017297.1	Matrin-3	8.61	5.43
IPI00012578.1	Importin subunit alpha-4	8.30	6.72
IPI00916767.1	Putative uncharacterized protein ATF2	8.30	13.62
IPI00954209.1	Putative uncharacterized protein HSPD1	8.07	36.21
IPI00021304.1	Keratin, type II cytoskeletal 2 epidermal	7.91	3.72
IPI00922744.1	Complement protein C4B frameshift mutant (Fragment)	7.51	10.45
IPI00018971.8	52 kDa Ro protein	7.10	6.74
IPI00786995.1	similar to protein kinase, DNA-activated, catalytic polypeptide	6.70	0.73
IPI00013485.3	40S ribosomal protein S2	6.66	8.53
IPI00013296.3	40S ribosomal protein S18	6.59	13.82
IPI00909143.1	Dihydrolipoyl dehydrogenase	5.25	4.12
IPI00402184.4	Isoform 4 of Heterogeneous nuclear ribonucleoprotein Q	4.99	3.98
IPI00916763.1	Putative uncharacterized protein HSPE1	4.97	13.86
IPI00879086.1	Putative uncharacterized protein KLHL22	4.54	7.11
IPI00477179.1	Isoform 2 of Nucleolar RNA helicase 2	4.44	3.08
IPI00816063.1	Isoform 2 of 60S ribosomal protein L12	4.38	12.12
IPI00916896.1	Putative uncharacterized protein RBM14	4.35	12.40
IPI00916188.1	Putative uncharacterized protein NCL	4.29	7.41
IPI00028931.2	Desmoglein-2	4.25	1.61
IPI00797941.2	cDNA FLJ57770, moderately similar to ADP-ribosylation factor 3	4.23	12.50
IPI00645459.1	Isoform 3 of ATPase WRNIP1	4.23	2.70
IPI00642454.1	Ribosomal protein L7a	4.20	8.61
IPI00008527.3	60S acidic ribosomal protein P1	4.19	14.04
IPI00003935.6	Histone H2B type 2-E	4.12	11.90
IPI00008433.4	40S ribosomal protein S5	4.00	7.35
IPI00940164.1	Putative uncharacterized protein ENSP00000412264 (Fragment)	3.99	9.63
IPI00173589.2	17 kDa protein	3.87	9.68
IPI00096899.7	DNA replication factor Cdt1	3.77	3.11
IPI00930144.1	Histone H2A	3.76	17.12
IPI00745302.1	Isoform 2 of Serine/threonine-protein kinase Nek11	3.74	5.32

Table 1. ATF2 Interacting Proteins Identified by Mass Spectrometry

IPI00029629.3	E3 ubiquitin/ISG15 ligase TRIM25	3.62	2.86
IPI00791342.1	13 kDa protein	3.59	10.71
IPI00549561.3	Isoform 2 of BTB/POZ domain-containing protein KCTD15	3.58	7.69
IPI00382804.1	EEF1A protein (Fragment)	3.56	4.85
IPI00894365.2	cDNA FLJ52842, highly similar to Actin, cytoplasmic 1	3.49	6.55
IPI00479058.2	40S ribosomal protein S15	3.48	13.10
IPI00935432.1	similar to ubiquitin protein ligase E3 component n-recognin 5 isofo	3.47	0.97
IPI00794267.1	18 kDa protein	3.46	7.19
IPI00555902.1	Isoform 1 of OCIA domain-containing protein 2	3.46	8.44
IPI00329389.8	60S ribosomal protein L6	3.44	6.94
IPI00744535.2	ATF7 protein	3.44	17.95
IPI00793271.1	12 kDa protein	3.43	11.93
IPI00003362.2	HSPA5 protein	3.43	2.29
IPI00187140.1	Putative 40S ribosomal protein S26-like 1	3.37	10.43
IPI00747764.3	cDNA FLJ53229, highly similar to Importin alpha-7 subunit	3.35	3.88
IPI00658013.1	nucleophosmin 1 isoform 3	3.32	8.11
IPI00718829.2	Isoform 2 of Protein-L-isoaspartate O-methyltransferase domain-c	3.30	7.66
IPI00217465.5	Histone H1.2	3.30	6.10
IPI00028954.1	80 kDa MCM3-associated protein	3.29	1.46
IPI00019359.4	Keratin, type I cytoskeletal 9	3.29	2.25
IPI00922330.1	Putative uncharacterized protein	3.29	15.66
IPI00829737.1	Isoform 2 of Zinc finger protein 658	3.29	3.40
IPI00885004.1	Isoform 2 of Xin actin-binding repeat-containing protein 2	3.28	0.66
IPI00464990.1	Isoform 2 of Platelet glycoprotein Ib beta chain	3.28	5.11
IPI00008965.1	Transcription factor AP-1	3.26	4.23
IPI00909383.1	cDNA FLJ56021, highly similar to Bifunctional aminoacyl-tRNA syn	3.22	2.53
IPI00941764.1	Ribophorin II	3.22	7.19
IPI00026781.3	Fatty acid synthase	3.21	1.04
IPI00939811.1	Ribosomal protein S3	3.18	8.60
IPI00916308.1	Putative uncharacterized protein FAM128A	3.14	17.11
IPI00453473.6	Histone H4	3.09	9.71

THE INTERPLAY OF CREB AND ATF2 IN REGULATING IONIZING RADIATION-INDUCED NEUROENDOCRINE DIFFERENTIATION IN PROSTATE CANCER CELLS

Xuehong Deng[1], Han Liu[1], Jiaoti Huang[2], Liang Cheng[3], Evan T. Keller[4], Sarah J. Parsons[5], and Chang-Deng Hu[1]

[1]Department of Medicinal Chemistry & Molecular Pharmacology, Purdue University; [2]Department of Pathology, University of Rochester Medical Center; [3]Department of Pathology and Laboratory Medicine, Indiana University School of Medicine; [4]Department of Urology, University of Michigan; [5]Department of Microbiology, University of Virginia Health System.

Radiation therapy is a first line treatment for prostate cancer patients with localized tumors. Although most patients respond well to the treatment, approximately 10-60% of prostate cancer patients experience recurrent tumors. However, the molecular mechanisms underlying tumor recurrence remain largely unknown. Here we show that ionizing radiation (IR) induces transdifferentiation of LNCaP prostate cancer cells into neuroendocrine (NE)-like cells, which are known to be implicated in prostate cancer progression, androgen independent growth and poor prognosis. Further analyses reveal that two CRE-binding transcription factors CREB and ATF2 play opposing roles in NE-like transdifferentiation, and that IR induces NE-like transdifferentiation by increasing nuclear content of phospho-CREB and impairing nuclear import of ATF2, a favorable ratio of pCREB over ATF2 in the nucleus for neuroendocrine differentiation. The IR-induced NE-like cells are reversible, and three IR-resistant clones isolated from dedifferentiated cells have acquired the ability to proliferate, but respond poorly to IR- and androgen depletion treatment in terms of NE-like redifferentiation. Significantly, these clones are cross-resistant to IR, chemotherapy, and androgen depletion treatments. These results suggest that radiotherapy-induced NE-like transdifferentiation represents a novel pathway by which prostate cancer cells survive the treatment and contribute to tumor recurrence.

Prostate Cancer: Basic Research III

Moderated Poster 10

Sunday, May 30, 2010 **1:00 PM-3:00 PM**

373
BIOLOGICAL EFFECTS OF FETAL EXPOSURE TO BISPHENOL A ON UROGENITAL SINUS

Kenichiro Ishii, Shigeki Arase, Yuko Yoshio, Tsu, Japan; Katsuhide Igarashi, Kenichi Aisaki, Tokyo, Japan; Yasuhide Hori, Kohei Nishikawa, Norihito Soga, Hideaki Kise, Kiminobu Arima, Tsu, Japan; Jun Kanno, Tokyo, Japan; Yoshiki Sugimura, Tsu, Japan*

INTRODUCTION AND OBJECTIVES: In prostate, both androgens and estrogens play a significant role in development and differentiation. Since the balance of these hormones is quite important, even small changes in the levels of estrogens including estrogen-mimicking chemicals can lead to serious changes. Bisphenol A (BPA), one of endocrine disrupting chemicals (EDCs), is well known as a widespread estrogenic chemical. The problem is that BPA has been detected in fetal plasma, implicating in development of toxicity in the fetus. In this study, to investigate the effects of fetal exposure to BPA on prostatic development, we first evaluated the morphological changes of BPA-treated mouse urogenital sinus (UGS). Next, we examined the changes of in situ hormonal environment in BPA-treated UGS.

METHODS: From GD13 to GD16, pregnant female C57BL/6 mice were treated with BPA (20 ug/kg/day) or synthetic estrogen diethylstilbestrol (DES, 0.2 ug/kg/day) by oral gavage. On E17-P1 and P5, male UGS were assembled. The E2 level and aromatase activity in UGS were determined by liquid chromatography-tandem mass spectrometry and the tritiated water release assay, respectively.

RESULTS: In both BPA- and DES-treated UGS, the number of basal epithelial cells in the primary ducts of dorsolateral prostate was approximately twice as compared with control. The mRNAs of EGF, TGF-alpha, and FGF-7 but not IGF-I were up-regulated. In organ culture analysis, the number of basal epithelial cells was significantly increased in EGF- or TGF-alpha-treated fetal mouse UGS. In analyses of in situ hormonal environment, the E2 level and aromatase activity were significantly increased only in BPA-treated UGS. The mRNA up-regulations of Cyp19a1 (aromatase), Cyp11a1, and Ad4BP/SF-1 were observed. The number of aromatase-positive stromal cells in BPA-treated UGS was approximately twice as compared with control.

CONCLUSIONS: Alteration of in situ hormonal environment in UGS may be responsible for prostatic anomalies associated with fetal exposure to EDCs. We demonstrated that BPA had unique action in addition to the common action to estrogen receptor. The common action was the increased number of basal epithelial cells similar to DES treatment, by a suggest mechanism via cellular EGFR signals. On the other hand, the unique action was the increases of in situ E2 level and aromatase activity observed only in BPA treatment. Our data suggested that BPA might interact with in situ steroidogeneis by altering tissue component, e.g., accumulation of aromtase-expressed stromal cells, in particular organs.

Source of Funding: Grants-in Aid from the Ministry of Health, Labour and Welfare, Japan

374
ANDROGEN DEPRIVATION UP REGULATES EXPRESSION OF STEM CELL AND NEUROENDOCRINE MARKERS IN PROSTATE CANCER CELLS IN VITRO AND IN VIVO

Markus Germann, Marco G. Cecchini, Antoinette Wetterwald, Urs E. Studer, George N. Thalmann, Bern, Switzerland*

INTRODUCTION AND OBJECTIVES: To evaluate changes in expression of genes related to tumor progression and the cancer stem cell concept in response to androgen deprivation (AD) in different in vitro and in vivo models of castration resistant prostate cancer.

METHODS: LNCaP, LNCaP-Bic, C4-2 and C4-2B4 cell lines were used for in vitro experiments. Gene specific mRNA expression was measured by RT-PCR and compared to the parental LNCaP cells. Tumors of the androgen dependent CaP xenograft model BM18 show an almost complete regression after castration of tumor bearing mice. Tumor growth can be reinitiated even months after castration by re-administration of testosterone. After tumor regression only very small clusters of residual epithelial cells can be observed. To investigate the nature of these cells, BM18 tumors were harvested before castration (intact), 14 days after castration (regressed) or 3 days after testosterone readministration to regressed tumors and tested gene specific mRNA expression.

RESULTS: Overall AD induced expression of proliferation and anti-apoptotic genes as well as the putative stem/progenitor cell markers á2-integrin, Oct4, Nanog, Nestin and Sca1 in all LNCaP derived cell lines in vitro. In vivo, compared to intact BM18 tumors, regressed tumors show a significant higher expression of Bcl2 together with a 10-20 fold higher expression of the self-renewal markers Oct4, Sox2 and Nanog. Regressed tumors express low PSA mRNA levels but maintain high expression of markers of luminal cell differentiation (AR, CK18 and PSP94). Furthermore, regressed tumors show a 40-1000 fold increased expression of markers of neuroendocrine differentiation (Chromogranin A, Synaptophysin, Enolase 2 and Nestin). Interestingly, 3 days after testosterone readministration, relapsed tumors show at least partial reversal of these alterations in gene expression. These results were confirmed in the cell lines in vitro.

CONCLUSIONS: AD up regulates stem/progenitor and neuroendocrine cell markers, as well as markers of proliferative potential, self-renewal and inhibition of apoptosis in LNCaP cells in vitro and in BM18 tumors in vivo suggesting the outgrowth of a more malignant phenotype with stem cell properties by AD leading to castration resistance.

Source of Funding: None

375
RADIATION INDUCES NEUROENDOCRINE DIFFERENTIATION OF PROSTATE CANCER CELL LINES IN VITRO AND IN VIVO

Chang-Deng Hu, Bennett Elzey, Jean Poulson, Wallace Morrison, Xuehong Deng, Sandra Torregrosa-Allen, Timothy Ratliff, West Lafayette, IN*

INTRODUCTION AND OBJECTIVES: Although localized prostate cancer (PCa) can be cured by radiotherapy, approximately 30-60% of patients with high grade tumors will experience recurrence. However, the molecular mechanisms underlying tumor recurrence remain largely unknown. Accumulated evidence suggests that an increased number of neuroendocrine (NE) cells in PCa correlates with disease progression and poor prognosis. The objective of this study was to test if radiation induces neuroendocrine differentiation (NED) *in vitro* and *in vivo*.

METHODS: Prostate cancer cell lines were subjected to ionizing radiation (IR) according to clinical radiotherapy protocol (Co-60 photons, 2 Gy/day, 5 days/week for 7 weeks; total dose 70 Gy) and NED was determined based on morphological changes and the induction of NE markers chromogranin A (CgA) and neuron-specific enolase (NSE). To determine the effect of radiation on NED of prostate cancer cells *in vivo*, LNCaP cells were implanted subcutaneously in the hind legs of nude mice. Upon reaching 100-200 mm^3, LNCaP tumor-xenografts were irradiated (6-MV X-rays, 5 Gy, twice weekly for 4 weeks; total dose 40 Gy). NED was determined based on the increase of serum CgA levels and increased expression of CgA in irradiated tumor tissues.

RESULTS: We previously reported that IR can induce NED in LNCaP cells. In the present study, we extended our finding to several other cell lines and confirmed that IR does induce neurite extension and the expression of CgA and NSE in DU-145, PC-3 and VCaP cell lines *in vitro*. We also found that radiation increased serum CgA levels in 4

out of 5 mice bearing LNCaP xenografts. Immunofluorescence analysis confirmed that irradiated tumors had higher expression of CgA when compared to non-irradiated tumors.

CONCLUSIONS: Radiation can induce NED in several prostate cancer cell lines and in LNCaP xenograft nude mouse models. These findings suggest that radiotherapy may induce NED in PCa patients and warrant a clinical evaluation of radiotherapy-induced NED in PCa patients.

Source of Funding: This worked was supported by Purdue University Center for Cancer Research Small Grants Program and the U.S. Army Medical Research Acquisition Activity, Prostate Cancer Research Program grant (PC073098).

376

HEDGEHOG/GLI SUPPORTS ANDROGEN SIGNALING IN ANDROGEN DEPRIVED AND ANDROGEN INDEPENDENT PROSTATE CANCER CELLS

Mengqian Chen, Elina Levina, Matthew Tanner, Albany, NY; Alexandre de la Taille, Francis Vacherot, Stephane Terry, Creteil, France; Ralph Buttyan, Albany, NY*

INTRODUCTION AND OBJECTIVES: Hedgehog (Hh) is a developmental cell signaling pathway that regulates Gli-mediated transcription. Previously we showed that androgen deprivation induces expression of Hh ligands and awakens autocrine Hh signaling in prostate cancer cells. Here we evaluated the effect of inhibitors of autocrine Hh or of hyperactive Gli on androgen signaling activity and cell growth in androgen deprived (AD) and androgen independent (AI) prostate cancer cells.

METHODS: LNCaP and AI variants (LNCaP-AI, C4-2B or LN3) or VCaP cells were cultured in androgen-free medium in the presence or absence of the Hh inhibitor, cyclopamine. Smoothened (Smo) siRNA was transfected into cells to mimic cyclopamine action. Gli1 and Gli2 expression vectors were transfected into LNCaP cells to mimic hyperactivity of Hh. Expression of androgen regulated genes were evaluated by real-time reverse-transcriptase PCR (qPCR). Luciferase (luc) reporter vectors promoted by the androgen-responsive probasin (PRB) or PGC gene promoters were transfected into cells to serve as a surrogate marker of AR activity. Cell growth was measured by cell counting and by a WST-assay. Human 293-FT cells were co-transfected with AR and myc-tagged Gli2 to identify interaction between AR and Gli2 by co-immunoprecipitation with anti-AR or anti-myc antibodies.

RESULTS: Cyclopamine treatment dose-dependently downregulated expression of KLK2, KLK3 and PGC and upregulated androgen-repressed SHH expression in all cell lines. Cyclopamine also downregulated expression of luc from PRB or PGC promoters. These responses were mimicked by Smo but not by control siRNAs. Gli1 and Gli2 overexpression in LNCaP cells upregulated KLK2, KLK3 and PGC expression in a bicalutamide-independent manner. Gli1 and Gli2 overexpression also confered AI growth on LNCaP cells. Gli2 co-immunoprecipitates with AR from 293-FT cell extracts.

CONCLUSIONS: Inhibition of autocrine Hh suppressed residual androgen signaling in AD and AI prostate cancer cells and blocked AI growth. Overexpression of Gli increased residual androgen signaling and conferred AI growth. We conclude that autocrine Hh signaling supports androgen action under low/no androgen conditions. Gli2 protein interacts with AR and this interaction might represent the point of cross-talk between Hh and androgen signaling in prostate cancer.

Source of Funding: NCI RO1-CA111618; DOD W81XWH-06

377

WHAT CAN THE HAIR FOLLICLES AND SALIVARY GLANDS TELL US ABOUT THE OXIDATIVE STRESS STATUS OF THE PROSTATE? A PRECLINICAL STEP TOWARDS INDIVIDUALIZATION OF PROSTATE CANCER PREVENTION STRATEGIES

Kaitlyn Whelan, Jian Ping Lu, Edduard Fridman, Jehonathan Pinthus, Hamilton, Canada*

INTRODUCTION AND OBJECTIVES: Oxidative stress (OS) is a key event in the development of prostate cancer (PC). Prostatic OS is influenced by androgenic stimulation and by the expression/activity of anti-oxidative and stress molecules in a setting that is unique for each individual. Negative results from the recent SELECT study may relate in part to generalization of the prevention protocol. Surrogate markers that can predict the individual's oxidative status can complement a more rationalized selection of candidates for PC prevention. We opted to determine if the individual's prostatic OS status can be determined by examining OS in surrogate androgen regulated tissues from the same host.

METHODS: Adult male rats were divided equally into three groups: (A-) underwent bilateral orchiectomy (lack of endogenous/exogenous androgens), (A+) received continues testosterone supplementation (endogenous + exogenous androgens) and (C) left intact (eugonadal). Serum testosterone levels were determined after 72hrs and the prostate, salivary glands and dermal papillary cells (DPC) of the hair follicles from each animal were harvested and examined for the expression of 8-OHdG (OS marker), and the OS adaptation molecules; catalase and clustrin by immunostaining and immunoblotting. Staining intensity was graded blindly by two pathologists. Statistical analysis was completed using two-tail t-test. Normally distributed data were analyzed using ANOVA model. When needed, Box-Cox transformation was used to reach normality.

RESULTS: OS intensity and the expression of catalase and clusterin directly correlated with testosterone levels in all three target tissues; prostate ($p=0.001$), salivary glands ($p=0.007$) and DPC ($p=0.005$). Although different levels of prostatic OS were noted in-between rats with similar serum testosterone levels, there were no inter-individual differences between the OS status of the prostate, salivary glands and DPC ($p>0.01$).

CONCLUSIONS: The intensity of prostatic OS and the expression of OS adaptation molecules are individually influenced by androgens in a mode mirrored by other androgen regulated tissues. One needs to examine the OS at the tissue level as serum levels of testosterone alone can not predict the OS status within these androgen regulated tissues. Clinical studies are needed to validate these findings in humans and their potential prognostic implication in the individualization of PC prevention and therapeutics.

Source of Funding: SELF

378

STROMA REACTION IN MOUSE XENOGRAFT MODELS OF PROSTATE CANCER BONE METASTASIS

Berna Özdemir, Chiara Secondini, Ruth Schwaninger, Antoinette Wetterwald, Bern, Switzerland; Mauro Delorenzi, Lausanne, Switzerland; Marco G. Cecchini, George N. Thalmann, Bern, Switzerland*

INTRODUCTION AND OBJECTIVES: We present an experimental method of global gene expression analysis of stromal-epithelial interaction in cancer in bulk tissue specimens able to dissect the cancer cell-specific from the stromal cell-specific transcriptome induced by the stromal-epithelial interaction based on species-specific (mouse and human, respectively) cDNA gene arrays.

METHODS: The human osteoinductive prostate cancer (PC) cell line C4-2B4 was xenografted into the tibia of SCID mice. RNA was extracted from the radiologically confirmed tumour bearing bone shaft. Intact bone served as "mouse-only" control, and from cultured C4-2B4

Abstract for 2011 IMPaCT Meeting

Radiation induces neuroendocrine differentiation of prostate cancer cells *in vitro* and *in vivo:* Implications for prostate cancer radiotherapy

Chang-Deng Hu, Xuehong Deng, Christopher Suarez, Bennett D. Elzey, Jean M. Poulson, Wallace B. Morrison, Sandra Torregrosa-Allen, Jiaoti Huang, Liang Cheng, Evan T. Keller, Sarah J. Parsons, Timothy L. Ratliff

Background and Objectives: Although localized prostate cancer (PCa) can be cured by radiotherapy, approximately 30-60% of patients with high grade tumors experience biochemical recurrence within five years. However, the molecular mechanisms underlying tumor recurrence remain largely unknown. Accumulated evidence suggests that an increased number of neuroendocrine (NE)-like cells in PCa correlates with disease progression and poor prognosis. The objective of this award is to determine the role of two transcription factors ATF2 and CREB in radiation-induced neuroendocrine differentiation (NED) and to identify signaling pathways for development of targeted therapy.

Methods: Prostate cancer cell lines were subjected to ionizing radiation (IR) according to clinical radiotherapy protocol (Co-60 photons, 2 Gy/day, 5 days/week for 7 weeks; total dose 70 Gy) and NED was determined based on morphological changes and the induction of NE markers chromogranin A (CgA) and neuron-specific enolase (NSE). To determine the effect of radiation on NED of prostate cancer cells *in vivo*, LNCaP cells were implanted subcutaneously in the hind legs of nude mice. Upon reaching 100-200 mm^3, LNCaP tumor-xenografts were irradiated (6-MV X-rays, 5 Gy, twice weekly for 4 weeks; total dose 40 Gy). NED was determined based on the increase of serum CgA levels and increased expression of CgA in irradiated tumor tissues. To study the role of ATF2 and CREB in radiation-induced NED, the expression and activation of these transcription factors were analyzed using cell lysates from irradiated cells or using tissues from irradiated xenograft tumors. Furthermore, constitutive active or dominant negative mutants of ATF2 and CREB were stably expressed in prostate cancer cells and their impact on radiation-induced NED was assessed.

Results to date: Under the support of the PCRP Idea Development Award, we have accomplished the followings. (1) Radiation induces NED in several prostate cancer cell lines including LNCaP, DU-145, PC-3 and VCaP to various degrees. (2) Radiation induces NED in LNCaP xenografts in nude mice and elevates serum CgA levels. (3) ATF2 acts as a transcriptional repressor of NED whereas CREB functions as a transcriptional activator of NED. (4) Radiation induces cytoplasmic sequestration of ATF2 and increases phosphorylation of CREB at S133 in the nucleus. (5) Expression of a constitutively nuclear-localized ATF2 can inhibit radiation-induced NED. (6) Expression of several dominant negative CREB or CREB knockdown can inhibit radiation-induced NED. (7) Preliminary screen of upstream protein

kinases has identified PKA and CaMKII as potential protein kinases that may mediate radiation-induced CREB activation and NED.

Conclusions: We have demonstrated that radiation-induced NED is a general response in prostate cancer cells *in vitro* and *in vivo*. Furthermore, we have identified CREB, ATF2, PKA and CaMKII as signaling molecules that regulate radiation-induced NED.

Impact: Preliminary studies of radiation-induced NED using *in vitro* and *in vivo* models have demonstrated that radiation can induce NED in prostate cancer cells. The identified signaling molecules and possible signaling pathways that mediate radiation-induced NED are promising molecular targets for development of novel NED-based targeted therapy. Current effort is focused on the clinical evaluation of our findings.

Abstract for 2011 SBUR Fall Symposium

TARGETING RADIATION−INDUCED NEUROENDOCRINE DIFFERENTIATION AS A NOVEL RADIOSENSITIZATION APPROACH FOR PROSTATE CANCER RADIOTHERAPY

Chang−Deng Hu PhD[1], Xuehong Deng BS[1], Christopher Suarez BS[1], Bennett Elzey PhD[1], Jean Poulson DVM, PhD[1], Wallace Morrison DVM, MS[1], Song−Chu Ko MD, PhD[2], Noah Hahn MD[2] and Timothy Ratliff PhD[1]
[1]Purdue University, West Lafayette, Indiana; [2]Indiana University School of Medicine, Indianapolis, Indiana

Introduction: Although the majority of localized low−risk prostate cancer (PCa) can be cured by radiotherapy, approximately 30−60% of patients with high−risk PCa experience biochemical recurrence within five years. Our recent evidence suggests that upon 4−week irradiation, fractionated ionizing radiation (IR) can induce neuroendocrine differentiation (NED) in prostate cancer cells, a phenotypic change implicated in prostate cancer progression. Interestingly, IR−induced NED involves two distinct phases: the selection of radioresistant cells during the first two weeks and the differentiation during the last two weeks. Molecular analysis demonstrated that the transcription factor cAMP response element−binding (CREB) is involved in both phases. The objective of our research is to determine whether targeting radiation−induced NED can be explored as a novel radiosensitization approach.
Methods: Since CREB is involved in both phases during the course of NED, we employed two CREB targeting approaches to test our hypothesis. First, we established stable cell lines that can inducibly express A−CREB, a dominant negative mutant of CREB, to compete with endogenous CREB for function. Second, we established stable cell lines that can inducibly express CREB short−hairpin RNAs to knockdown CREB. Expression of A−CREB or CREB knockdown was induced at different times while subjecting LNCaP cells to fractionated IR (2 Gy/day, 5 days/week). MTT assays, flow cytometery and morphological analysis were employed to assess the impact of CREB targeting on cell viability and IR−induced NED.
Results: We observed that expression of A−CREB significantly sensitized LNCaP cells to IR during the first two weeks. We also observed that CREB knockdown during the second phase only was sufficient to inhibit IR−induced neurite outgrowth and sensitize cells to radiation.
Conclusions: Based on recent findings that IR can induce NED in multiple prostate cancer cell lines in vitro, in LNCaP xenograft tumors, and in a subset of human prostate cancer patients, we conclude that targeting IR−induced NED can be utilized as a novel radiosensitization approach.
Funding provided by Department of Defense PCRP Idea Development Award.

Ionizing Radiation Induces Prostate Cancer Neuroendocrine Differentiation through Interplay of CREB and ATF2: Implications for Disease Progression

Xuehong Deng,[1] Han Liu,[1] Jiaoti Huang,[2] Liang Cheng,[3] Evan T. Keller,[4] Sarah J. Parsons,[5] and Chang-Deng Hu[1]

[1]Department of Medicinal Chemistry and Molecular Pharmacology and the Purdue Cancer Center, Purdue University, West Lafayette, Indiana; [2]Department of Pathology, University of Rochester Medical Center, Rochester, New York; [3]Department of Pathology and Laboratory Medicine, Indiana University School of Medicine, Indianapolis, Indiana; [4]Department of Urology, University of Michigan, Ann Arbor, Michigan; and [5]Department of Microbiology, University of Virginia Health System, Charlottesville, Virginia

Abstract

Radiation therapy is a first-line treatment for prostate cancer patients with localized tumors. Although some patients respond well to the treatment, ~10% of low-risk and up to 60% of high-risk prostate cancer patients experience recurrent tumors. However, the molecular mechanisms underlying tumor recurrence remain largely unknown. Here we show that fractionated ionizing radiation (IR) induces differentiation of LNCaP prostate cancer cells into neuroendocrine (NE)-like cells, which are known to be implicated in prostate cancer progression, androgen-independent growth, and poor prognosis. Further analyses revealed that two cyclic AMP–responsive element binding transcription factors, cyclic AMP–response element binding protein (CREB) and activating transcription factor 2 (ATF2), function as a transcriptional activator and a repressor, respectively, of NE-like differentiation and that IR induces NE-like differentiation by increasing the nuclear content of phospho-CREB and cytoplasmic accumulation of ATF2. Consistent with this notion, stable expression of a non-phosphorylatable CREB or a constitutively nuclear-localized ATF2 in LNCaP cells inhibits IR-induced NE-like differentiation. IR-induced NE-like morphologies are reversible, and three IR-resistant clones isolated from dedifferentiated cells have acquired the ability to proliferate and lost the NE-like cell properties. In addition, these three IR-resistant clones exhibit differential responses to IR- and androgen depletion–induced NE-like differentiation. However, they are all resistant to cell death induced by IR and the chemotherapeutic agent docetaxel and to androgen depletion–induced growth inhibition. These results suggest that radiation therapy–induced NE-like differentiation may represent a novel pathway by which prostate cancer cells survive the treatment and contribute to tumor recurrence. [Cancer Res 2008;68(23):9663–70]

Introduction

Radiation therapy is a first-line treatment for prostate cancer. Although some patients with localized tumors respond well to the treatment (1), ~10% of low-risk and up to 60% of high-risk prostate cancer patients experience recurrent tumors (2). However, the molecular mechanisms underlying tumor recurrence remain largely unknown.

Neuroendocrine (NE) cells are one of three types of epithelial cells in the human prostate and are present in 30% to 100% cases of prostatic adenocarcinoma (3, 4). Although the physiologic role of NE cells remains unclear, increased numbers of NE-like cells seem to be associated with prostate cancer progression, androgen-independent growth, and poor prognosis (5, 6). Interestingly, androgen ablation, cytokines such as interleukin 6 (IL-6), and agents that elevate the intracellular levels of cyclic AMP (cAMP) can induce NE-like differentiation (NED) in LNCaP prostate cancer cells by activating several distinct signaling pathways (5, 6). Like NE cells, the differentiated NE-like cells also produce a number of neuropeptides that facilitate the growth of surrounding tumor cells in a paracrine manner (5–7). They are generally androgen receptor negative (8, 9), highly resistant to apoptosis (10, 11), and their differentiation state is reversible (12). Thus, NE-like cells may survive in a dormant state and contribute to prostate cancer recurrence on dedifferentiation (12).

cAMP response element binding protein (CREB) belongs to the basic region leucine zipper (bZIP) family of transcription factors (13–15). It functions as a homodimer or heterodimer to bind a specific DNA sequence, the cAMP responsive element (16), to regulate transcription of target genes responsible for many cellular processes including cell proliferation and differentiation (15). CREB is implicated in prostate cancer growth (17), acquisition of androgen-independent growth (18), and transcription of chromogranin A (CgA; ref. 19) and prostate-specific antigen (20). Although it is known that CREB is activated by protein kinase A through the phosphorylation at Ser^{133} of CREB1B in response to cAMP (14, 21), whether CREB itself can induce NED remains to be determined.

Activating transcription factor 2 (ATF2) also belongs to the bZIP family of transcription factors (22, 23) and is a member of the activator protein 1 (AP-1; ref. 24). AP-1 activity is required for many cellular processes, and deregulated AP-1 activity is implicated in many cancers including prostate cancer (25). Interestingly, ATF2 and CREB share the same cAMP responsive element sequence and regulate the transcription of cAMP responsive element–containing genes. Whereas some cAMP responsive element–containing target

Note: Supplementary data for this article are available at Cancer Research Online (http://cancerres.aacrjournals.org/).

Requests for reprints: Chang-Deng Hu, Department of Medicinal Chemistry and Molecular Pharmacology, Purdue University, West Lafayette, IN 47907. Phone: 765-496-1971; Fax: 765-494-1414; E-mail: cdhu@pharmacy.purdue.edu.

doi:10.1158/0008-5472.CAN-08-2229

genes are activated by CREB and ATF2 equally or cooperatively (26), differential regulation of other target genes by CREB and ATF2 has also been observed (27–31). Unlike CREB, the role of ATF2 in prostate cancer is little known. A recent study reported that increased cytoplasmic localization of phospho-ATF2 in prostate cancer specimens correlates with the clinical progression of prostate cancer (32), suggesting that alteration of ATF2 subcellular localization may contribute to clinical progression of prostate cancer.

We recently showed that ATF2 is a nucleocytoplasmic shuttling protein and its subcellular localization is regulated by AP-1 dimerization (33). Here we present evidence that ATF2 constantly shuttles between the cytoplasm and nucleus in proliferating LNCaP cells and that fractionated ionizing radiation (IR) induces NED by impairing the nuclear import of ATF2 and increasing the nuclear phospho-CREB at Ser^{133} (pCREB).

Materials and Methods

Plasmid construction. To construct a constitutively activated form of CREB, cDNA encoding residues 413 to 490 of VP16 was amplified by PCR from VP16 (Clontech) and subcloned into pHA-CMV. To make VP16-bCREB fusion proteins, cDNA encoding the bZIP domain of CREB1B (residues 285–314) was amplified by PCR from a human cDNA library and subcloned into pHA-VP16. A flexible glycine spacer ($GGGGSx_4$) was inserted between VP16 and bCREB. For the construction of nuclear-localized ATF2 (nATF2), the sequence encoding a nuclear localization signal (PKKKRKV) from the large T antigen of SV40 (34) was subcloned upstream of ATF2 coding sequences in pFlag-ATF2. pFlag-cATF2 is a deletion mutant of ATF2 in which two nuclear localization signals are deleted (33). Both cytoplasmic-localized ATF2 (cATF2) and nATF2 were expressed as a fusion protein with the fluorescent protein, Venus, in transient transfection experiments. To knock down ATF2, sense and antisense oligos (19-mer) were synthesized and subcloned into pSUPER (OligoEngine). Four short interference RNA (siRNA) constructs were made, and their effect on ATF2 expression in LNCaP cells was verified by transient transfection, followed by immunoblotting of ATF2. One ATF2 siRNA construct targeting the 5′ untranslated region (148–167 of ATF2 mRNA) proved to be the most potent and was used in this work. All plasmids were verified by DNA sequencing.

IR-induced NE-like differentiation. Cells were cultured in 10-cm dishes in RPMI 1640 supplemented with 10% fetal bovine serum (FBS) and antibiotics and were continuously irradiated (2 Gy/d, 5 d/wk) in a GC-220 Co-60 for the indicated times. NE-like cells were visualized by morphologic changes, and the induction of the NE markers, CgA and neuron-specific enolase (NSE), was determined by immunoblotting with anti-CgA and anti-NSE antibodies (Abcam). To determine the effect of CREB-S133A and nATF2 on IR-induced NED, we used a tetracycline-on system (Invitrogen) to establish stable cell lines that inducibly expressed HA-CREB-S133A or Flag-nATF2. The established cell lines were maintained in the presence of selectable markers (zeocin and blasticidin), and 5 μg/mL tetracycline was applied while cells were irradiated as described above. Media were changed twice a week, and antibiotics and tetracycline were added accordingly. Cells that extended neurites longer than two cell bodies were scored as differentiated, and the induction of CgA and NSE was analyzed by immunoblotting and quantified using ImageJ software. Values were normalized to β-actin.

Analysis of ATF2 and CREB subcellular localization. LNCaP cells were fixed in ice-cold 3.7% formaldehyde for 20 min, followed by permeabilization in ice-cold 0.2% Triton X-100 for 5 min. Cells were incubated with anti-ATF2 (c-19; Santa Cruz Biotechnology) overnight, followed by three washes and incubation with the secondary antibody conjugated with Texas red (Jackson ImmunoResearch Laboratories) for 1 h. To stain DNA, 4′,6-diamidino-2-phenylindole (DAPI) was added to the secondary antibody staining reaction at the final concentration of 0.5 μg/mL. Subcelluar localization of ATF2 was examined by microscopic analysis, and fluorescent images were captured using a charge-coupled device camera mounted on a Nikon TE2000 inverted fluorescence microscope with the DAPI and Texas red filters.

For biochemical subcellular fractionation analysis, cytosolic and nuclear fractions were prepared as described before (33). Cytosolic and nuclear fractions were verified by anti–β-tubulin (Sigma) or anti–histone 3 (Abcam), respectively, in immunoblotting assays. The amounts of ATF2, pCREB, and CREB were determined with anti-ATF2, anti-pCREB, and anti-CREB (Cell Signaling) antibodies. The amounts of ATF2 and pCREB in the cytoplasm or nucleus, respectively, relative to total protein were quantified using ImageJ software.

Transient transfection. To evaluate the effect of ATF2 knockdown, mutant ATF2, or mutant CREB on NED, 60% to 80% confluent LNCaP cells cultured in 10-cm dishes were transfected with the indicated plasmids using FuGENE HD (Roche). Transfected cells were examined for morphologic changes and harvested for determination of expression of NE markers CgA and NSE by immunoblotting 6 d after transfection. The induction of CgA and NSE was quantified using ImageJ software and normalized to β-actin.

IR- and androgen depletion–induced NE-like differentiation in IR-resistant clones. To study IR-induced NED in IR-resistant clones, cells were similarly treated as described above for wild-type LNCaP cells. NE-like cells were visualized by morphologic changes, and the induction of NE markers CgA and NSE and the expression of androgen receptor were determined by immunoblotting with anti-CgA, anti-NSE, and anti–androgen receptor (Santa Cruz Biotechnology) antibodies. To determine the response of IR-resistant clones to androgen depletion treatment, cells were cultured in phenol-free RPMI 1640 supplemented with 10% charcoal-dextran–treated FBS (CD-FBS) for 3 wk and similarly assayed for morphologic changes and the induction of NE markers CgA and NSE. Note that although androgen depletion treatment for 1 wk was sufficient to induce neurite outgrowth, the induction of CgA and NSE expression was barely detectable by immunoblotting even for wild-type LNCaP cells.

Cell viability and growth inhibition assay. Wild-type or IR-resistant clones were cultured in 48-well plates and irradiated with fractionated IR (2 Gy/d) or treated with docetaxel (5 nmol/L) or cultured in phenol-free RPMI 1640 supplemented with 10% CD-FBS for the indicated times. Cell viability for IR- and docetaxel-treated cells was determined by a 3-(4,5-dimethylthiazol-2-yl)-2,5-diphenyltetrazolium bromide assay as described previously (33). Because irradiated cells only showed cell death starting from the 2nd week of irradiation, the cell viability of wild-type LNCaP or IR-resistant clones was determined by comparing to cells that had received 10-Gy irradiation. Because wild-type and IR-resistant clones showed different growth rates and because CD-FBS treatment only inhibited cell growth without inducing cell death, cells cultured in normal FBS were used as controls to first calculate the percentage of growth inhibition (percentage of viable cells in CD-FBS over those in normal FBS), which was subsequently used to calculate the percentage of growth inhibition at different times when compared with cells immediately after treatment (day 0). A Student's t test was applied for statistical analysis.

Results

IR induces NE-like differentiation in LNCaP cells. In an attempt to isolate radiation-resistant clones by following a clinical protocol (70 Gy; ref. 1), we surprisingly found that on 40-Gy irradiation (2 Gy/d, 5 d/wk), the majority of cells (~80%) died whereas cells that survived the treatment displayed the growth of extended neurites (Fig. 1*A*), a NE-like phenotype. Expression of two NE cell markers, CgA and NSE, was significantly induced (Fig. 1*B* and *C*). Similar treatments failed to induce NED in DU145 and PC-3 prostate cancer cells. Consistent with previous reports that NE cells are apoptosis resistant (10, 11), IR-induced NE-like cells were resistant to IR and survived another 3-wk irradiation until the completion of the entire radiation protocol (70 Gy). Addition of the chemotherapeutic agent docetaxel into the IR-induced NE-like cells did not cause any change in cell viability either.

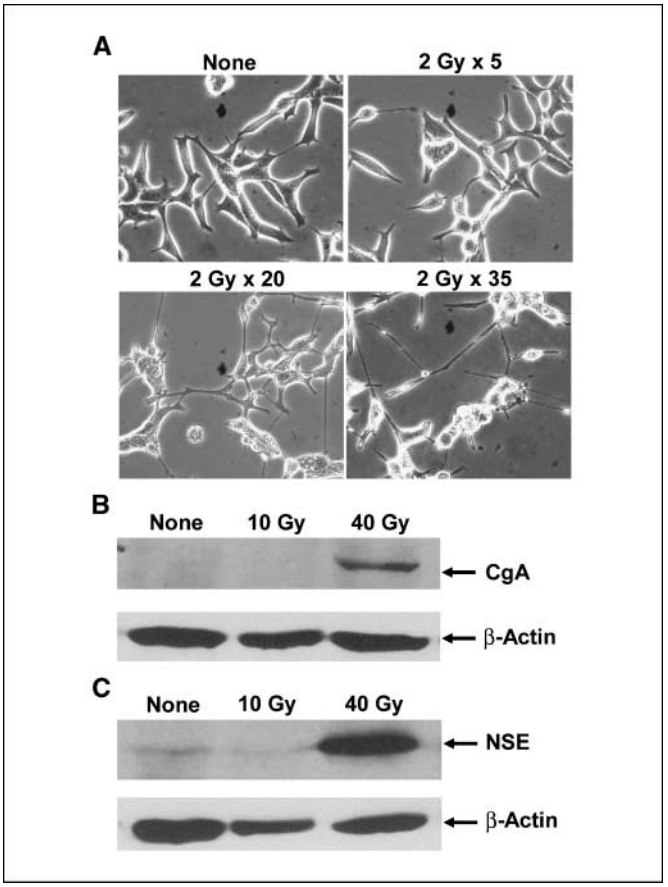

Figure 1. IR induces NE-like differentiation in LNCaP prostate cancer cells. *A,* representative images of cells that received the indicated times of exposures (2 Gy/d, 5 d/wk). Note that cells irradiated 20 times display significant neurite outgrowth and branching. *B* and *C,* immunoblotting of CgA and NSE. Cells that received the indicated dose of radiation were harvested and 20 μg of total protein was used for immunoblotting of CgA and NSE.

IR induces cytoplasmic accumulation of ATF2 and an increase in nuclear pCREB. To determine the subcellular localization of ATF2 in IR-induced NE-like cells, we performed immunostaining and found that ATF2 localization in the cytoplasm was increased compared with nontreated cells (Supplementary Fig. S1*A*). No significant changes in expression and nuclear localization of c-Jun, JunB, and JunD were observed (data not shown), suggesting that the increased cytoplasmic localization of ATF2 is not due to a decrease in Jun proteins to anchor ATF2 in the nucleus (33). In contrast, ATF2 was predominantly localized in the nucleus with some cytoplasmic localization in proliferating LNCaP cells, and treatment with the nuclear export inhibitor leptomycin B (33, 35) increased nuclear localization of ATF2 (Fig. 2*A*). The nuclear sequestration of ATF2 in proliferating LNCaP cells by leptomycin B was also confirmed by subcellular fractionation analysis (data not shown). These results show that ATF2 constantly shuttles between the cytoplasm and nucleus in proliferating LNCaP cells. Consistent with our previous observation that phosphorylation at residues T69 and T71 does not regulate ATF2 subcellular localization (33), the subcellular localization of phospho-ATF2 was similar to that of ATF2 in proliferating and the NE-like cells (data not shown).

To determine whether ATF2 cytoplasmic localization is a consequence or a potential cause of NED, we examined ATF2 subcellular localization at different time points before cells underwent morphologic changes. Irradiation of cells up to five times increased cytoplasmic ATF2 without inducing striking morphologic alterations (Fig. 2*A*). However, treatment of the irradiated cells with leptomycin B failed to induce nuclear accumulation of ATF2 in irradiated cells (Fig. 2*A*), indicating that IR impairs the nuclear import of ATF2. No significant change in ATF2 subcellular localization was observed when irradiated less than five times. Subcellular fractionation analysis showed that IR treatment increased cytoplasmic ATF2 from 24% to 45% of total ATF2 (Fig. 2*B*).

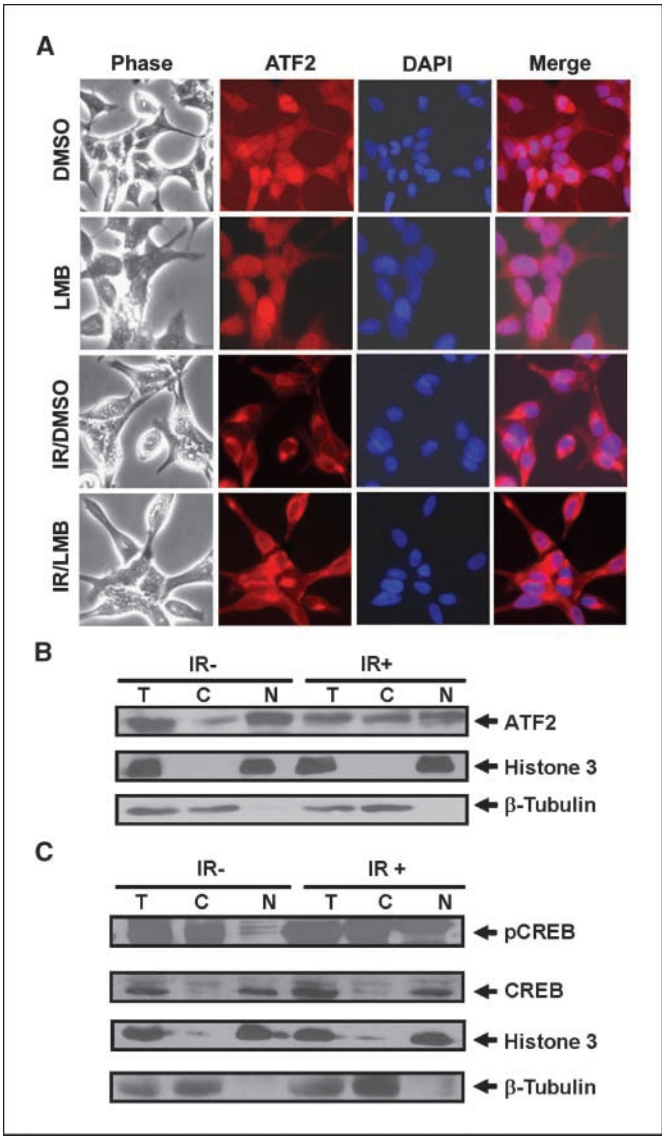

Figure 2. IR induces cytoplasmic accumulation of ATF2 and an increase in nuclear pCREB in LNCaP cells. *A,* LNCaP prostate cancer cells cultured in 12-well plates were treated with DMSO or leptomycin B (*LMB*; 40 ng/mL) overnight or irradiated (2 Gy/d) for 5 d, followed by treatment with DMSO or leptomycin B overnight. Subcellular localization of ATF2 was determined by immunostaining with anti-ATF2 antibody, and DNA in the nucleus was stained with DAPI. *B* and *C,* nonirradiated (*IR−*) or irradiated (2 Gy × 5; *IR+*) LNCaP cells were harvested, and cytosolic, nuclear, and total cellular extracts were prepared. Approximately 20 μg of total cellular extracts (*T*) and an equal portion of cytosolic (*C*) and nuclear (*N*) extracts were used for immunoblotting of ATF2, pCREB, and CREB.

Because CREB regulates transcription of CgA (19), we examined expression and subcellular localization of CREB and pCREB in proliferating and IR-irradiated cells, as we did for ATF2. Because all available pCREB antibodies we tested cross-reacted with phospho-ATF1 and another ~80-kDa cytoplasmic protein (data not shown), we performed subcellular fractionation analysis and determined that IR treatment increased nuclear pCREB from 25% to 49% of the total pCREB (Fig. 2*C*). Unlike pCREB, the nuclear content of CREB was not altered by IR treatment (Fig. 2*C*). Interestingly, pCREB was also detected in the cytoplasm in proliferating LNCaP cells, and IR treatment did not seem to alter the phosphorylation extent of cytoplasmic CREB. IR-induced NE-like cells maintained a high level of pCREB in the nucleus (Supplementary Fig. S1*B*). Taken together, these results show that IR-induced cytoplasmic accumulation of ATF2 and increase in nuclear pCREB occur before cells undergo differentiation.

CREB and ATF2 play opposing roles in NE-like differentiation. The IR-induced cytoplasmic accumulation of ATF2 and increase in nuclear pCREB prompted us to test the hypothesis that nuclear CREB and ATF2 may play opposing roles in NED. Indeed, 50% knockdown of ATF2 resulted in a NE-like morphologic change (Supplementary Fig. S2*A*) and a 1.6-fold induction of NSE (Fig. 3*A*). No induction of CgA was observed (data not shown). In contrast, transient expression of VP16-bCREB, a constitutively activated and nuclear-localized mutant of CREB (36, 37), induced a NE-like morphologic change (Supplementary Fig. S2*B*) and increased CgA and NSE expression by 2- to 3-fold (Fig. 3*B*). However, overexpression of a constitutively nuclear-localized ATF2 (nATF2), which has a nuclear localization signal from the large T antigen of SV40 fused to the NH_2 terminus of ATF2 as others did (34), inhibited VP16-bCREB–mediated morphologic changes and the induction of NSE. To determine whether increased cytoplasmic accumulation of endogenous ATF2 can induce NED, we overexpressed a constitutively cytoplasmic-localized ATF2 (cATF2), which lacks the two nuclear localization signals (33), in LNCaP cells. Because ATF2 homodimerization impairs ATF2 nuclear import (33), overexpression of cATF2 increased cytoplasmic localization of ATF2 to ~50% of total ATF2 (data not shown). Indeed, cATF2, but not nATF2, induced neurite outgrowth (Supplementary Fig. S2*C*) and a 5.4-fold increase in NSE expression (Fig. 3*C*). No induction of CgA by cATF2 or nATF2 was observed. Transiently expressed cATF2-Venus and nATF2-Venus were predominantly localized to the cytoplasm and nucleus, respectively (Supplementary Fig. S2*D*). Immunoblotting analysis confirmed the exogenous expression of VP16-bCREB, cATF2-Venus, and nATF2-Venus in these experiments (data not shown). Knockdown of ATF2 or expression of cATF2 had no effect on the localization and amount of pCREB, and overexpression of VP16-bCREB did not alter subcellular localization of ATF2 (data not shown). Taken together, these results support the hypothesis that CREB and ATF2 play opposing roles in NED.

Stable expression of a nonphosphorylatable CREB or nATF2 inhibits IR-induced NE-like differentiation. To further determine the role of CREB and ATF2 in IR-induced NED, we established tetracycline-inducible stable cell lines that express nATF2 or a nonphosphorylatable CREB (CREB-S133A), which has been used as a dominant negative mutant form of CREB (13, 15). In the absence of tetracycline, these stable cell lines exhibited normal morphology like vector-only cells (Fig. 4*A*). However, addition of tetracycline significantly induced expression of CREB-S133A or nATF2 (Fig. 4*B*) and reduced the percentage of cells displaying extended neurites in response to irradiation (Fig. 4*C*).

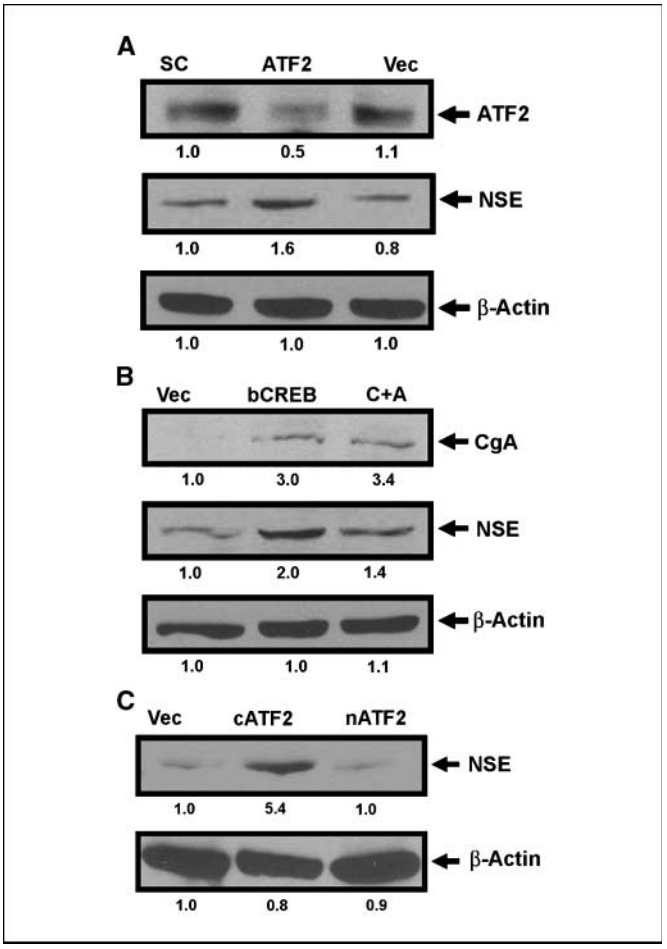

Figure 3. ATF2 and CREB play opposing roles in NE-like differentiation. *A,* immunoblotting analysis of ATF2 and NSE expression from LNCaP cells transfected with siRNA constructs for scrambled sequences (*SC*), ATF2 siRNA (*ATF2*), or pSUPER vector only (*Vec*). *B,* immunoblotting analysis of CgA and NSE from LNCaP cells transfected with the vector control (*Vec*), the plasmid encoding VP16-bCREB (*bCREB*), or cotransfected with plasmids encoding VP16-bCREB and nATF2 (*C+A*). *C,* immunoblotting analysis of NSE from LNCaP cells transfected with the vector control (*Vec*) or the plasmid encoding cATF2 or nATF2. The number below each lane is the quantified fold change when compared with the first lane.

Interestingly, induction of CgA and NSE by IR was inhibited by nATF2, but not by CREB-S133A (Fig. 4*D*). These results further support the conclusion that nuclear ATF2 and pCREB play different roles in IR-induced neurite outgrowth.

To determine the relationship between the expression of nATF2 and IR-induced phosphorylation of CREB and the relationship between the expression of CREB-S133A and the subcellular localization of ATF2, we irradiated cells for 5 days while constantly inducing expression of nATF2 or CREB-S133A. Expression of CREB-S133A did not affect IR-induced cytoplasmic localization of ATF2 (data not shown), whereas expression of nATF2 significantly inhibited IR-induced phosphorylation of CREB (Supplementary Fig. S3). However, expression of nATF2 only did not affect phosphorylation of CREB in the absence of IR (data not shown). These results suggest that IR-induced cytoplasmic sequestration of ATF2 may be a prerequisite for IR-induced phosphorylation of CREB and the subsequent NE-like differentiation.

IR-induced NE-like differentiation is reversible, and dedifferentiated cells lose NE-like properties. Because cAMP-induced

NE-like cells are reversible (12), we sought to determine whether IR-induced NE-like cells are also reversible. We irradiated cells for 4 weeks (40 Gy) to allow all surviving cells to differentiate into NE-like cells and then waited for the growth of any cells that were reversible. Although differentiated NE-like cells were maintained without obvious cell death or growth for the first 2 months, we isolated three independent clones 3 months after the completion of the irradiation. We named these clones LNCaP-IRR1 (IRR refers to IR resistant), LNCaP-IRR2, and LNCaP-IRR3. These IR-resistant cells showed similar morphology to wild-type LNCaP cells (Supplementary Fig. S4). All three clones lost CgA and NSE expression but retained levels of androgen receptor comparable to wild-type LNCaP cells (Fig. 5*A*), suggesting that these clones have lost their NE-like cell properties.

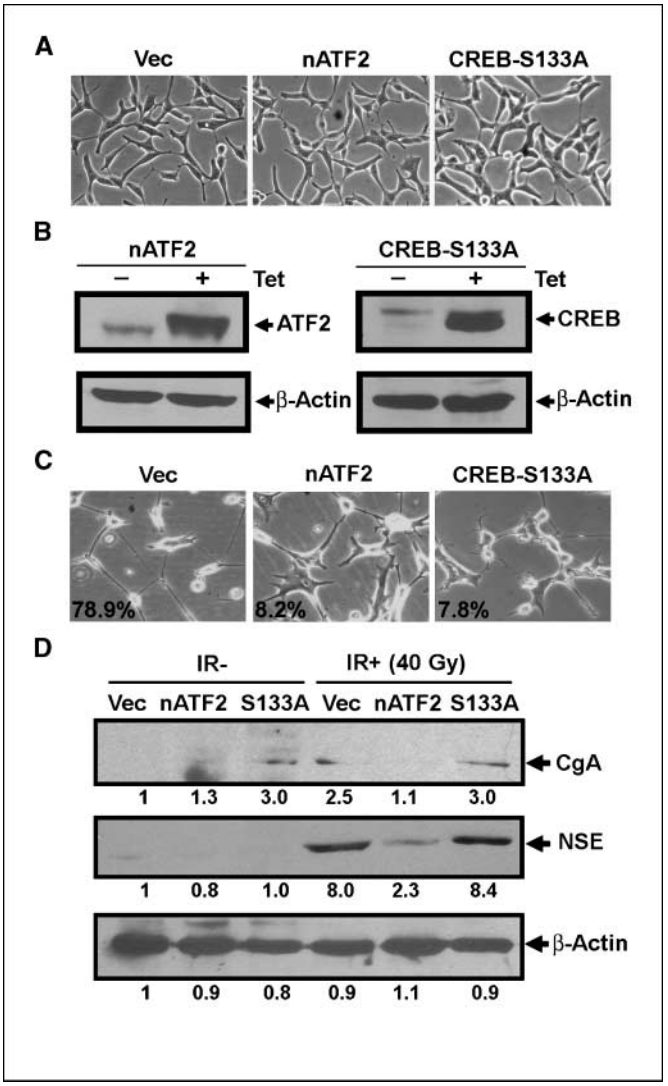

Figure 4. Inhibition of IR-induced NE-like differentiation by dominant negative CREB and nATF2. *A,* representative images of stable cell lines that have pcDNA4/TO (*Vec*), pcDNA4-TO-Flag-nATF2 (*nATF2*), or pcDNA4/TO-HA-CREB-S133A (*CREB-S133A*) integrated. *B,* immunoblotting analysis of induced nATF2 and CREB-S133A by tetracycline. Total cell lysates were prepared 3 d after the induction, and Flag-nATF2 and HA-CREB-S133A were detected with anti-ATF2 and anti-HA antibodies, respectively. *C,* representative images acquired from stable cell lines that received 40-Gy irradiation in the presence of tetracycline. The number indicates the percentage of cells showing extended neurites. *D,* immunoblotting analysis of CgA and NSE from experiments in *C*. The number below each lane is the quantified fold change when compared with the first lane.

To determine whether these IR-resistant clones can still be induced to redifferentiation, we irradiated them at 40 Gy and examined for morphologic changes and the induction of CgA and NSE. Whereas all three clones exhibited extended neurite outgrowth (Supplementary Fig. S5*A*), the induction of CgA and NSE was completely abrogated (Fig. 5*A*). Interestingly, androgen receptor expression in LNCaP-IRR2 clone was significantly inhibited like in parental cells whereas androgen receptor expression in LNCaP-IRR1 and LNCaP-IRR3 cells was only slightly attenuated. These distinct responses to IR treatment suggest that these three IR-resistant clones are likely heterogeneous. To determine how these clones respond to androgen depletion treatment, we treated cells in phenol-free medium supplemented with 10% CD-FBS for 3 weeks. Whereas LNCaP-IRR1 and LNCaP-IRR3 cells exhibited extended neurite outgrowth, LNCaP-IRR2 cells showed only short neurites (Supplementary Fig. S5*B*). Interestingly, an induction of CgA expression by CD-FBS similar to parental cells was observed in LNCaP-IRR2; no induction was observed in LNCaP-IRR1; and a significantly attenuated induction was seen in LNCaP-IRR3 cells (Fig. 5*B*). On the contrary, the induction of NSE in LNCaP-IRR2 was abolished, whereas LNCaP-IRR1 and IRR3 responded to the treatment to some extent. Like the parental cells, however, the expression of androgen receptor in all three clones was significantly down-regulated by the CD-FBS treatment. Taken together, these results suggest that the three IR-resistant clones are heterogeneous and likely have distinct molecular defects in their responses to IR and androgen depletion treatments.

IR-resistant and dedifferentiated cells acquire cross-resistance to therapy. To explore the potential implication of dedifferentiated cells in prostate cancer progression, we examined their response to radiation, the chemotherapeutic agent docetaxel (38), and androgen depletion treatments. Like the parental LNCaP cells, all three clones stopped growth during the 1st week of irradiation (10 Gy) and no cell death was observed (Fig. 6*A*). During the 2nd week of irradiation, however, all three clones showed significantly reduced cell death when compared with the parental cells. Interestingly, all three IR-resistant cells began to resume growth during the 3rd week of irradiation whereas the parental cells did not show obvious growth or death as all surviving cells differentiated into NE-like cells. Similar to their response to IR treatment, all three IR-resistant clones were resistant to cell death induced by the chemotherapeutic agent docetaxel (Fig. 6*B*), as well as to growth inhibition on androgen depletion (Fig. 6*C*). These results suggest that IR-induced NE-like cells have the potential to dedifferentiate back into a proliferating state with the acquisition of cross-resistance to radiotherapy, chemotherapy, and hormonal therapy.

Discussion

NE-like cells are implicated in prostate cancer progression, androgen-independent growth, and poor prognosis (3–6, 39, 40). Because androgen ablation treatment can induce NED *in vitro* and *in vivo* (3–6), it has been proposed that the presence of NE-like cells may contribute to androgen-independent growth, a critical factor leading to the failure of current prostate cancer therapy. We present here the first evidence that in addition to androgen ablation, IR also induces NED in the prostate cancer cell line LNCaP.

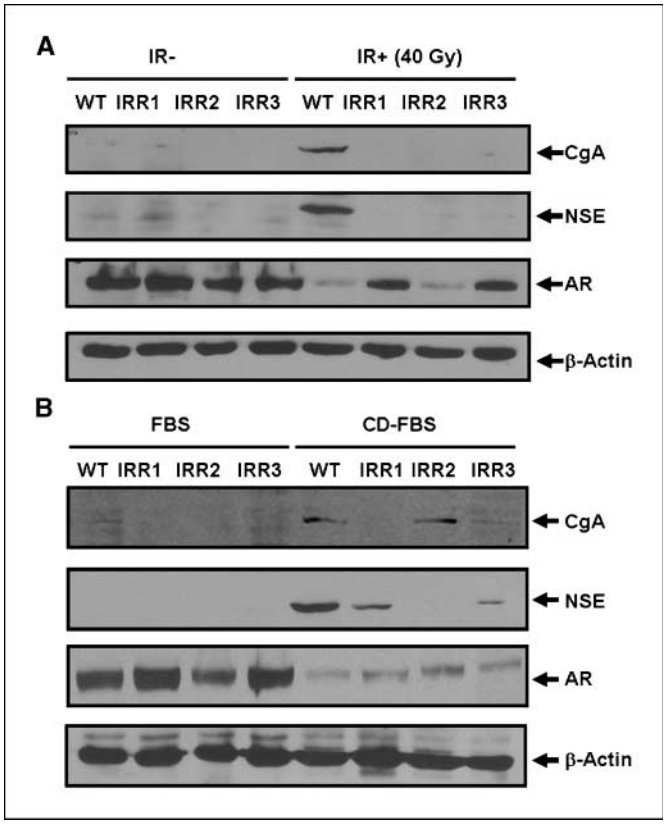

Figure 5. Response of IR-resistant clones to IR- and androgen depletion–induced NE-like redifferentiation. *A,* wild-type LNCaP (*WT*) and the indicated IR-resistant clones were subjected to fractionated IR (40 Gy), and the induction of CgA and NSE as well as the expression of androgen receptor (*AR*) was compared with that of nonirradiated cells. *B,* wild-type LNCaP and IR-resistant clones were cultured in medium supplemented with 10% FBS or CD-FBS for 3 wk, and the induction of CgA and NSE as well as the expression of androgen receptor was determined by immunoblotting.

Significantly, IR-induced NED is reversible, and dedifferentiated cells have lost the NE-like properties. However, all isolated three IR-resistant clones derived from dedifferentiated cells are cross-resistant to radiation, docetaxel, and androgen depletion treatments. These findings, along with other reports (41–46), strongly suggest that radiation- or hormonal therapy–induced NED may represent a common pathway by which cancer cells survive treatment and contribute to prostate cancer recurrence.

Although it has been reported that signal transducer and activator of transcription-3 (47) and β-catenin (48) can mediate IL-6– and androgen depletion–induced NED in prostate cancer cells, respectively, it remains largely unexplored how the switch from proliferation to differentiation is turned on at the transcriptional level. Several pieces of evidence presented in this work show that CREB functions as a transcriptional activator and ATF2 acts as a transcriptional repressor of NED. First, IR induced cytoplasmic accumulation of ATF2 and increased nuclear pCREB. Second, knockdown of ATF2 or overexpression of VP16-bCREB induced NED. Third, overexpression of nATF2 inhibited NED induced by VP16-bCREB, whereas overexpression of cATF2 induced NED. Last, stable expression of CREB-S133A or nATF2 inhibited IR-induced NED.

The transcriptional regulation of cAMP responsive element–containing genes by ATF2 and CREB is dependent on individual genes. For example, the insulin promoter contains one cAMP responsive element–binding site, and both ATF2 and CREB can bind it. However, ATF2 activates the transcription of insulin, whereas CREB inhibits it (31). In the present work, we also observed that overexpression of VP16-bCREB increased expression of endogenous CgA and NSE, whereas overexpression of nATF2 inhibited VP16-bCREB–induced expression of NSE, but not CgA. Likewise, knockdown of ATF2 or overexpression of cATF2 increased expression of NSE, but not CgA. These results support the notion that the effect of CREB and ATF2 on target gene transcription is dependent on gene context. Although VP16-bCREB can induce CgA and NSE expression (Fig. 3*B*), stable expression of nATF2, but not CREB-S133A, inhibited IR-induced expression of CgA and NSE (Fig. 4*D*). Despite the fact that the CREB-S133A–expressing stable cell line seems to have a basal level of CgA

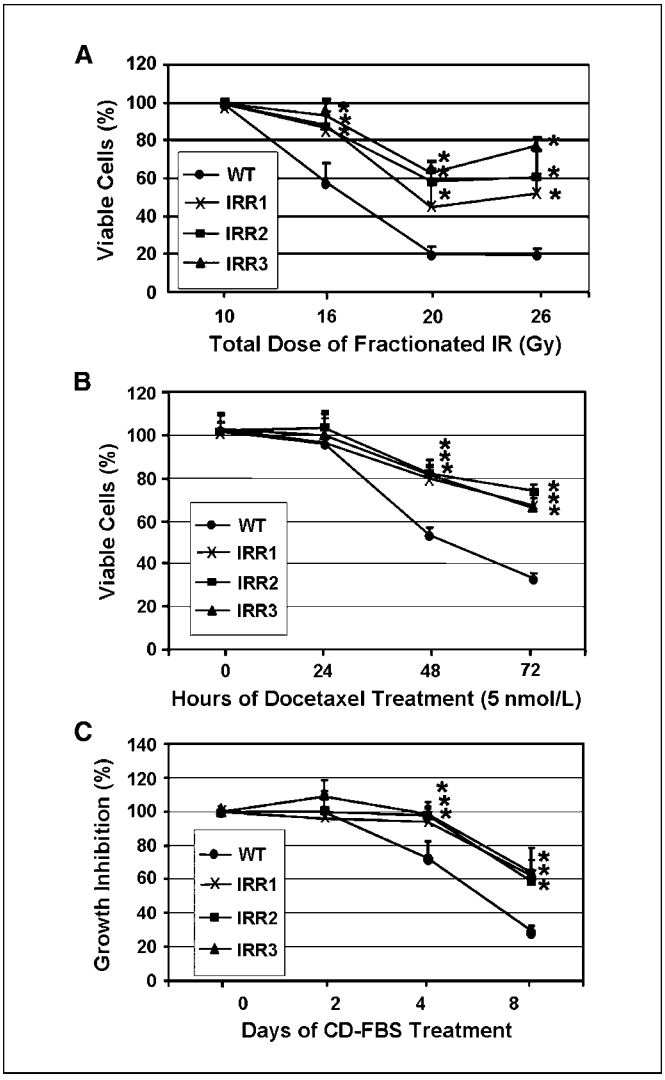

Figure 6. Cross-resistance of IR-resistant clones to therapeutic treatments. *A,* wild-type LNCaP and the indicated IR-resistant clones were cultured in 48-well plates and subjected to fractionated IR for the indicated doses. Cell viability was determined 1 d after the indicated irradiation as the percentage of viable cells that received 10-Gy irradiation. *B,* cells were treated with docetaxel for the indicated time and cell viability was determined as the percentage of viable cells at 0 h. *C,* cells were cultured in 10% FBS or CD-FBS for the indicated time and the inhibition of cell growth by CD-FBS was determined as described in Materials and Methods. *, $P < 0.01$, compared with wild-type LNCaP cells.

expression in the absence of tetracycline, which is likely due to leaky expression of CREB-S133A, induction of CREB-S133A by tetracycline did not alter the CgA expression in response to IR (Fig. 4*D*). Given that overexpression of VP16-bCREB induced expression of both CgA and NSE (Fig. 3*B*), these observations suggest that CREB is not responsible for IR-induced CgA and NSE expression. Alternatively, phosphorylation of CREB at different sites (21) may contribute to IR-induced CgA and NSE expression. Future studies are needed to distinguish these two possibilities. Interestingly, overexpression of CREB-S133A and nATF2 did not inhibit the growth of shorter neurites but rather inhibited the elongation of neurites (Fig. 4*C*). Consistent with a role of CREB in neurite elongation in hippocampal neurons (49), it is likely that CREB and ATF2 may oppose each other in irradiated LNCaP cells to regulate transcription of target genes essential for neurite elongation, one of the phases during neuritogenesis (50). Further identification of the target genes will provide insight into the molecular mechanisms by which CREB and ATF2 play opposing roles in IR-induced NED. Because expression of nATF2 inhibited IR-induced phosphoryaltion of CREB (Supplementary Fig. S3), it is possible that nuclear ATF2 may also antagonize an upstream signaling pathway that contributes to IR-induced phosphorylation of CREB. It will be interesting to determine whether this effect is independent of or dependent on ATF2 transcriptional activity. In addition, identification of cell signaling that regulates cytoplasmic accumulation of ATF2 and phosphorylation of CREB will provide opportunities to develop novel therapeutics for prostate cancer.

The finding that IR can induce NED is clinically important, given that ~10% to 60% of patients treated with radiation therapy experience recurrent tumors (2). Although a detailed and well-controlled examination of NE-like cells in recurrent tumors would shed light on our *in vitro* findings here, the fact that patients who have biochemical recurrence after radiotherapy normally do not undergo surgery or even biopsy prevents us from performing this type of study. In addition, the transient nature of NE-like cells may also not allow us to find a causative link between radiation therapy and the induction of NED in patients. We are therefore currently performing longitudinal analyses to evaluate the effect of radiation therapy on NED and its contribution to tumor recurrence in xenograft nude mouse prostate cancer models.

Disclosure of Potential Conflicts of Interest

No potential conflicts of interest were disclosed.

Acknowledgments

Received 6/12/2008; revised 8/18/2008; accepted 9/18/2008.

Grant support: Purdue Cancer Center Small Grants Program and the U.S. Army Medical Research Acquisition Activity, Prostate Cancer Research Program grant PC073098. DNA sequencing was done in Purdue Genomic Core Facility supported by National Cancer Institute grant CCSG CA23168 to the Purdue Cancer Center.

The costs of publication of this article were defrayed in part by the payment of page charges. This article must therefore be hereby marked *advertisement* in accordance with 18 U.S.C. Section 1734 solely to indicate this fact.

We thank Drs. Robert Geahlen, David Riese, Jian Jian Li, and Timothy Ratliff for their support and consultation during the course of this work, and the members of the Hu laboratory for helpful discussions.

References

1. Ganswindt U, Paulsen F, Anastasiadis AG, Stenzl A, Bamberg M, Belka C. 70 Gy or more: which dose for which prostate cancer? J Cancer Res Clin Oncol 2005;131:407–19.
2. Allen GW, Howard AR, Jarrard DF, Ritter MA. Management of prostate cancer recurrences after radiation therapy-brachytherapy as a salvage option. Cancer 2007;110:1405–16.
3. Daneshmand S, Quek ML, Pinski J. Neuroendocrine differentiation in prostate cancer. Cancer Ther 2005;3:383–96.
4. Nelson EC, Cambio AJ, Yang JC, Ok JH, Lara PN, Jr., Evans CP. Clinical implications of neuroendocrine differentiation in prostate cancer. Prostate Cancer Prostatic Dis 2007;10:6–14.
5. Amorino GP, Parsons SJ. Neuroendocrine cells in prostate cancer. Crit Rev Eukaryot Gene Expr 2004;14:287–300.
6. Yuan TC, Veeramani S, Lin MF. Neuroendocrine-like prostate cancer cells: neuroendocrine transdifferentiation of prostate adenocarcinoma cells. Endocr Relat Cancer 2007;14:531–47.
7. Deeble PD, Cox ME, Frierson HF, Jr., et al. Androgen-independent growth and tumorigenesis of prostate cancer cells are enhanced by the presence of PKA-differentiated neuroendocrine cells. Cancer Res 2007;67:3663–72.
8. Nakada SY, di Sant'Agnese PA, Moynes RA, et al. The androgen receptor status of neuroendocrine cells in human benign and malignant prostatic tissue. Cancer Res 1993;53:1967–70.
9. Bonkhoff H. Neuroendocrine differentiation in human prostate cancer. Morphogenesis, proliferation and androgen receptor status. Ann Oncol 2001;12 Suppl 2:S141–4.
10. Fixemer T, Remberger K, Bonkhoff H. Apoptosis resistance of neuroendocrine phenotypes in prostatic adenocarcinoma. Prostate 2002;53:118–23.
11. Vanoverberghe K, Vanden Abeele F, Mariot P, et al. Ca^{2+} homeostasis and apoptotic resistance of neuroendocrine-differentiated prostate cancer cells. Cell Death Differ 2004;11:321–30.
12. Cox ME, Deeble PD, Lakhani S, Parsons SJ. Acquisition of neuroendocrine characteristics by prostate tumor cells is reversible: implications for prostate cancer progression. Cancer Res 1999;59:3821–30.
13. Mayr B, Montminy M. Transcriptional regulation by the phosphorylation-dependent factor CREB. Nat Rev Mol Cell Biol 2001;2:599–609.
14. Brindle PK, Montminy MR. The CREB family of transcription activators. Curr Opin Genet Dev 1992;2:199–204.
15. Shaywitz AJ, Greenberg ME. CREB: a stimulus-induced transcription factor activated by a diverse array of extracellular signals. Annu Rev Biochem 1999;68:821–61.
16. Montminy MR, Bilezikjian LM. Binding of a nuclear protein to the cyclic-AMP response element of the somatostatin gene. Nature 1987;328:175–8.
17. Garcia GE, Nicole A, Bhaskaran S, Gupta A, Kyprianou N, Kumar AP. Akt-and CREB-mediated prostate cancer cell proliferation inhibition by Nexrutine, a Phellodendron amurense extract. Neoplasia 2006;8:523–33.
18. Unni E, Sun S, Nan B, et al. Changes in androgen receptor nongenotropic signaling correlate with transition of LNCaP cells to androgen independence. Cancer Res 2004;64:7156–68.
19. Canaff L, Bevan S, Wheeler DG, et al. Analysis of molecular mechanisms controlling neuroendocrine cell specific transcription of the chromogranin A gene. Endocrinology 1998;139:1184–96.
20. Kim J, Jia L, Stallcup MR, Coetzee GA. The role of protein kinase A pathway and cAMP responsive element-binding protein in androgen receptor-mediated transcription at the prostate-specific antigen locus. J Mol Endocrinol 2005;34:107–18.
21. Johannessen M, Moens U. Multisite phosphorylation of the cAMP response element-binding protein (CREB) by a diversity of protein kinases. Front Biosci 2007;12:1814–32.
22. Hai TW, Liu F, Coukos WJ, Green MR. Transcription factor ATF cDNA clones: an extensive family of leucine zipper proteins able to selectively form DNA-binding heterodimers. Genes Dev 1989;3:2083–90.
23. Maekawa T, Sakura H, Kanei-Ishii C, et al. Leucine zipper structure of the protein CRE-BP1 binding to the cyclic AMP response element in brain. EMBO J 1989;8:2023–8.
24. Wagner EF. AP-1-Introductory remarks. Oncogene 2001;20:2334–5.
25. Eferl R, Wagner EF. AP-1: a double-edged sword in tumorigenesis. Nat Rev Cancer 2003;3:859–68.
26. Gueorguiev VD, Cheng SY, Sabban EL. Prolonged activation of cAMP-response element-binding protein and ATF-2 needed for nicotine-triggered elevation of tyrosine hydroxylase gene transcription in PC12 cells. J Biol Chem 2006;281:10188–95.
27. Ionescu AM, Drissi H, Schwarz EM, et al. CREB Cooperates with BMP-stimulated Smad signaling to enhance transcription of the Smad6 promoter. J Cell Physiol 2004;198:428–40.
28. Ionescu AM, Schwarz EM, Zuscik MJ, et al. ATF-2 cooperates with Smad3 to mediate TGF-β effects on chondrocyte maturation. Exp Cell Res 2003;288:198–207.
29. Niwano K, Arai M, Koitabashi N, et al. Competitive binding of CREB and ATF2 to cAMP/ATF responsive element regulates eNOS gene expression in endothelial cells. Arterioscler Thromb Vasc Biol 2006;26:1036–42.
30. Flint KJ, Jones NC. Differential regulation of three members of the ATF/CREB family of DNA-binding proteins. Oncogene 1991;6:2019–26.
31. Hay CW, Ferguson LA, Docherty K. ATF-2 stimulates the human insulin promoter through the conserved CRE2 sequence. Biochim Biophys Acta 2007;1769:79–91.
32. Ricote M, Garcia-Tunon I, Bethencourt F, et al. The p38 transduction pathway in prostatic neoplasia. J Pathol 2006;208:401–7.

33. Liu H, Deng X, Shyu YJ, Li JJ, Taparowsky EJ, Hu CD. Mutual regulation of c-Jun and ATF2 by transcriptional activation and subcellular localization. EMBO J 2006;25: 1058–69.

34. Paulmurugan R, Gambhir SS. Firefly luciferase enzyme fragment complementation for imaging in cells and living animals. Anal Chem 2005;77:1295–302.

35. Kudo N, Wolff B, Sekimoto T, et al. Leptomycin B inhibition of signal-mediated nuclear export by direct binding to CRM1. Exp Cell Res 1998;242:540–7.

36. Reusch JE, Colton LA, Klemm DJ. CREB activation induces adipogenesis in 3T3-1 cells. Mol Cell Biol 2000; 20:1008–20.

37. Barco A, Alarcon JM, Kandel ER. Expression of constitutively active CREB protein facilitates the late phase of long-term potentiation by enhancing synaptic capture. Cell 2002;108:689–703.

38. de Wit R. Chemotherapy in hormone-refractory prostate cancer. BJU Int 2008;101 Suppl 2:11–5.

39. di Sant'Agnese PA. Neuroendocrine differentiation in prostatic carcinoma: an update on recent developments. Ann Oncol 2001;12 Suppl 2:S135–40.

40. Huang J, Wu C, di Sant'Agnese PA, Yao JL, Cheng L, Na Y. Function and molecular mechanisms of neuroendocrine cells in prostate cancer. Anal Quant Cytol Histol 2007;29:128–38.

41. Yuan TC, Veeramani S, Lin FF, et al. Androgen deprivation induces human prostate epithelial neuroendocrine differentiation of androgen-sensitive LNCaP cells. Endocr Relat Cancer 2006;13:151–67.

42. Ismail AH, Landry F, Aprikian AG, Chevalier S. Androgen ablation promotes neuroendocrine cell differentiation in dog and human prostate. Prostate 2002; 51:117–25.

43. Wright ME, Tsai MJ, Aebersold R. Androgen receptor represses the neuroendocrine transdifferentiation process in prostate cancer cells. Mol Endocrinol 2003;17: 1726–37.

44. Jin RJ, Wang Y, Masumori N, et al. NE-10 neuroendocrine cancer promotes the LNCaP xenograft growth in castrated mice. Cancer Res 2004;64:5489–95.

45. Jiborn T, Bjartell A, Abrahamsson PA. Neuroendocrine differentiation in prostatic carcinoma during hormonal treatment. Urology 1998;51:585–9.

46. Zhang XQ, Kondrikov D, Yuan TC, Lin FF, Hansen J, Lin MF. Receptor protein tyrosine phosphatase α signaling is involved in androgen depletion–induced neuroendocrine differentiation of androgen-sensitive LNCaP human prostate cancer cells. Oncogene 2003; 22:6704–16.

47. Spiotto MT, Chung TD. STAT3 mediates IL-6-induced neuroendocrine differentiation in prostate cancer cells. Prostate 2000;42:186–95.

48. Yang X, Chen MW, Terry S, et al. A human- and male-specific protocadherin that acts through the wnt signaling pathway to induce neuroendocrine transdifferentiation of prostate cancer cells. Cancer Res 2005;65:5263–71.

49. Karasewski L, Ferreira A. MAPK signal transduction pathway mediates agrin effects on neurite elongation in cultured hippocampal neurons. J Neurobiol 2003;55: 14–24.

50. Aletta JM, Greene LA. Growth cone configuration and advance: a time-lapse study using video-enhanced differential interference contrast microscopy. J Neurosci 1988;8:1425–35.

Legends to Supplementary Figures

Supplementary SFig. 1. **IR induces cytoplasmic accumulation of ATF2 and nuclear accumulation of pCREB in NE-like cells.** (*A*). LNCaP cells cultured in 10 cm dishes were irradiated with fractionated IR (2 Gy/day, 5 days/week) for four weeks to induce NE-like differentiation. Subcellular localization of ATF2 in NE-like cells was determined using immunostaining. DAPI staining was used to mark the nucleus. Subcellular localization of ATF2 in proliferating LNCaP cells was shown in Fig. 2A. (*B*). LNCaP cells were similarly treated as described in (*A*) and cytosolic and nuclear extracts were prepared. For the purpose of comparison, non-irradiated cells (-) and cells that received 5 times of exposure to IR (10 Gy) were also included. Note that only 10 μg of cytosolic extract and the equal portion of nuclear extract were loaded for immunoblotting of pCREB.

Supplementary SFig. 2 ATF2 and CREB play an opposing role in NE-like differentiation. Shown are representative images acquired from cells transfected with plasmids encoding the indicated siRNA constructs (*A*), mutant CREB (*B*), or mutant ATF2 (*C*) as presented in Fig. 3. (*D*) Shown are subcellular localization of cATF2 and nATF2 as Venus fusions.

Supplementary SFig. 3. Effect of nATF2 on IR-induced phosphorylation of CREB. The LNCaP cells that stably express inducible nATF2 were cultured in 10 cm dishes and subjected to IR (2 Gy/day) for five days while nATF2 expression was constantly induced by tetracycline (Tet +) or not induced (Tet -). Irradiated cells were harvested, and

cytosolic (C) and nuclear (N) fractions were prepared. The amount of pCREB, CREB, and ATF2 in the cytosolic and nuclear fractions was determined using immunoblotting.

Supplementary SFig. 4. Morphology of wild-type LNCaP (WT) and the indicated isolated IR-resistant clones from dedifferentiated NE-like cells.

Supplementary SFig. 5. IR- and androgen depletion-induced NE-like morphological changes in wild-type LNCaP (WT) cells and IR-resistant clones. (*A*) Shown are representative images of irradiated cells acquired at the end of 40 Gy-irradiation. (*B*) Shown are representative images of cells acquired at the end of three-week treatment with C/D-FBS.

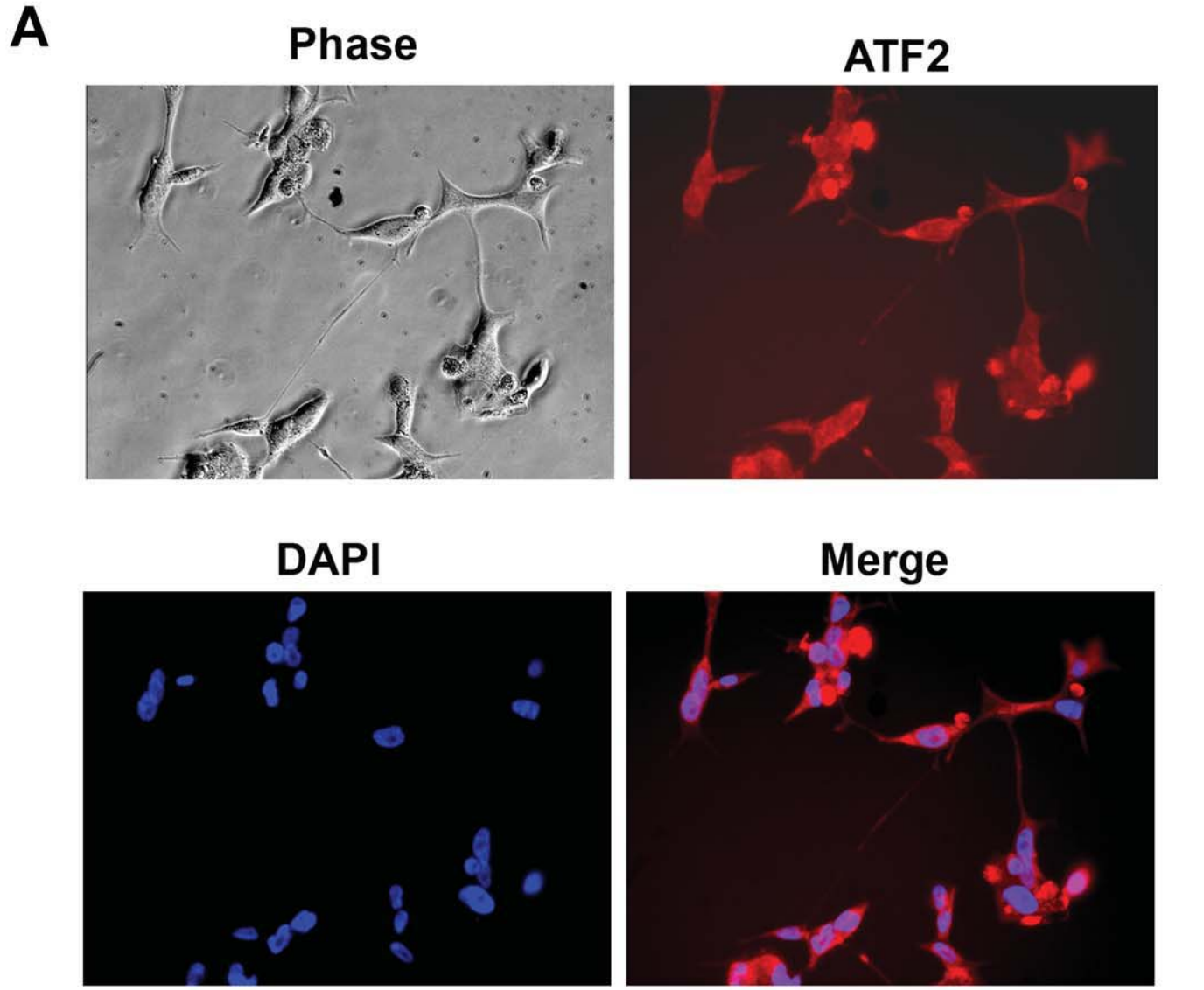
A
Phase
ATF2
DAPI
Merge
B
–
10 Gy
40 Gy
C
N
C
N
C
N
pCREB
Histone 3
β–tubulin

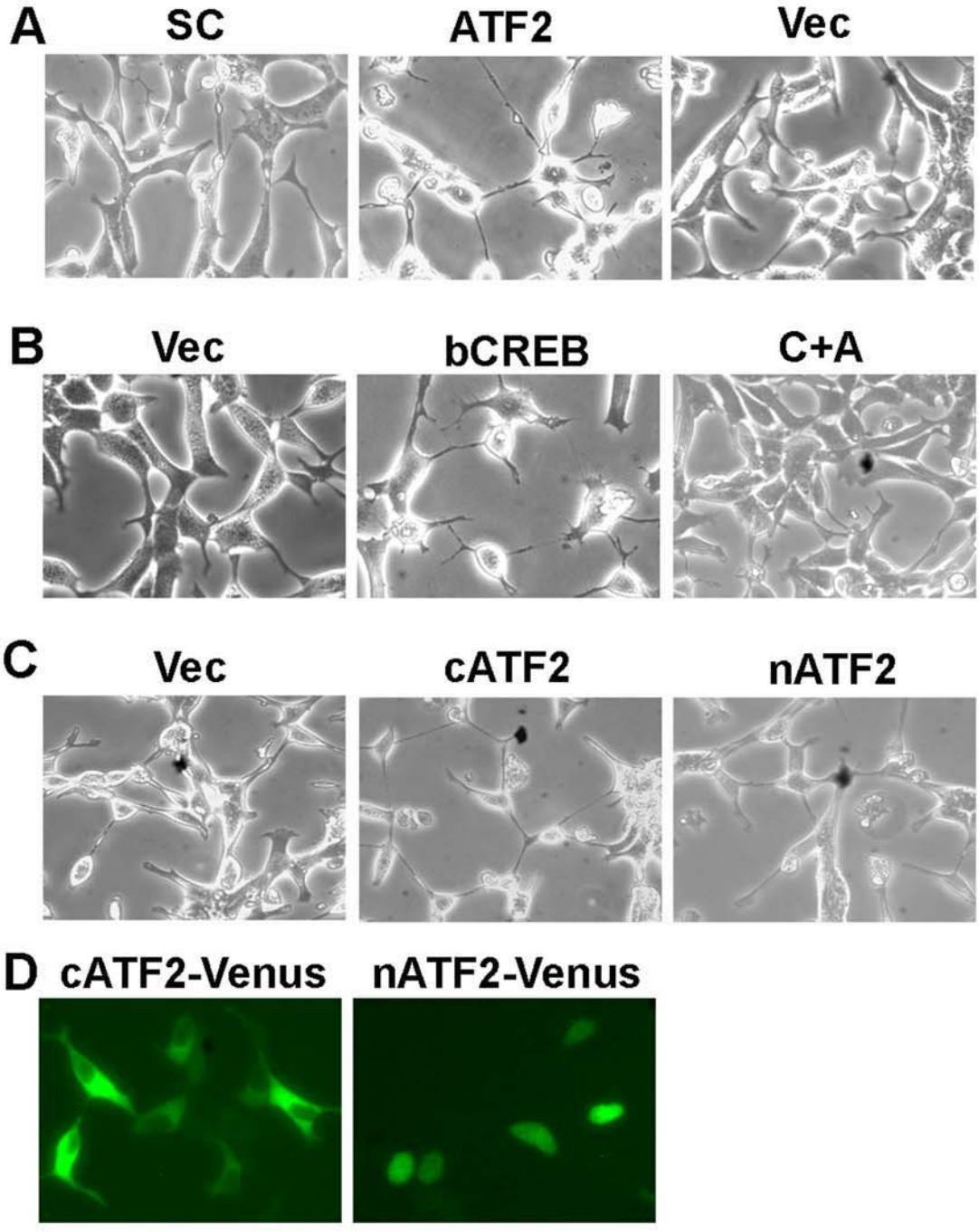
A
SC
ATF2
Vec
B
Vec
bCREB
C+A
C
Vec
cATF2
nATF2
D
cATF2-Venus
nATF2-Venus

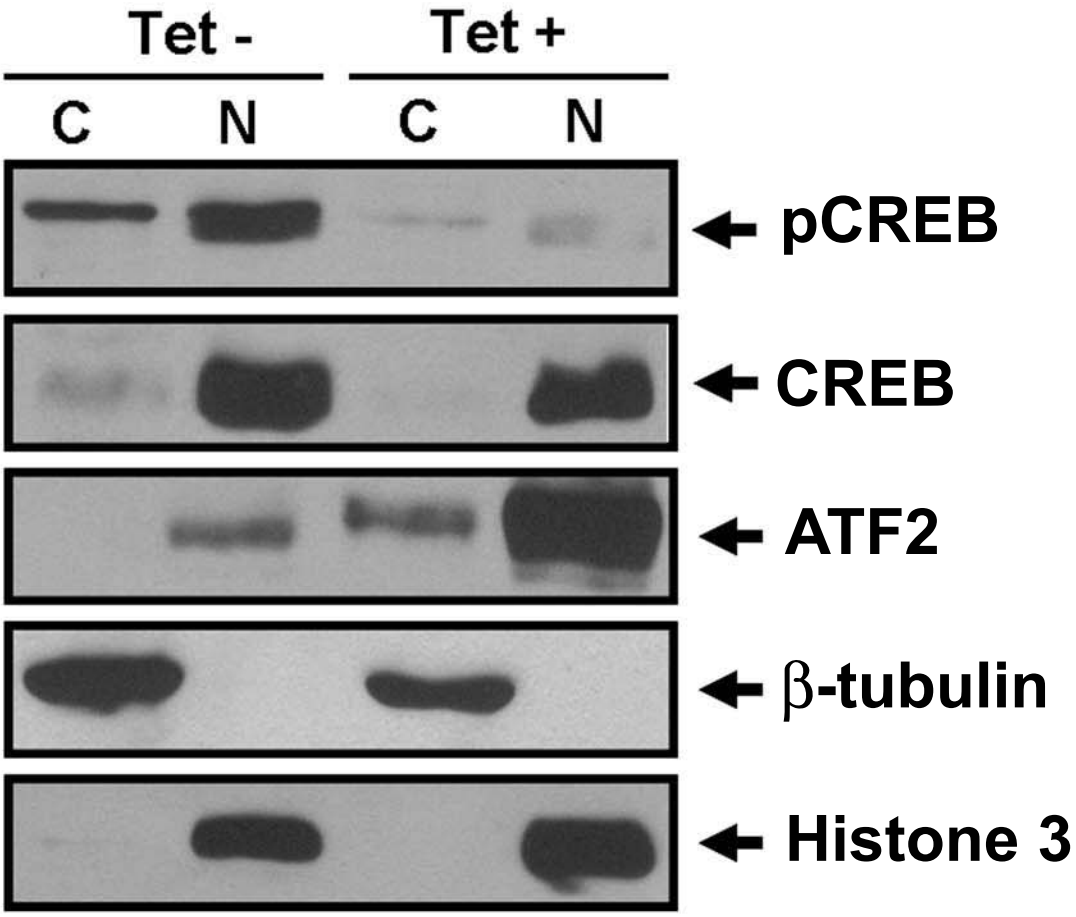
Tet -
Tet +
C
N
C
N
pCREB
CREB
ATF2
β-tubulin
Histone 3

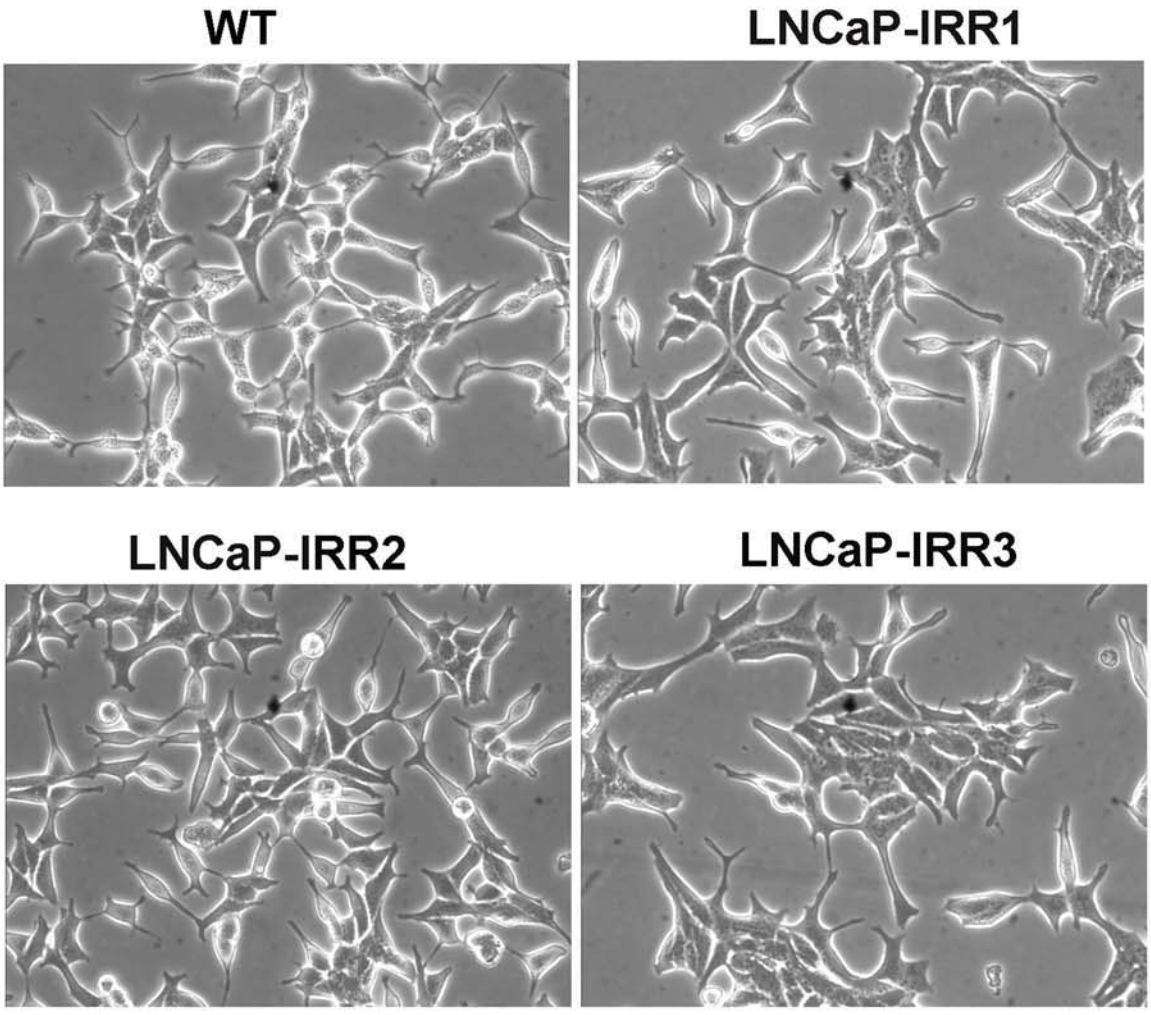
WT
LNCaP-IRR1
LNCaP-IRR2
LNCaP-IRR3

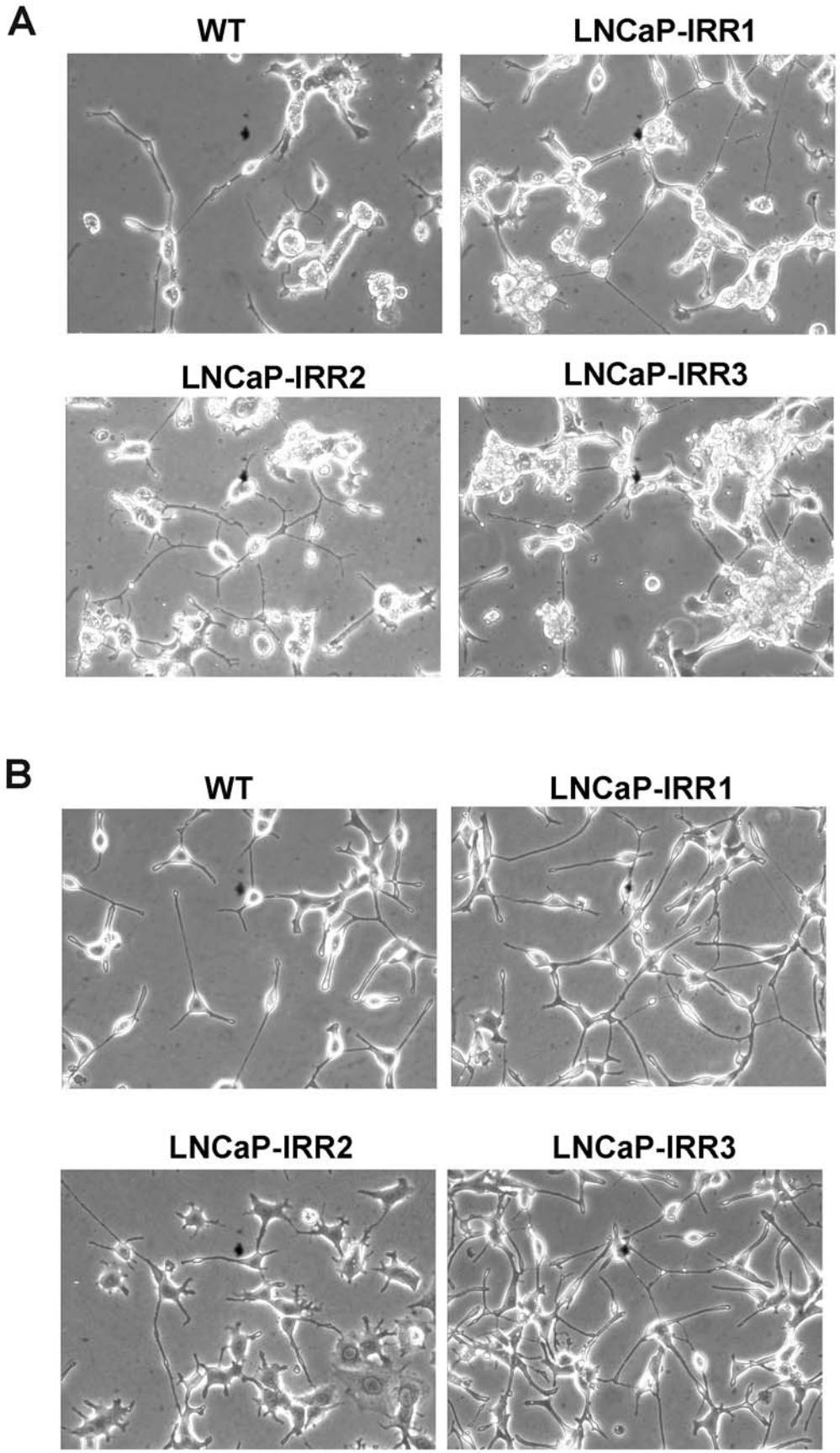
A
WT
LNCaP-IRR1
LNCaP-IRR2
LNCaP-IRR3
B
WT
LNCaP-IRR1
LNCaP-IRR2
LNCaP-IRR3

Am J Cancer Res 2011;1(7):834-844
www.ajcr.us /ISSN:2156-6976/ajcr0000075

Original Article

Ionizing radiation induces neuroendocrine differentiation of prostate cancer cells *in vitro*, *in vivo* and in prostate cancer patients

Xuehong Deng[1], Bennett D. Elzey[2], Jean M. Poulson[3], Wallace B. Morrison[3], Song-Chu Ko[4], Noah M. Hahn[5], Timothy L. Ratliff[2], Chang-Deng Hu[1]

[1]Department of Medicinal Chemistry and molecular pharmacology, [2]Department of Comparative Pathobiology, and [3]Department of Veterinary Clinical Sciences[3], Purdue University, West Lafayette, IN 47907, USA, [4]Department of Radiation Oncology and [4]Department of Medicine, Indiana University Melvin and Bren Simon Cancer Center, Indianapolis, IN 46202, USA

Received July 3, 2011; accepted July 27, 2011; Epub August 18, 2011; Published August 30, 2011

Abstract: Prostate cancer remains the most common noncutaneous cancer among American men. Although most patients can be cured by surgery and radiotherapy, 32,050 patients still died of the disease in 2010. Many patients receive radiotherapy either as a primary therapy, salvage therapy, or in combination with surgery or hormonal therapy. Despite initial treatment, several studies suggest that approximately 10% of low-risk prostate cancer patients and up to 30-60% with more advanced cancer patients experience biochemical recurrence within five years after radiotherapy. Thus, elucidating the molecular mechanisms underlying radioresistance and tumor recurrence has the potential to significantly reduce prostate cancer mortality. We previously demonstrated that fractionated ionizing radiation (IR) can induce the prostate cancer cell line LNCaP to undergo neuroendocrine differentiation (NED) by activation of cAMP response element binding protein (CREB) and cytoplasmic sequestration of ATF2, two CRE-binding transcription factors that oppose each other to regulate NED. Importantly, IR-induced NED is reversible and de-differentiated cells are cross-resistant to IR, androgen depletion and docetaxel treatments. These findings suggest that radiation-induced NED may allow prostate cancer cells to survive treatment and contribute to tumor recurrence. In the present study, we further demonstrated that IR also induces NED in a subset of DU-145 and PC-3 cells. In addition, we confirmed that IR induces NED in LNCaP xenograft tumors in nude mice, and observed that the plasma chromogranin A (CgA) level, a biomarker for NED, is increased by 2- to 5-fold in tumor-bearing mice after fractionated radiation doses of 20 and 40 Gy, respectively. Consistent with these *in vivo* findings, a pilot study in prostate cancer patients showed that the serum CgA level is elevated in 4 out of 9 patients after radiotherapy. Taken together, these findings provide evidence that radiation-induced NED is a general therapeutic response in a subset of prostate cancer patients. Thus, a large scale analysis of radiotherapy-induced NED in prostate cancer patients and its correlation to clinical outcomes will likely provide new insight into the role of NED in prostate cancer radiotherapy and prognosis.

Keywords: Ionizing radiation, prostate cancer, neuroendocrine differentiation, ATF2, CREB, radiotherapy

Introduction

Prostate cancer is the second leading cause of cancer death in men in the US [1]. Despite progress over the last two decades, the only curative treatments for localized prostate cancer are surgery and radiotherapy (RT). Although most patients can be cured, several large scale studies suggest that 10% of patients with low-risk prostate cancer and up to 30-60% of patients with high-risk prostate cancer experience biochemical recurrence within 5 years after RT. Among patients with recurrent disease, 20-30% die within 10 years [2-6]. Given that only 2.4% of prostate cancer patients in the US initially present with metastatic disease, the majority of prostate cancer deaths occur in patients who underwent the primary treatment of localized cancer, local recurrence, salvage therapy, and eventually distant recurrence, hormonal therapy, and death. Because RT is: 1) one of the primary treatments for low-risk localized prostate cancer, 2) a major treatment for high-risk prostate cancer when combined with hormonal

therapy, 3) a major salvage therapy for local recurrence, and 4) a recommended adjuvant therapy for patients undergoing surgery [7-13], enhancing the sensitivity of prostate cancer cells to RT will likely reduce, or even prevent, tumor recurrence and impact the management of advanced prostate cancer.

The prostate gland contains three types of epithelial cells including luminal, basal and neuroendocrine cells. While luminal and basal cells are the majority of the prostatic epithelial cells, NE cells are less than 1% of total epithelial cells. Although the physiological role of NE cells remains ill-defined, increased number of NE-like cells is observed in advanced prostate cancer patients [14, 15]. NE-like cells are androgen receptor (AR) negative and they do not proliferate [16]. However, NE-like cells secrete a number of peptide hormones and growth factors to support the growth of surrounding tumor cells [17]. In addition, NE-like cells are reversible and can de-differentiate back to a proliferating state, which may contribute to tumor recurrence [18, 19]. Further, NE-like cells express high levels of Bcl-2 and are highly apoptosis resistant [7, 20, 21]. Because the quantification of NED by identifying chromogranin A (CgA) or neuron specific enolase (NSE) positive cells from prostate cancer tissues is affected by several factors such as location of sampling and tumor volume, controversial results regarding the clinical correlation of NED to disease progression have been reported [15, 17, 22-25]. To overcome this challenge, several studies measured serum biomarkers of NED and demonstrated that the serum CgA level is the best biomarker to reflect the extent of NED in prostate cancer tissues [26-28]. Importantly, an increase in the serum CgA level correlates with disease progression and the acquisition of castration-resistant prostate cancer [25, 27, 29-32], suggesting that NED may represent a novel mechanism by which prostate cancer cells survive treatment and contribute to recurrence. Thus, targeting NE-like cells has recently been proposed and developed as a treatment for prostate cancer [7, 8, 14, 17, 22, 33].

A number of stimuli, such as cAMP [18, 34-36], IL-6 [23, 36-42], androgen ablation therapy [43-48], and EGF [21], have been reported to induce prostate cancer cells to undergo NED. We recently observed that the prostate cancer LNCaP cells also underwent NED after receiving a clinically relevant dose of fractionated ionizing radiation (IR) [19]. Upon IR doses spanning four weeks, the remaining viable cells (~20%) all differentiated into NE-like cells and expressed higher levels of CgA and NSE [19]. Furthermore, we observed that two transcription factors, cAMP response element binding protein (CREB) and activating transcription factor 2 (ATF2), oppose each other to regulate NED. Consistent with this notion, IR induced cytoplasmic sequestration of ATF2 and increased phosphorylation of nuclear CREB. In the present study, we extend these findings to two other prostate cancer cell lines, and provide evidence that radiation also induces NED in LNCaP xenograft tumors in nude mice and in human prostate cancer patients.

Materials and methods

Cell culture and analysis of NED

Cell culture and NED analysis were exactly the same as previously reported [19] except that LNCaP cells were cultured in RPMI1640, DU-145 in MEM, and PC-3 cells in F-12K media. The irradiation protocol (2 Gy/day, 5 days/week), VP16-bCREB, and an ATF2 short-hairpin RNA (shRNA) plasmid used in the present work to determine the effect of IR, VP16-bCREB and ATF2 knockdown on NED in DU-145 and PC-3 cells were also described before [19]. Likewise, immunofluorescence and subcellular fractionation methods were similarly used to determine the effect of IR on the phosphorylation of CREB and subcellular localization of ATF2.

IR-induced NED in xenograft tumors in nude mice

The LNCaP human prostate cancer cells were implanted subcutaneously by injecting $5x10^6$ cells 1:1 in Matrigel into the thighs of 6-week old male athymic nude mice (BALB/c strain). Implanted tumors were allowed to grow to a volume of 300-500 mm^3, prior to irradiation. All tumors were irradiated to a total dose of 40 Gy given in 8 twice weekly fractions of 5 Gy using 6-MV x-rays from a clinical linear accelerator in the Linda and William Fleischhauer Radiation Therapy Facility at the Purdue University School of Veterinary Medicine. Tumors were treated using parallel opposed beams with dose computed manually. Tumor volumes were measured twice a week or during blood sample collec-

tions. For immunohistochemical (IHC) analysis of NED in xenograft tumors, the mice were sacrificed one day after the last treatment (40 Gy total dose), and the resected tumors were fixed in formalin and embedded in paraffin. Tissue slides were prepared at 5 μm thickness, and CgA was stained by the anti-CgA antibody (Abcam). To determine the effect of x-ray irradiation on plasma CgA and PSA levels, veinous blood samples were drawn prior to treatment (0 Gy), after 2 weeks (20 Gy) and after 4 weeks (40 Gy). The plasma CgA and PSA were measured using the CgA EIA kit (Cosmo Bio) and the PSA ELISA Kit (Calbiotech) according to the manufacturer's instructions. Plasma CgA levels were normalized to plasma PSA levels, and fold change compared with the 0 Gy time point was determined. For control mice, the 0 Gy time point was designated when xenograft tumors reached 300-500 mm^3, and blood was drawn for pre-treatment time point. Blood was collected again after 2 weeks and 4 weeks, corresponding with samples collected after 20 Gy and 40 Gy in the irradiated groups. All animal experiments were approved by the Purdue Animal Care and Use Committee (PACUC No. 08-127), and all animal use followed the Assurance of Compliance with Public Health Services Policy on Human Care and Use of Laboratory Animals (Welfare Assurance #A3231-01).

Serum CgA and PSA measurement in human prostate cancer patients

Nine patients diagnosed with localized prostate cancer (six T1c and one of each pT2b, pT2c, and pT3a) were enrolled at Indiana University School of Medicine. All patients signed the consent form and agreed to participate in the pilot study according to the approved Institutional Review Board protocol (0805-43). The average age of patients was 54.6 years old. Five patients were Gleason score 7, one patient was Gleason score 9, and three patients were Gleason score 6. All patients were treated at either the Indiana University Hospital or the Midwest Proton Radiotherapy Institute with the total dose of 70.2-79.2 Gy delivered (2 Gy/day). To determine the effect of RT on serum CgA levels, three blood samples were drawn before the start of RT treatment, in the middle of the treatment (week 4-5), and after the treatment (end of week 7 or 8), designated pre-treatment, mid-treatment and post-treatment, respectively. Serum CgA and PSA levels were measured using the CgA EIA kit (Cosmo Bio) and the PSA ELISA Kit (Calbiotech) according to the manufacturer's instructions. Because some prostate cancer patients maintain a high level of serum CgA, which is likely determined by the number of pre-existing NE-like cells and cancer cells that secrete CgA, serum CgA levels were normalized to serum PSA levels for the calculation of fold change.

Results

IR induces morphological changes and expression of NED markers to various extents in prostate cancer cells

To determine whether our findings with LNCaP cells can be extended to other prostate cancer cells, we performed similar experiments on DU-145 and PC-3 cells as we did with LNCaP cells [19]. In LNCaP cells, cell bodies became smaller and the majority of cells were connected via longer neurites (**Figure 1A**) [19]. In contrast, enlarged and flat cell bodies were observed for both DU-145 and PC-3 cells. Unlike LNCaP cells in which almost all surviving cells showed extended neurites, only a subset of irradiated DU-145 cells (32%) showed neurite outgrowth whereas non-irradiated DU-145 cells did not show any neurite outgrowth (**Figure 1A**). Interestingly, approximately 6% of non-irradiated PC-3 cells already displayed neurite outgrowth whereas IR increased the number of cells with neurite outgrowth to 35%. Consistent with the morphological changes, NSE was also induced in DU-145 and PC-3, albeit to a lesser extent (**Figure 1B**). However, no significant induction of CgA in DU-145 and PC-3 was observed when compared with LNCaP cells. While these results confirm that IR can induce DU-145 and PC-3 cells to differentiate into NE-like cells, they also suggest that a subset of DU-145 and PC-3 cells is refractory to IR. This is also consistent with the differential responses of prostate cancer cell lines to androgen depletion, IL-6, cAMP and EGF treatments [21, 23].

Effect of IR on CREB activation and ATF2 subcellar localization

In LNCaP cells, we observed that IR-induced NED is associated with increased nuclear phospho-CREB and cytoplasmic-localized ATF2. To know whether IR also activates CREB and induces cytoplasmic localization of ATF2 in these

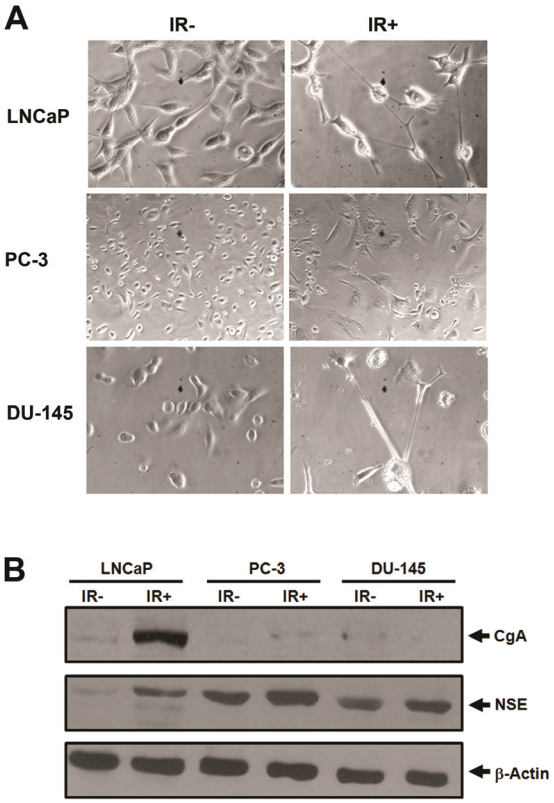

Figure 1. IR induces NED in prostate cancer cells. **A).** Representative images acquired from the indicated prostate cancer cells that were treated with 40 Gy of fractionated IR (IR+) or without IR treatment (IR-) (microscopy at 200x for LNCaP and 100x for PC-3 and DU-145). Note that enlarged and flat cell bodies were observed for irradiated PC-3 when compared with non-irradiated PC-3**. B).** Approximately 40 μg of total lysate from non-irradiated (IR-) and irradiated (40 Gy, IR+) cells was used for immunoblot analysis of CgA, NSE and β-actin. Similar results were reproduced from at least three independent experiments.

cell lines, we performed immunofluorescence analysis and subcellular fraction. We observed that CREB was highly phosphorylated in irradiated DU-145, but to a lesser extent in PC-3 (**Figure 2A**). Interestingly, increased cytoplasmic localization of ATF2 was observed in both DU-145 and PC-3 cells (**Figure 2B**). However, only a subset of cells (~50%) showed cytoplasmic localization of ATF2 in these two cell lines, whereas increased cytoplasmic localization was observed in almost all irradiated LNCaP cells. Consistent with immunofluorescence analysis, subcellular fractionation also showed only a slight increase of ATF2 in the cytosolic fraction in irradiated DU-145 and PC-3 cells, which is likely due to increased cytoplasmic localization of ATF2 in a subset of cells (data not shown). Thus, we conclude that IR can similarly induce CREB activation and impair ATF2 nuclear localization in a subset of DU-145 and PC-3 cells.

Overexpression of VP16-bCREB or ATF2 knockdown induces NED in DU-145 and PC-3 cells

The above results suggest that DU-145 and PC-3 cell may have intrinsic defects in activating CREB or sequestering ATF2 in the cytoplasm in some cells. To know whether these cells can still be induced by VP16-bCREB, a constitutively activated CREB, we performed similar experiments in these two cell lines as we did in LNCaP cells [19]. We observed that overexpression of VP16-bCREB also induced neurite extension in a subset of DU-145 (14%) and PC-3 cells (21%) (**Figure 3A**). Consistent with the morphological changes, a slight induction of both CgA and NSE was observed in DU-145 transfected with the VP16-bCREB plasmid (**Figure 3C**). However, only a slight induction of NSE, but not CgA, was observed in PC-3 cells transfected with the VP16-CREB plasmid (**Figure 3B**). Because the transfection efficiency is relatively low in these two cell lines, these results suggest that expression of VP16-bCREB also induced NED in a subset of DU-145 and PC-3 cells.

Similar results were obtained when ATF2 was knocked down in both DU-145 and PC-3 cells (**Figure 4**). While no extended neurites were observed in DU-145 cells transfected with scrambled control, approximately 25% of DU-145 transfected with the ATF2 shRNA plasmid for five days showed neurite outgrowth. Similarly, 26% of PC-3 cells transfected with the ATF2 shRNA plasmid for five days showed neurite outgrowth whereas 4.5% of cells transfected with the scrambled control plasmid showed neurite outgrowth.

Radiation induces NED in LNCaP xenograft tumors in nude mice

To determine whether IR can induce NED *in vivo*, we employed nude mouse xenograft models. For this purpose, we used LNCaP cells as they can be better induced by IR to undergo NED. We performed x-ray irradiation to xenograft tumors at 10 Gy/week (5 Gy/fraction). Our preliminary results with this irradiation protocol

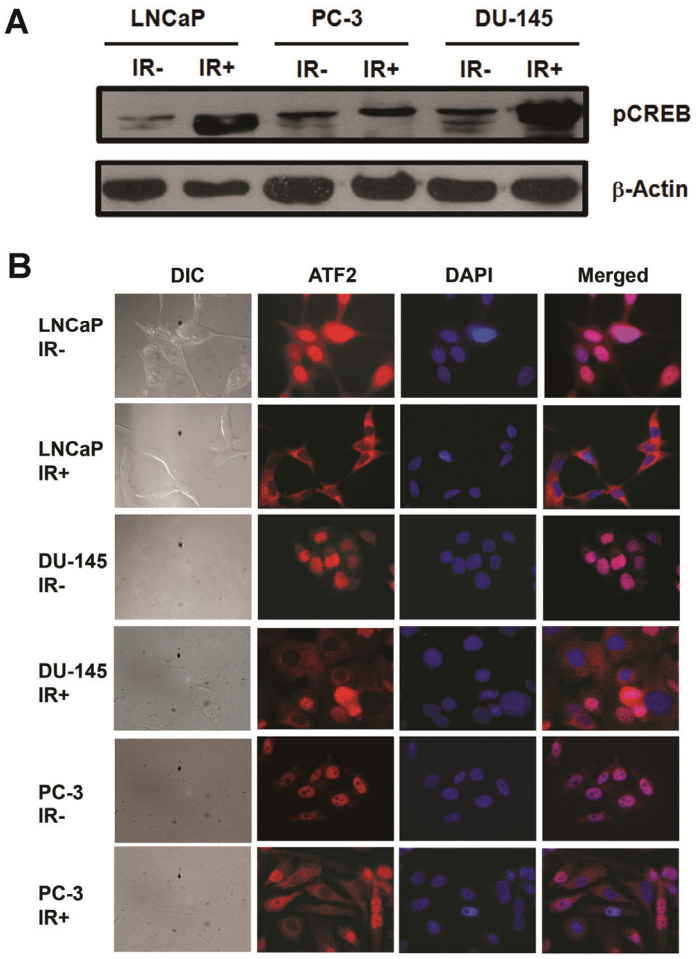

Figure 2. IR induces CREB activation and cytoplasmic sequestration of ATF2 in prostate cancer cells. **A).** A representative immunoblot analysis of phosphorylated CREB (pCREB) from non-irradiated cells (IR-) or from cells that received 10 Gy of fractionated IR (IR+). **B).** Shown are DIC and fluorescent images for ATF2 and DNA (DAPI) acquired from the indicated non-irradiated prostate cancer cells (IR-) or from cells that received 10 Gy of fractionated IR (IR+) (microscopy at 600x). These experiments were reproduced at least three times and similar results were obtained.

also induced NED *in vitro* (unpublished observation). At the end of four weeks, mice were sacrificed and residual tumor nodules were resected for IHC analysis of CgA expression. Compared to non-irradiated tumors (n=3), some cells in all irradiated tumors (n=10) showed higher expression of CgA, suggesting that radiation indeed induces NED in xenograft tumors (**Figure 5A**).

Because serum/plasma CgA levels can be used to quantify the extent of NED in prostate cancer tissues in human patients, we next performed similar fractionated IR to xenograft tumors and measured the plasma CgA level. We collected blood samples from tumor-bearing mice (n=10) before irradiation, and at 2 and 4 weeks of irradiation. As controls, blood samples from non-irradiated tumor-bearing mice (n=10) were also collected at corresponding time points (equivalent to 0, 20 and 40 Gy). Higher plasma CgA levels were observed in all mice bearing large tumors regardless of irradiation, likely due to the increased number of LNCaP cells that express basal levels of CgA. Since LNCaP cells secrete PSA, we normalized plasma CgA levels to plasma PSA levels to control for differing amounts of cells present in each tumor. Three out of 10 mice showed elevated plasma CgA levels after 20 Gy of irradiation, and 7 mice showed elevated plasma CgA levels after 40 Gy of irradiation. In contrast, none of the non-irradiated tumor-bearing mice showed any elevation of plasma CgA levels at the corresponding time points. Instead, their normalized CgA levels were lower after 2-4 weeks of observation. Because these non-irradiated xenograft tumors continued to grow and reached 1300 mm^3 to 2300 mm^3 at the end of the corresponding 4-week time point, the lower normalized CgA levels in non-irradiated mice are likely due to increased PSA production by LNCaP cells under hypoxic conditions in these large tumors [49]. When plasma CgA levels in all 10 irradiated mice were considered, the average plasma CgA levels increased by 2- and 5-fold at the end of 2- and 4-week irradiation, respectively, whereas the average plasma CgA levels for the control group decreased by 2-4 fold at the end of 2- to 4- weeks' observation, respectively (**Figure 5B**). Thus, we conclude that x-ray irradiation can induce NED in xenograft tumors.

Prostate cancer patients show elevated levels of serum CgA after radiotherapy

Because serum CgA has been used as a bio-

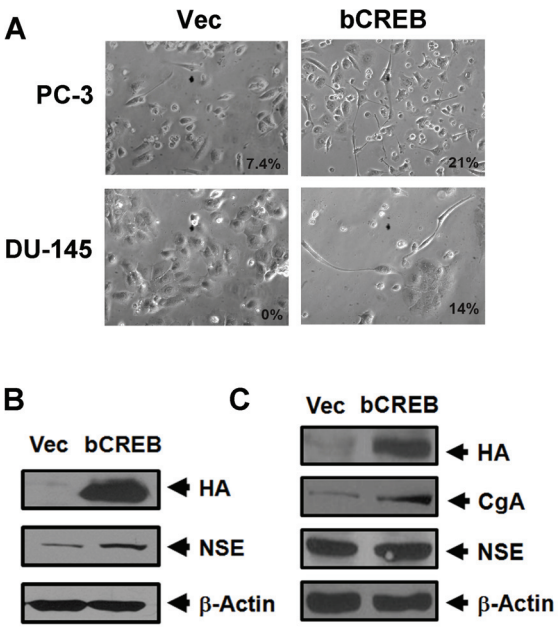

Figure 3. Activated CREB induces neurite outgrowth and the expression of CgA and NSE in PC-3 and DU-145 cells. **A)**. Prostate cancer cells PC-3 and DU-145 were transfected with a pHA-CMV plasmid encoding a constitutively activated CREB, VP16-bCREB (bCREB), or the pHA-CMV empty vector (Vec). Shown are phase contrast images acquired five days after the transfection (microscopy at 200x). The number indicates the percentage of cells showing neurite outgrowth. **B)** and **C)**. Expression of HA-VP16-bCREB (HA), CgA, NSE and β-actin in PC-3 cells (B) or DU-145 cells (C) from the experiments in A. Note that CgA was not detectable in PC-3 cells transfected with the vector control pHA-CMV or pHA-VP16-bCREB.

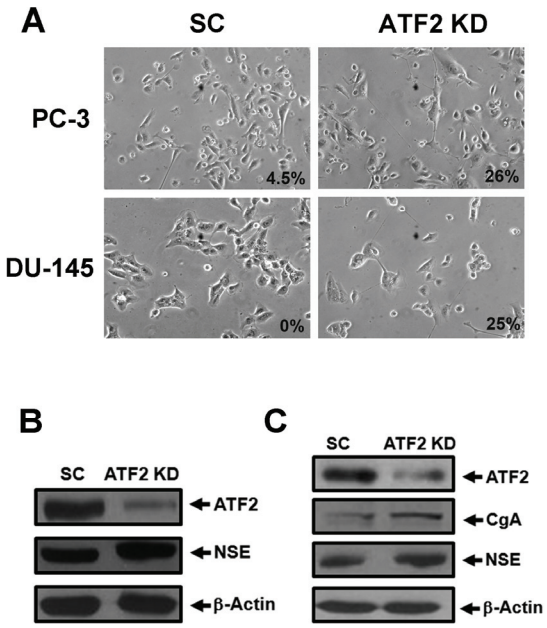

Figure 4. ATF2 knockdown induces neurite outgrowth and the expression of CgA and NSE in prostate cancer cells. **A)**. Prostate cancer cells PC-3 and DU-145 were transfected with the ATF2 shRNA plasmid (ATF2 KD) or the scrambled control (SC). Shown are phase contrast images acquired five days after the transfection (Microscopy at 200x). The number indicates the percentage of cells showing neurite outgrowth. **B)** and **C)**. Expression of ATF2, CgA, NSE and β-actin in PC-3 cells (B) or DU-145 cells (C) from the experiments in A. Note that CgA was not detectable in PC-3 cells transfected with either SC or ATF2 shRNA plasmids.

marker to monitor hormonal therapy-induced NED in prostate cancer patients [25, 27, 29-32], the above observations that x-ray irradiation to xenograft tumors increased plasma CgA levels in nude mice prompted us to test if RT also induces serum CgA elevation in human prostate cancer patients. To this end, we collected blood samples before RT, in the middle of RT, and immediately after RT from prostate cancer patients enrolled at Indiana University School of Medicine, and measured serum CgA and PSA levels. Except for one patient from whom we missed the collection of his blood sample at the middle time point, we collected blood samples at all three time points from the other 8 patients. Among these 8 patients, 2 showed an increase in the serum CgA level at the middle of the RT treatment, and interestingly, 6 patients showed a decrease in the serum CgA level. However, the CgA level at the end of the RT treatment in these 6 patients rebounded to the pre-treatment level or higher (**Figure 6**). When compared with the pre-treatment CgA level, 4 out of 9 patients showed 1.5-2.2 fold increase in serum CgA levels, 2 were unchanged, and 2 had a slight decrease (less than 2 fold) after RT treatment. Thus, approximately 44% (4 out of 9) of patients showed serum CgA elevation after RT.

Discussion

Based on our recent findings that IR can induce NED in LNCaP cells, we provide evidence here that IR also induces NED in DU-145 and PC-3 cells, albeit to a lesser extent. Consistent with this, IR treatment induced cytoplasmic localization of ATF2 and CREB phosphorylation in a sub-

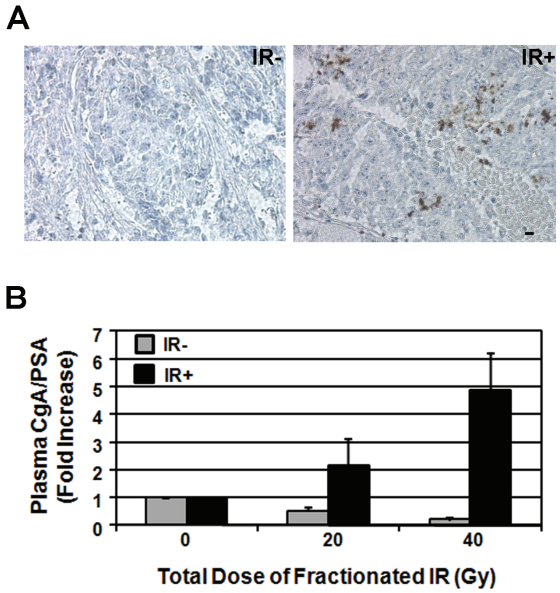

Figure 5. Ionizing radiation induces CgA expression in LNCaP xenograft tumors and an increase of plasma CgA levels in nude mice. **A)**. IHC analysis of CgA expression in irradiated LNCaP xenograft tumors after 40 Gy (IR+) or in non-irradiated xenograft tumors (IR-) (microscopy at 400x). Scale bar represents 10 μm. **B)**. Average fold change of plasma CgA levels normalized to plasma PSA at the end of week 2 (20 Gy) and week 4 (40 Gy) when compared with pre-irradiation (0 Gy). Similar time points were followed for blood collection from non-irradiated tumor-bearing mice. The average fold change presented is from all 10 mice for each group.

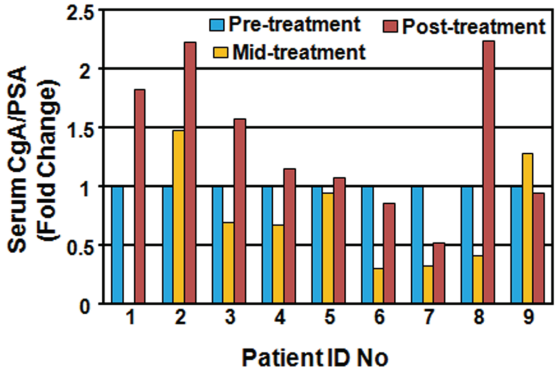

Figure 6. Radiotherapy increases serum CgA levels in prostate cancer patients. All 9 prostate cancer patients were diagnosed with localized tumors and treated at the Indiana University Hospital or the Midwest Proton Radiotherapy Institute with 70.2-79.2 Gy (2 Gy/fraction). Blood samples were collected for pre-treatment, mid-treatment, and post-treatment. The serum CgA levels were normalized to the serum PSA levels, and the fold change at mid- and post-treatment time points is presented for each patient.

set of cells. Likewise, expression of a constitutively activated CREB or ATF2 knockdown also induced the expression of NSE and/or CgA, and neurite extension in these two cell lines. Thus, it is likely that radiation-induced NED is a general phenomenon. Furthermore, we showed that IR also induced NED in LNCaP xenograft tumors in nude mice and that RT also induced elevation of serum CgA levels in 4 out of 9 prostate cancer patients. Our findings here together suggest that radiation-induced NED may represent a therapeutic response in a subset of prostate cancer patients undergoing radiotherapy.

Difference between LNCaP, DU-145 and PC-3 cells

The LNCaP cell line was established from a local metastasized lymph node whereas DU-145 and PC-3 were established from metastasized tumors in brain and bone, respectively [50]. Although the treatment history of these patients is not clear, it is possible that DU1-45 and PC-3 cells were established after extensive exposures to treatments. In addition, DU-145 and PC-3 cells do not express detectable levels of AR and other genetic, or possibly epigenetic, changes may be involved. These intrinsic differences may be responsible for the differential induction of NED by other stimuli as well [23, 34]. Consistent with these observations, three clones isolated from regrowing cells after IR-induced NED are poorly responsive to IR and ADT [19]. Interestingly, we observed that CREB activation and ATF2 cytoplasmic sequestration only occurred in a subset of DU-145 and PC-3 cells after fractionated IR whereas almost all LNCaP cells after 10 Gy showed increased pCREB in the nucleus and an increase of cytoplasmic localized ATF2. These observations suggest that while DU-145 and PC-3 cells do contain a subset of cells that are inducible by IR to undergo NED, there are also some cells that are refractory to NED. Further analysis of these intrinsic differences among these three cell lines may shed new light on the molecular mechanisms underlying IR-induced NED.

CgA as a biomarker to monitor RT-induced NED

IHC staining of CgA and NSE has been widely used to identify NE-like cells in prostate cancer

tissues. Because of the difficulty in quantifying NED using the IHC method, controversial results have been reported [15, 17, 22-25]. To resolve these controversies, several groups examined serum NED biomarkers and demonstrated that serum CgA is the best biomarker that can reflect NED in tissues [26-28]. In our xenograft nude mouse model, we not only observed increased numbers of tumor cells expressing higher levels of CgA in irradiated xenograft tumors, but we also observed an increase in the plasma CgA level in a dose-dependent manner in the majority of mice bearing irradiated xenograft tumors. In contrast, no increase in plasma CgA levels was observed in any of the non-irradiated tumor-bearing mice. Our results suggest that plasma or serum CgA levels can be used to monitor NED during treatment. In fact, results from a preliminary test with 9 prostate cancer patients suggest that RT increases serum CgA levels in 4 out of 9 patients after RT. It is worth noting that a previous study measured serum CgA levels in 100 prostate cancer patients before RT and three months after RT, and observed that 10 patients also showed elevated serum CgA levels three months after RT [51]. Since the number of prostate cancer cells has an impact on serum CgA levels, it is possible that many patients who underwent NED during treatment may eventually show lower CgA levels due to the decrease in tumor cells. Because prostate cancer patients also often have pre-existing NE-like cells, it is therefore important to monitor patient's responses during RT by measuring serum CgA at multiple time points and compare with the serum CgA level before treatment. Indeed, we observed that 6 patients showed an initial decrease in serum CgA levels by the middle of RT, but rebound to levels comparable to or higher than before RT. Because tumors start to shrink once treatment begins, an initial decrease in serum CgA levels and subsequent rebound after completion of the treatment may provide an interesting pattern to monitor RT-induced NED. Though one limitation of this pilot study is the small sample size, the preliminary finding warrants a detailed analysis of RT-induced NED and its correlation to clinical outcomes.

Can targeting NED be explored as a novel radiosensitization approach?

The extent of pre-existing NE-like cells and hormonal therapy-induced NED appear to contribute to disease progression and poor prognosis [25, 27, 29-32]. It is therefore proposed that targeting NED can be explored as a novel therapeutic approach [7, 8, 14, 17, 22, 33]. We have observed that CREB activation can be induced by radiation doses as low as 10 Gy in prostate cancer cells. In the case of LNCaP cells, approximately 80% of cells are killed by IR during the second week, after a total dose of 20 Gy, and the remaining 20% of cells surviving the treatment undergo NED by the end of 4 weeks after a total dose of 40 Gy [19]. After that, no cell death occurs after total doses of up to 72 Gy. These observations suggest an interesting model that radiation-induced NED likely includes at least two important phases. The first phase is the selection and enrichment of radioresistant cells during the first two weeks, and the second phase is the NED phase during the second two weeks. Since increased CREB phoshphorylation was observed in a dose-dependent manner during the course of treatment, it is likely that CREB activation is not only involved in radioresistance but also involved in IR-induced NED. Thus, targeting CREB signaling, in principle, may sensitize prostate cancer cells to IR. In fact, targeting of CREB upstream signaling molecules such as PKA and CaMKII in prostate cancer cells can induce cell death or sensitize cells to RT or ADT [52-57]. Because CREB can be phosphorylated and activated by more than 15 different protein kinases such as MAPKs, AKT, PKA, CaMKII, ATM [58] and because many of these protein kinases can be activated by IR [59, 60], future identification of upstream protein kinases involved in radiation-induced CREB activation and NED may enable development of effective radiosensitizers for prostate cancer treatment.

Acknowledgements

We appreciate the input from the Hu lab, and we also thank Drs. Sarah Parson, Evan Keller, Jiaoti Huang, Liang Cheng, Peter Johnstone, and Michael Koch for the support and consultation during the course of this work. Thanks to Sandra Torregrosa-Allen in the Molecular Discovery and Evaluation Shared Resource for the establishment of xenograft tumors, blood collections, and animal care. Thanks to Caroline Bolyard and Jill Huenemann in the Purdue Veterinary Teaching Hospital for technical assistance with mouse irradiation. This work was supported, in part, by grants from the U.S. Army Medical Re-

search Acquisition Activity, Prostate Cancer Research Program grant PC073098, Purdue University Center for Cancer Research Small Grants Program, and the Indiana Clinical and Translational Science Institute funded, in part, by RR025761 from the National Institutes of Health, National Center for Research Resources, Clinical and Translational Sciences Award. DNA sequencing and animal experiments were conducted in the Purdue University Center for Cancer Research Genomic Core Facility and the Molecular Discovery and Evaluation Shared Resource supported by NCI CCSG CA23168 to Purdue University Center for Cancer Research.

Address correspondence to: Dr. Chang-Deng Hu, Medicinal Chemistry and Molecular Pharmacology, Purdue University, West Lafayette, IN 47907, USA, Tel: 1-765-496-1971; Fax: 1-765-494-1414 E-mail: hu1@purdue.edu

References

[1] Jemal A, Siegel R, Ward E, Hao Y, Xu J, Thun MJ. Cancer statistics, 2009. CA Cancer J Clin 2009; 59: 225-49.

[2] Kuban DA, Thames HD, Levy LB, Horwitz EM, Kupelian PA, Martinez AA, Michalski JM, Pisansky TM, Sandler HM, Shipley WU, Zelefsky MJ, Zietman AL. Long-term multiinstitutional analysis of stage T1-T2 prostate cancer treated with radiotherapy in the PSA era. Int J Radiat Oncol Biol Phys 2003; 57: 915-28.

[3] Zietman AL, DeSilvio ML, Slater JD, Rossi CJ, Jr., Miller DW, Adams JA, Shipley WU. Comparison of conventional-dose vs high-dose conformal radiation therapy in clinically localized adenocarcinoma of the prostate: a randomized controlled trial. JAMA 2005; 294: 1233-9.

[4] D'Amico AV, Chen MH, Renshaw AA, Loffredo B, Kantoff PW. Risk of prostate cancer recurrence in men treated with radiation alone or in conjunction with combined or less than combined androgen suppression therapy. J Clin Oncol 2008; 26: 2979-83.

[5] Agarwal PK, Sadetsky N, Konety BR, Resnick MI, Carroll PR. Treatment failure after primary and salvage therapy for prostate cancer: likelihood, patterns of care, and outcomes. Cancer 2008; 112: 307-14.

[6] Kimura M, Mouraviev V, Tsivian M, Mayes JM, Satoh T, Polascik TJ. Current salvage methods for recurrent prostate cancer after failure of primary radiotherapy. BJU Int 2009; 105: 191-201.

[7] Raldow A, Hamstra DA, Kim SN, Yu JB. Adjuvant radiotherapy after radical prostatectomy: evidence and analysis. Cancer Treat Rev 2011; 37: 89-96.

[8] Rosenthal SA, Sandler HM. Treatment strategies for high-risk locally advanced prostate cancer. Nat Rev Urol 2010; 7: 31-8.

[9] Choe KS, Liauw SL. Radiotherapeutic strategies in the management of low-risk prostate cancer. ScientificWorldJournal 2010; 10: 1854-69.

[10] Cooperberg MR, Broering JM, Litwin MS, Lubeck DP, Mehta SS, Henning JM, Carroll PR. The contemporary management of prostate cancer in the United States: lessons from the cancer of the prostate strategic urologic research endeavor (CapSURE), a national disease registry. J Urol 2004; 171: 1393-401.

[11] Trock BJ, Han M, Freedland SJ, Humphreys EB, DeWeese TL, Partin AW, Walsh PC. Prostate cancer-specific survival following salvage radiotherapy vs observation in men with biochemical recurrence after radical prostatectomy. JAMA 2008; 299: 2760-9.

[12] Chin JL. Post-radical prostatectomy management options for the positive surgical margin: argument for adjuvant radiotherapy. Urol Oncol 2009; 27: 87-8.

[13] Bolla M, Van Tienhoven G, Warde P, Dubois JB, Mirimanoff RO, Storme G, Bernier J, Kuten A, Sternberg C, Billiet I, Torecilla JL, Pfeffer R, Cutajar CL, Van der Kwast T, Collette L. External irradiation with or without long-term androgen suppression for prostate cancer with high metastatic risk: 10-year results of an EORTC randomised study. Lancet Oncol 2010; 11: 1066-73.

[14] Daneshmand S, Quek ML, Pinski J. Neuroendocrine differentiation in prostate cancer. Cancer Therapy 2005; 3: 383-396.

[15] Nelson EC, Cambio AJ, Yang JC, Ok JH, Lara PN, Jr., Evans CP. Clinical implications of neuroendocrine differentiation in prostate cancer. Prostate Cancer Prostatic Dis 2007; 10: 6-14.

[16] Bonkhoff H. Neuroendocrine differentiation in human prostate cancer. Morphogenesis, proliferation and androgen receptor status. Ann Oncol 2001; 12 Suppl 2: S141-4.

[17] Amorino GP, Parsons SJ. Neuroendocrine cells in prostate cancer. Crit Rev Eukaryot Gene Expr 2004; 14: 287-300.

[18] Cox ME, Deeble PD, Lakhani S, Parsons SJ. Acquisition of neuroendocrine characteristics by prostate tumor cells is reversible: implications for prostate cancer progression. Cancer Res 1999; 59: 3821-30.

[19] Deng X, Liu H, Huang J, Cheng L, Keller ET, Parsons SJ, Hu CD. Ionizing radiation induces prostate cancer neuroendocrine differentiation through interplay of CREB and ATF2: Implications for disease progression. Cancer Res 2008; 68: 9663-9670.

[20] Wang JC. Finding primary targets of transcriptional regulators. Cell Cycle 2005; 4: 356-8.

[21] Humez S, Monet M, Legrand G, Lepage G,

Delcourt P, Prevarskaya N. Epidermal growth factor-induced neuroendocrine differentiation and apoptotic resistance of androgen-independent human prostate cancer cells. Endocr Relat Cancer 2006; 13: 181-95.

[22] Huang J, Wu C, di Sant'Agnese PA, Yao JL, Cheng L, Na Y. Function and molecular mechanisms of neuroendocrine cells in prostate cancer. Anal Quant Cytol Histol 2007; 29: 128-38.

[23] Zelivianski S, Verni M, Moore C, Kondrikov D, Taylor R, Lin MF. Multipathways for transdifferentiation of human prostate cancer cells into neuroendocrine-like phenotype. Biochim Biophys Acta 2001; 1539: 28-43.

[24] di Sant'Agnese PA. Neuroendocrine differentiation in prostatic carcinoma: an update on recent developments. Ann Oncol 2001; 12 Suppl 2: S135-40.

[25] Komiya A, Suzuki H, Imamoto T, Kamiya N, Nihei N, Naya Y, Ichikawa T, Fuse H. Neuroendocrine differentiation in the progression of prostate cancer. Int J Urol 2009; 16: 37-44.

[26] Kamiya N, Suzuki H, Kawamura K, Imamoto T, Naya Y, Tochigi N, Kakuta Y, Yamaguchi K, Ishikura H, Ichikawa T. Neuroendocrine differentiation in stage D2 prostate cancers. Int J Urol 2008; 15: 423-8.

[27] Berruti A, Mosca A, Porpiglia F, Bollito E, Tucci M, Vana F, Cracco C, Torta M, Russo L, Cappia S, Saini A, Angeli A, Papotti M, Scarpa RM, Dogliotti L. Chromogranin A expression in patients with hormone naive prostate cancer predicts the development of hormone refractory disease. J Urol 2007; 178:838-43.

[28] Angelsen A, Syversen U, Haugen OA, Stridsberg M, Mjolnerod OK, Waldum HL. Neuroendocrine differentiation in carcinomas of the prostate: do neuroendocrine serum markers reflect immunohistochemical findings? Prostate 1997; 30: 1-6.

[29] Berruti A, Dogliotti L, Mosca A, Bellina M, Mari M, Torta M, Tarabuzzi R, Bollito E, Fontana D, Angeli A. Circulating neuroendocrine markers in patients with prostate carcinoma. Cancer 2000; 88: 2590-7.

[30] Taplin ME, George DJ, Halabi S, Sanford B, Febbo PG, Hennessy KT, Mihos CG, Vogelzang NJ, Small EJ, Kantoff PW. Prognostic significance of plasma chromogranin a levels in patients with hormone-refractory prostate cancer treated in Cancer and Leukemia Group B 9480 study. Urology 2005; 66: 386-91.

[31] Sciarra A, Monti S, Gentile V, Mariotti G, Cardi A, Voria G, Lucera R, Di Silverio F. Variation in chromogranin A serum levels during intermittent versus continuous androgen deprivation therapy for prostate adenocarcinoma. Prostate 2003; 55: 168-79.

[32] Sasaki T, Komiya A, Suzuki H, Shimbo M, Ueda T, Akakura K, Ichikawa T. Changes in chromogranin a serum levels during endocrine therapy in metastatic prostate cancer patients. Eur Urol 2005; 48: 224-9.

[33] Vashchenko N, Abrahamsson PA. Neuroendocrine differentiation in prostate cancer: implications for new treatment modalities. Eur Urol 2005; 47: 147-55.

[34] Bang YJ, Pirnia F, Fang WG, Kang WK, Sartor O, Whitesell L, Ha MJ, Tsokos M, Sheahan MD, Nguyen P and et al. Terminal neuroendocrine differentiation of human prostate carcinoma cells in response to increased intracellular cyclic AMP. Proc Natl Acad Sci U S A 1994; 91: 5330-4.

[35] Farini D, Puglianiello A, Mammi C, Siracusa G, Moretti C. Dual effect of pituitary adenylate cyclase activating polypeptide on prostate tumor LNCaP cells: short- and long-term exposure affect proliferation and neuroendocrine differentiation. Endocrinology 2003; 144: 1631-43.

[36] Deeble PD, Murphy DJ, Parsons SJ, Cox ME. Interleukin-6- and cyclic AMP-mediated signaling potentiates neuroendocrine differentiation of LNCaP prostate tumor cells. Mol Cell Biol 2001; 21: 8471-82.

[37] Lee SO, Chun JY, Nadiminty N, Lou W, Gao AC. Interleukin-6 undergoes transition from growth inhibitor associated with neuroendocrine differentiation to stimulator accompanied by androgen receptor activation during LNCaP prostate cancer cell progression. Prostate 2007; 67: 764-73.

[38] Qiu Y, Robinson D, Pretlow TG, Kung HJ. Etk/Bmx, a tyrosine kinase with a pleckstrin-homology domain, is an effector of phosphatidylinositol 3'-kinase and is involved in interleukin 6-induced neuroendocrine differentiation of prostate cancer cells. Proc Natl Acad Sci U S A 1998; 95: 3644-9.

[39] Spiotto MT, Chung TD. STAT3 mediates IL-6-induced neuroendocrine differentiation in prostate cancer cells. Prostate 2000; 42: 186-95.

[40] Wang Q, Horiatis D, Pinski J. Inhibitory effect of IL-6-induced neuroendocrine cells on prostate cancer cell proliferation. Prostate 2004; 61: 253-9.

[41] Wang Q, Horiatis D, Pinski J. Interleukin-6 inhibits the growth of prostate cancer xenografts in mice by the process of neuroendocrine differentiation. Int J Cancer 2004; 111: 508-13.

[42] Xie S, Lin HK, Ni J, Yang L, Wang L, di Sant'Agnese PA, Chang C. Regulation of interleukin-6-mediated PI3K activation and neuroendocrine differentiation by androgen signaling in prostate cancer LNCaP cells. Prostate 2004; 60: 61-7.

[43] Ismail AH, Landry F, Aprikian AG, Chevalier S. Androgen ablation promotes neuroendocrine cell differentiation in dog and human prostate. Prostate 2002; 51: 117-25.

[44] Jiborn T, Bjartell A, Abrahamsson PA. Neuroendocrine differentiation in prostatic carcinoma during hormonal treatment. Urology 1998; 51: 585-9.
[45] Jin RJ, Wang Y, Masumori N, Ishii K, Tsukamoto T, Shappell SB, Hayward SW, Kasper S, Matusik RJ. NE-10 neuroendocrine cancer promotes the LNCaP xenograft growth in castrated mice. Cancer Res 2004; 64: 5489-95.
[46] Wright ME, Tsai MJ, Aebersold R. Androgen receptor represses the neuroendocrine transdifferentiation process in prostate cancer cells. Mol Endocrinol 2003; 17: 1726-37.
[47] Yuan TC, Veeramani S, Lin FF, Kondrikou D, Zelivianski S, Igawa T, Karan D, Batra SK, Lin MF. Androgen deprivation induces human prostate epithelial neuroendocrine differentiation of androgen-sensitive LNCaP cells. Endocr Relat Cancer 2006; 13: 151-67.
[48] Zhang XQ, Kondrikov D, Yuan TC, Lin FF, Hansen J, Lin MF. Receptor protein tyrosine phosphatase alpha signaling is involved in androgen depletion-induced neuroendocrine differentiation of androgen-sensitive LNCaP human prostate cancer cells. Oncogene 2003; 22: 6704-16.
[49] Horii K, Suzuki Y, Kondo Y, Akimoto M, Nishimura T, Yamabe Y, Sakaue M, Sano T, Kitagawa T, Himeno S, Imura N, Hara S. Androgen-dependent gene expression of prostate-specific antigen is enhanced synergistically by hypoxia in human prostate cancer cells. Mol Cancer Res 2007; 5: 383-91.
[50] Sobel RE, Sadar MD. Cell lines used in prostate cancer research: a compendium of old and new lines--part 1. J Urol 2005; 173: 342-59.
[51] Lilleby W, Paus E, Skovlund E, Fossa SD. Prognostic value of neuroendocrine serum markers and PSA in irradiated patients with pN0 localized prostate cancer. Prostate 2001; 46: 126-33.
[52] Deeble PD, Cox ME, Frierson HF, Jr., Sikes RA, Palmer JB, Davidson RJ, Casarez EV, Amorino GP, Parsons SJ. Androgen-independent growth and tumorigenesis of prostate cancer cells are enhanced by the presence of PKA-differentiated neuroendocrine cells. Cancer Res 2007; 67: 3663-72.
[53] Rokhlin OW, Taghiyev AF, Bayer KU, Bumcrot D, Koteliansk VE, Glover RA, Cohen MB. Calcium/calmodulin-dependent kinase II plays an important role in prostate cancer cell survival. Cancer Biol Ther 2007; 6: 732-42.
[54] Mamaeva OA, Kim J, Feng G, McDonald JM. Calcium/calmodulin-dependent kinase II regulates notch-1 signaling in prostate cancer cells. J Cell Biochem 2009; 106: 25-32.
[55] Merkle D and Hoffmann R. Roles of cAMP and cAMP-dependent protein kinase in the progression of prostate cancer: cross-talk with the androgen receptor. Cell Signal 2011; 23: 507-15.
[56] Hensley HH, Hannoun-Levi JM, Hachem P, Mu Z, Stoyanova R, Khor LY, Agrawal S, Pollack A. PKA knockdown enhances cell killing in response to radiation and androgen deprivation. Int J Cancer 2011; 128: 962-73.
[57] Rokhlin OW, Guseva NV, Taghiyev AF, Glover RA, Cohen MB. KN-93 inhibits androgen receptor activity and induces cell death irrespective of p53 and Akt status in prostate cancer. Cancer Biol Ther 2010; 9: 224-35.
[58] Johannessen M, Moens U. Multisite phosphorylation of the cAMP response element-binding protein (CREB) by a diversity of protein kinases. Front Biosci 2007; 12: 1814-32.
[59] Dent P, Yacoub A, Contessa J, Caron R, Amorino G, Valerie K, Hagan MP, Grant S, Schmidt-Ullrich R. Stress and radiation-induced activation of multiple intracellular signaling pathways. Radiation Research 2003; 159: 283-300.
[60] Dent P, Yacoub A, Fisher PB, Hagan MP, Grant S. MAPK pathways in radiation responses. Oncogene 2003; 22: 5885-96.

THE JOURNAL OF BIOLOGICAL CHEMISTRY VOL. 287, NO. 11, pp. 8621–8632, March 9, 2012

Critical Role of N-terminal End-localized Nuclear Export Signal in Regulation of Activating Transcription Factor 2 (ATF2) Subcellular Localization and Transcriptional Activity*[S]

Received for publication, August 18, 2011, and in revised form, January 23, 2012 Published, JBC Papers in Press, January 24, 2012, DOI 10.1074/jbc.M111.294272

Chih-Chao Hsu[1] **and Chang-Deng Hu**[2]

From the Department of Medicinal Chemistry and Molecular Pharmacology and the Purdue University Center for Cancer Research, Purdue University, West Lafayette, Indiana 47907

Background: Alteration of ATF2 subcellular localization is involved in multiple human diseases.
Results: A second nuclear export signal was identified in the most N-terminal end of ATF2.
Conclusion: The newly identified nuclear export signal negatively regulates ATF2 nuclear localization and transcriptional activity.
Significance: Understanding how ATF2 subcellular localization is regulated will provide insight into the pathological role of ATF2 in human diseases.

Activating transcription factor 2 (ATF2) belongs to the basic leucine zipper family of transcription factors. ATF2 regulates target gene expression by binding to the cyclic AMP-response element as a homodimer or a heterodimer with c-Jun. Cytoplasmic localization of ATF2 was observed in melanoma, brain tissue from patients with Alzheimer disease, prostate cancer specimens, and ionizing radiation-treated prostate cancer cells, suggesting that alteration of ATF2 subcellular localization may be involved in the pathogenesis of these diseases. We previously demonstrated that ATF2 is a nucleocytoplasmic shuttling protein, and it contains two nuclear localization signals in the basic region and one nuclear export signal (NES) in the leucine zipper domain (named LZ-NES). In the present study, we demonstrate that a hydrophobic stretch in the N terminus, ^{1}MKFKLHV^{7}, also functions as an NES (termed N-NES) in a chromosome region maintenance 1 (CRM1)-dependent manner. Mutation of both N-NES and LZ-NES results in a predominant nuclear localization, whereas mutation of each individual NES only partially increases the nuclear localization. These results suggest that cytoplasmic localization of ATF2 requires function of at least one of the NESs. Further, mutation of N-NES enhances the transcriptional activity of ATF2, suggesting that the novel NES negatively regulates the transcriptional potential of ATF2. Thus, ATF2 subcellular localization is probably modulated by multiple mechanisms, and further understanding of the regulation of ATF2 subcellular localization under various pathological conditions will provide insight into the pathophysiological role of ATF2 in human diseases.

ATF2 (activating transcription factor 2) is a basic leucine zipper (bZIP)[3] protein and is an important member of the activator protein-1 (AP-1) family (1). Like other bZIP transcription factors, ATF2 utilizes its basic region to bind DNA and its leucine zipper region to dimerize with its partners. ATF2 binds the cAMP-response element, T(G/T)ACGTCA, as a homodimer or ATF2·c-Jun heterodimer (2–4), and regulates transcription of a large set of genes, including those involved in anti-apoptosis (5, 6), cell growth (7, 8), and DNA damage response (9).

The transcriptional activity of ATF2 can be regulated by multiple mechanisms. First, the transcriptional activity of ATF2 is regulated by phosphorylation at Thr-69 and Thr-71 within the N-terminal transactivation domain (10–12). In response to growth and stress signals, these two residues can be phosphorylated by mitogen-activated protein kinases (MAPKs), including extracellular signal regulated kinase (ERK), c-Jun N-terminal kinase (JNK), and p38 (10–12). The phosphorylation-induced transcriptional activity may be achieved by increasing the intrinsic histone acetylase activity of ATF2 (13), promoting DNA binding (14), and/or preventing it from ubiquitination (15, 16). Second, the transcriptional activity of ATF2 is regulated by an intramolecular interaction between the N-terminal transactivation domain and the bZIP domain (17). This is largely based on the observation that the activity of ATF2 is limited when it is exogenously expressed without coexpression with its dimerization partners or coactivators (17–20). It was proposed that the activity of ATF2 is repressed by an intramolecular interaction between the N-terminal domain and the bZIP domain (17). However, when coexpressed with coactivators, such as CREB-binding protein or E1A (21), the intramolecular interaction is disrupted. Third, the transcriptional activity is regulated by its subcellular localization. We recently demonstrated that ATF2 is a nucleocytoplasmic shuttling protein, and its subcellular localization is regulated by its

* This work is supported in part by grants from the National Science Foundation, American Heart Association, and the United States Department of Defense and by Purdue University Center for Cancer Research Small Grants.
[S] This article contains supplemental Figs. 1–9.
[1] Supported by the Purdue Research Foundation Graduate Fellowship and Ronal W. Dollens Graduate Scholarship in the Life Sciences.
[2] To whom correspondence should be addressed: 575 Stadium Mall Dr., West Lafayette, Indiana 47907. Tel.: 765-496-1971; Fax: 765-494-1414; E-mail: hu1@purdue.edu.

[3] The abbreviations used are: bZIP, basic leucine zipper; NLS, nuclear localization signal; NES, nuclear export signal; LMB, leptomycin B; CREB, cAMP-response element-binding protein; IP, immunoprecipitation; NTD, N-terminal domain.

dimerization (19). Interestingly, overexpressed ATF2 is predominantly localized in the cytoplasm due to the inadequate level of Jun proteins anchoring ATF2 in the nucleus (19). This finding not only uncovers a novel regulatory mechanism of ATF2 transcriptional activity but also provides an alternative mechanism, that the limited transcriptional activity of overexpressed ATF2 may be due to its insufficient nuclear localization in addition to the intramolecular interaction.

Alteration of ATF2 subcellular localization appears to be implicated in the pathogenesis of several human diseases. In melanoma specimens, cytoplasmic localized ATF2 is associated with a better outcome, whereas strong nuclear staining correlates with a poor prognosis (22). In skin cancer, reduced nuclear ATF2 was observed in most basal and squamous cell carcinoma cells (23). In the brain, cytoplasmic ATF2 was observed in cortical neurons of patients with Alzheimer disease (24). In prostate cancer, increased cytoplasmic phosphorylated ATF2 was linked to disease progression (25). Moreover, we recently reported that ionizing radiation-induced cytoplasmic sequestration of ATF2 is involved in neuroendocrine differentiation in prostate cancer cells (26, 27). Although the impact of ATF2 subcellular localization appears to be dependent on disease context, these reports highlight the importance of understanding the molecular mechanisms regulating ATF2 subcellular localization.

Currently, the mechanism by which ATF2 subcellular localization is regulated is not well understood. We have found that ATF2 is a nucleocytoplasmic shuttling protein with a nuclear export signal (NES) and two nuclear localization signals (NLSs) in its leucine zipper and basic region, respectively (19). We have also demonstrated that heterodimerization with the Jun family proteins anchors ATF2 in the nucleus by preventing its nuclear export. On the contrary, homodimerization of ATF2 in the cytoplasm hampers the nuclear import (19). Here, we further show that ATF2 possesses another NES located in the most N-terminal end, which functions in cooperation with the previously identified NES to export ATF2 out of the nucleus. Importantly, this NES negatively regulates ATF2 transcriptional activity.

EXPERIMENTAL PROCEDURES

Antibodies—Monoclonal anti-FLAG M2 antibody and monoclonal anti-hemagglutinin (HA) antibody were purchased from Sigma. Monoclonal anti-Myc antibody is from Clontech (Palo Alto, CA). Monoclonal anti-phospho-ATF2 (Thr(P)-71) antibody (sc-8398), polyclonal anti-GFP antibody (sc-8334), and anti-c-Jun antibody (sc-1694) were obtained from Santa Cruz Biotechnology, Inc. (Santa Cruz, CA).

Plasmid Construction—Localization of wild-type and mutant ATF2 proteins was determined by expressing ATF2 as fusion proteins with Venus(A206K), a monomeric mutant of Venus (28–30). A flexible poly-glycine-serine linker $(GGGGS)_3$ was introduced to the N terminus of Venus (A206K) by PCR. The amplified cDNA encoding $(GGGGS)_3$-Venus(A206K) was cloned into the SalI/BamHI site of pFLAG-CMV2 (Sigma) to produce pFLAG-$(4G1S)_3$-Venus(A206K). cDNAs encoding wild-type and all mutant ATF2 proteins were cloned in frame into NotI/KpnI sites of pFLAG-$(4G1S)_3$-Venus(A206K). All deletions and mutations of ATF2 were made by PCR or ligation PCR (31), and cDNAs encoding these mutant ATF2 proteins were subcloned into pFLAG-$(4G1S)_3$-Venus(A206K). For luciferase reporter gene assays, cDNAs encoding ATF2(N-NES4A), ATF2(LZ-NES3A), and ATF2(N/LZ-NESm) were released from the Venus(A206K) fusion constructs and were subcloned into NotI/KpnI sites of pFLAG-CMV2. To generate C-terminal Myc tag fusion protein, sequence encoding Myc epitope (MASMQKLISEEDL) was introduced in frame downstream of the BamHI site by the PCR method to produce pFLAG-MCS-Myc. The cDNA encoding wild-type or mutant ATF2 was then subcloned into NotI/KpnI sites of pFLAG-MCS-Myc. To make double Venus(A206K) fusion proteins, a PCR-amplified DNA fragment encoding Venus(A206K) was cloned into KpnI/SalI sites of pFLAG-$(4G1S)_3$-Venus(A206K) to produce pFLAG-2xVenus(A206K). PCR-amplified DNA fragments encoding ATF2(1–73) and ATF2(1–73, N-NES4A) were then cloned into NotI/KpnI sites of pFLAG-2xVenus-(A206K) to generate pFLAG-ATF2(1–73)-2xVenus(A206K) and pFLAG-ATF2(1–73, N-NES4A)-2xVenus(A206K), respectively. All constructs generated by the PCR-based method were confirmed by DNA sequencing. The *jun2-luc* reporter plasmid was a gift from Dr. Dorien Peters (32). LZ-NES3A is a substitution of three leucine residues in the NES in the leucine zipper region. N-NES4A, PNES1m, PNES2m, PNES3m, and PNES4m are substitutions of hydrophobic residues in the putative NES within the ATF2 N-terminal domain (NTD), as shown in Figs. 2*A* and 4*B*.

Cell Culture and Fluorescence Imaging Analysis—COS-1 cells were cultured in Dulbecco's modified Eagle's medium supplemented with 5% fetal bovine serum and antibiotics at 37 °C in 5% CO_2. Forty thousand cells per well were seeded in 12-well plates to grow overnight and then transfected with 2 μg of expression vectors indicated in each experiment using Fugene 6 (Roche Applied Science). At 16–18 h post-transfection, cells were fixed with 3.7% formaldehyde in phosphate-buffered saline (PBS) for 20 min. To inhibit nuclear export of ATF2 fusion proteins, transfected cells, at 14 h after transfection, were treated with 20 ng/ml leptomycin B (LMB) for 3.5 h before fixation. Fixed cells were permeabilized with 0.2% Triton X-100 in PBS for 5 min followed by counterstaining with 2.5 μg/ml 4′,6-diamidino-2-phenylindole (DAPI) to visualize nuclei. Localization of various ATF2-Venus(A206K) fusion proteins were examined by a Nikon TE2000-U inverted fluorescence microscope with YFP filters as reported previously (19). All images for purposes of quantification were taken at ×300 magnification. To determine ATF2 localization, five regions of interest, with a diameter of ~4.5 μm, were randomly selected from the nucleus and perinuclear regions, respectively, followed by measuring the intensity of Venus fluorescence within regions of interest using MetaMorph II software. The acquired emission intensities were background-corrected by subtracting mean fluorescence intensity of fields without cells. The localization of wild-type or mutant ATF2-Venus(A206K) within a cell was determined by calculating the ratio of mean nuclear fluorescence intensity to mean cytoplasmic fluorescence intensity. More than 50 individual cells were quantified in each set of experiments, and the ratio of nuclear to cytoplasmic intensity of each fusion protein was presented as mean ± S.E. from at least

three independent experiments. The integrity of all Venus fusion proteins was confirmed by Western blot (supplemental Fig. 1).

Co-Immunoprecipitation (Co-IP)—To determine the interaction between CRM1 (chromosome region maintenance 1) and N-NES, COS-1 cells cultured in a 10-cm dish were co-transfected with 5 μg of pMyc-CRM1 and 5 μg of pFLAG-Venus(A206K)-ATF2(1–341) or pFLAG-Venus(A206K)-ATF2(1–341, N-NES4A) for 2 days. Cells were trypsinized and resuspended in co-IP buffer (50 mM Tris-HCl, pH 7.4, 100 mM NaCl, 10 mM EDTA, 0.1% Triton X-100, 1 mM DTT, 5 μg/ml chymostatin, 5 μg/ml pepstatin A, 5 μg/ml leupeptin, 5 μg/ml antipain, and 5 mM PMSF). Cells were then sonicated to disrupt plasma and nuclear membrane, followed by centrifugation at 14,000 rpm for 10 min at 4 °C. The supernatant containing whole cell lysate (800 μg) was subjected to co-IP using 10 μg of anti-FLAG antibody for 2 h at 4 °C, followed by incubation with protein G beads (Santa Cruz Biotechnology, Inc.) for another 2 h at 4 °C. Bead-bound immune complexes were washed with co-IP buffer four times and subjected to SDS-PAGE followed by immunoblotting analysis with anti-Myc and anti-FLAG antibodies.

To determine the effect of the LZ-NES mutation on ATF2·c-Jun heterodimerization, HEK 293T cells were transfected with 5 μg of FLAG-ATF2-Venus(A206K) or FLAG-ATF2(LZ-NES3A)-Venus(A206K) for 1 day. Cell lysate was prepared as described above and then subjected to co-IP with anti-FLAG antibody (10 μg) at 4 °C overnight, followed by incubation with protein G beads at 4 °C for 2 h. The beads were washed with co-IP buffer six times with a 3-min rotation at 4 °C each time. The associated c-Jun was then detected by Western blot.

Luciferase Reporter Gene Assay—COS-1 cells were cultured in 12-well plates and serum-starved for 18 h. Cells were transfected with 2 μg of each indicated plasmid along with 0.5 μg of the *jun2-luc* reporter plasmid (luciferase reporter construct driven by five tandem repeats of *Jun2*) (32) and 100 ng of pRL-TK (Promega) for 24 h. Firefly and *Renilla* luciferase activities were measured by the Dual Luciferase Reporter Assay kit (Promega) according to the manufacturer's protocol with the following minor modifications. Firefly luciferase activity was measured by mixing 10 μl of cell lysate with 50 μl of LARII reagent. *Renilla* luciferase activity was then determined by mixing the sample with 50 μl of Stop & Glo reagent. The luciferase activity was measured by a TopCount NXT microplate luminescence counter (Packard). Luciferase data were presented as mean ± S.E. from at least three independent experiments performed in duplicate.

Immunostaining—COS-1 cells were fixed at 16 h post-transfection or at the end of LMB treatment with 3.7% formaldehyde for 20 min. Cells were then permeabilized with 0.2% Triton X-100 for 5 min, followed by incubation with mouse monoclonal anti-Myc or anti-HA antibody (1:200 dilution) for 1 h. After three washes with PBS, cells were stained with Texas Red-conjugated anti-mouse IgG secondary antibody and DAPI for another 1 h. Microscopy was similarly performed as reported previously (26). To quantify the nuclear distribution of ATF2 mutants in Fig. 5, COS-1 cells were seeded on coverslips and co-transfected with indicated plasmids and pHA-Venus for 16 h. After performing Myc and DAPI staining, the coverslips were mounted on glass slides with Vectashield Hard Set mounting medium (Vector Laboratories, Burlingame, CA). Venus fluorescent signal was used to define the region of the whole cell body. The percentage of nucleus-localized ATF2 in each individual cell was calculated as (integrated intensity of Myc signal in the nucleus/integrated intensity of Myc signal in the whole cell body) × 100%. Results were presented as means ± S.E. quantified from more than 60 cells.

UV Irradiation—COS-1 cells expressing ATF2(LZ-NES3A)-Venus were irradiated with UVC (120 J/m^2) in a Spectrolinker XL-1000 UV cross-linker (Spectronic Corp.). Cells were harvested at the indicated time points and subjected to Western blot with anti-phospho-ATF2 antibody. The phosphorylation status of the exogenous ATF2 was quantified by ImageJ software.

Statistical Analysis—The data were expressed as means ± S.E. and analyzed by GraphPad Prism 5 (La Jolla, CA). Student's *t* test was used to determine the difference between two groups. For multiple-group comparisons, data were analyzed by one-way analysis of variance, followed by Tukey post-test if significant differences were found.

RESULTS

N-terminal Domain Promotes ATF2 Nuclear Export in CRM1-dependent Manner—We previously demonstrated that ATF2 contains an NES in the leucine zipper region (termed LZ-NES), which, in conjunction with two NLSs in the basic region, regulates ATF2 nucleocytoplasmic shuttling (Fig. 1*A*). We also observed that deletion of the NTD (residues 1–341) of ATF2 increased nuclear localization of Jun-ATF2 heterodimers (33), whereas overexpressed full-length ATF2 was predominantly localized in the cytoplasm despite possession of the two NLS motifs (19). These results suggest that the NTD of ATF2 may negatively regulate ATF2 nuclear localization. To test this possibility, we examined the effect of an NTD deletion on ATF2 subcellular localization. Wild-type and NTD-deleted ATF2 were expressed as fusion proteins with a monomeric form (A206K mutant) of the fluorescent protein Venus in COS-1 cells. As shown in Fig. 1*B*, deletion of the NTD alone resulted in a predominant nuclear localization, demonstrating that the NTD does play a negative role in the nuclear localization of ATF2. To determine the subcellular localization of the NTD, we expressed ATF2(1–341) as a fusion with Venus(A206K) and observed that ATF2(1–341)-Venus(A206K) was predominantly localized in the cytoplasm (Fig. 1*B*). This result suggests that the NTD of ATF2 may possess a cytoplasmic localization activity. Interestingly, treatment of cells with LMB, a CRM1-specific nuclear export inhibitor (34), significantly increased the nuclear localization of ATF2(1–341)-Venus(A206K) (Fig. 1*C*). Thus, predominant cytoplasmic localization of the ATF2 NTD is probably mediated by a CRM1-dependent nuclear export mechanism. To determine whether the nuclear export activity conferred by the NTD is sufficient to drive ATF2 export, we tested the effect of LMB on the localization of ATF2(LZ-NES3A), a previously identified LZ-NES mutant (^{405}VAQLKQLLL^{413} to ^{405}VAQAKQALA^{413}) (19). As we

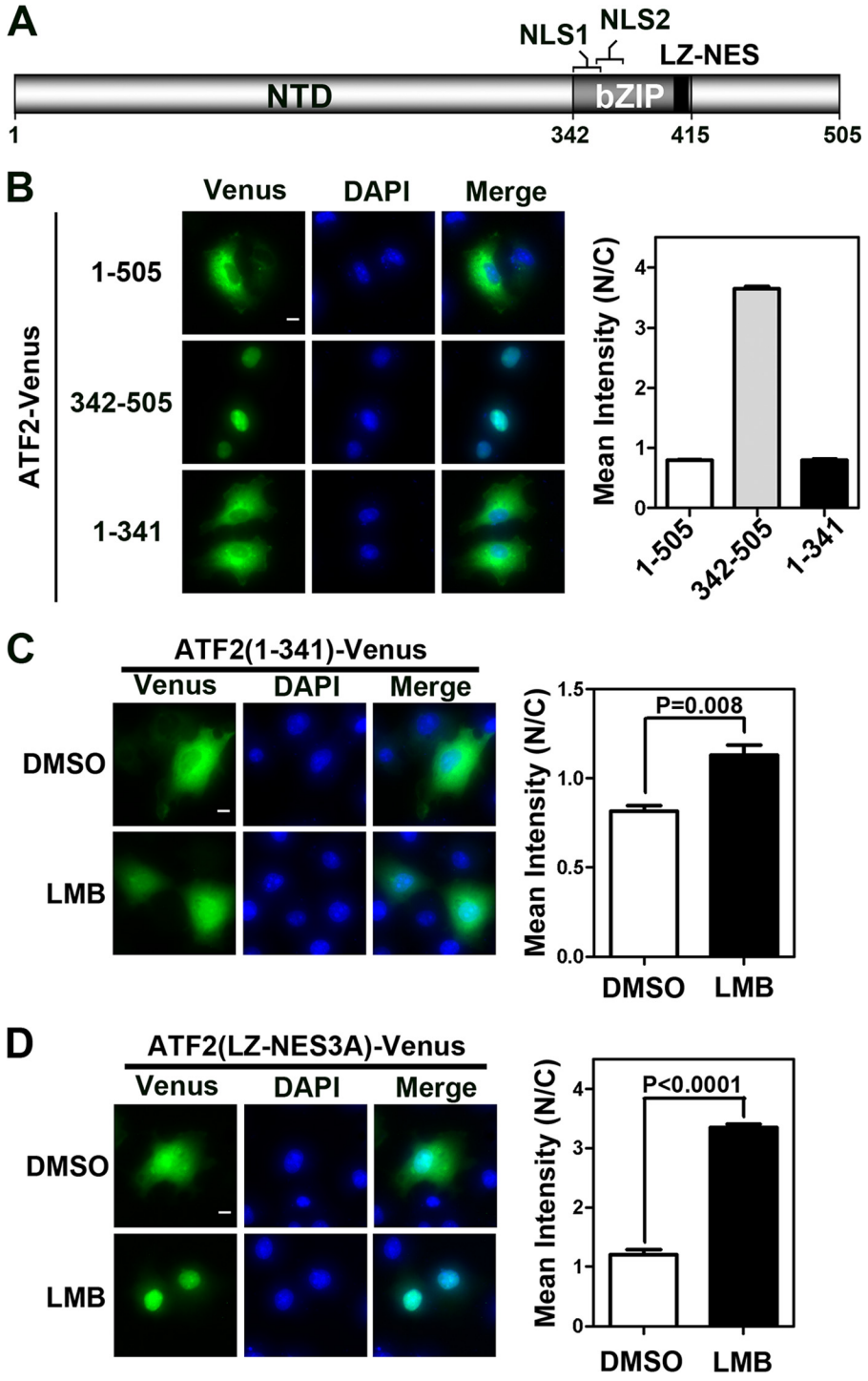

FIGURE 1. **The N-terminal domain contributes to CRM1-dependent nuclear export of ATF2.** *A*, schematic representation of previously identified NLS and NES motifs in ATF2. Two NLSs (NLS1 (residues 342–353) and NLS2 (residues 356–372)) are in the basic region, and one NES (*black box*; residues 405–413) is located in the leucine zipper region. *B*, subcellular localization of the indicated ATF2-Venus(A206K) fusion proteins. COS-1 cells were transfected with plasmids encoding FLAG-ATF2(1–505)-Venus(A206K) (full-length ATF2), FLAG-ATF2(342–505)-Venus(A206K), or FLAG-ATF2(1–341)-Venus(A206K) for 16 h. *Left*, representative images acquired after the cells were fixed, permeabilized, and stained with DAPI. *Scale bar*, 10 μm. *Right*, quantitative results of the ratio of nuclear to cytoplasmic fluorescence intensity from three independent experiments. *C*, effect of LMB on subcellular localization of ATF2(1–341)-Venus(A206K). COS-1 cells were transfected with the plasmid encoding FLAG-ATF2(1–341)-Venus(A206K) for 14 h, followed by LMB (20 ng/ml) or DMSO treatment for 3.5 h. *Left*, representative images. *Scale bar*, 10 μm. *Right*, quantitative results of the ratio of nuclear to cytoplasmic fluorescence intensity from three independent experiments. *D*, effect of LMB on subcellular localization of ATF2(LZ-NES3A)-Venus(A206K). COS-1 cells were transfected with the plasmid encoding FLAG-ATF2(LZ-NES3A)-Venus(A206K) for 14 h, followed by LMB or DMSO treatment for 3.5 h. *Left*, representative images. *Scale bar*, 10 μm. *Right*, quantitative results of the ratio of nuclear to cytoplasmic fluorescence intensity from three independent experiments. *Error bars*, S.E.

observed previously (19), mutation of LZ-NES significantly increased nucleus-localized ATF2 (Fig. 1*D*). Interestingly, treatment of cells with LMB further sequestered ATF2(LZ-NES3A) in the nucleus. Taken together, these results suggest that the ATF2 NTD may possess an additional CRM1-dependent nuclear export activity.

ATF2 NTD Does Not Contain Canonical NES—To determine whether the NTD has any NES motifs, we searched the N-terminal 341 residues of ATF2 using Net NES1.1 (35). We also manually compared the amino acid sequence within the NTD against the canonical NES sequence $\Phi^1X_{2-3}\Phi^2X_{2-3}\Phi^3X\Phi^4$ (where Φ represents Leu, Ile, Val, Phe, or Met, and *X* is any amino acid) (35, 36). These searches identified four putative NES motifs: PNES1, PNES2, PNES3, and PNES4 (Fig. 2*A*). To determine if these motifs are functional NESs, we mutated the conserved hydrophobic residues (shown in *boldface type* in Fig. 2*A*) within each putative NES to alanines in the context of ATF2(LZ-NES3A). As shown in Fig. 2, *B* and *C*, all of these mutations did not increase the nuclear localization of ATF2(LZ-NES3A) in the absence of LMB, whereas LMB treatment still sequestered the mutant fusions in the nucleus. Moreover, ATF2(PNES1–4m, LZ-NES3A)-Venus(A206K), a mutant with all four putative NESs and LZ-NES mutated, remained responsive to LMB. These results suggest that these four putative NES motifs in the NTD do not confer the CRM1-dependent nuclear export activity of ATF2 and that they are not functional NESs.

Residues 1–73 of ATF2 Contain Sequence Required for CRM1-dependent Nuclear Export—Because mutation analysis suggested that the ATF2 NTD does not possess a canonical NES, we then made an N-terminal truncation and a series of internal deletions in the NTD to map the region responsible for mediating the CRM1-dependent nuclear export. To exclude the potential impact of LZ-NES on ATF2 subcellular localization, all of these mutants were generated in the context of ATF2(LZ-NES3A) (Fig. 3*A*). As shown in Fig. 3, *B* and *C*, ATF2(Δ1–73, LZ-NES3A)-Venus(A206K) was almost completely localized in the nucleus, whereas other ATF2 mutants did not show any significant increase in the nuclear localization. Importantly, LMB treatment further increased the nuclear localization of all other ATF2 mutants but not ATF2(Δ1–73, LZ-NES3A)-Venus(A206K). These results suggest that the first 73 residues of ATF2 contribute to the CRM1-dependent nuclear export of ATF2 NTD. Consistent with this notion, the ATF2(1–341) fragment only was predominantly localized in the cytoplasm, whereas the ATF2(74–341) fragment was distributed in both the nucleus and the cytoplasm (supplemental Fig. 2).

Identification of Non-canonical NES in Most N-terminal End of ATF2—To confirm that the first 73 residues of ATF2 may contain an autonomous NES, we fused ATF2(1–73) to the N terminus of 2xVenus(A206K). The fusion to two Venus proteins increases the molecular mass (to ~65 kDa) of the fusion protein and thus attenuates its passive diffusion rate across the nuclear pore complex. Similar strategies have been utilized by others to evaluate NES activity (37–39). As shown in Fig. 4*A*, ATF2(1–73)-2xVenus(A206K) was predominantly localized in the cytoplasm. Importantly, treatment of cells with LMB altered its predominant cytoplasmic localization and increased its localization in the nucleus, reinforcing our hypothesis that a CRM1-dependent NES resides in this region. Because canonical NES is a hydrophobic residue-enriched motif, we then searched for hydrophobic residue-enriched regions within the first 73 residues and identified ^{1}MKFKLHV^7 (termed N-NES) as the only potential hydrophobic stretch. Although this sequence does not match the consensus NES, a similar atypical NES has been reported in Eps15 (40) (Fig. 4*B*). To determine if the hydrophobic stretch functions as an NES, we mutated the four hydrophobic residues to alanines (N-NES4A: ^{1}MKFKLHV^7 to ^{1}AKAKAHA^7) in ATF2(1–73). As shown in Fig. 4*B*, transiently expressed ATF2(1–73, N-NES4A)-2xVenus(A206K) was distributed throughout the cell, suggesting that the hydrophobic residues in the most N-terminal end of ATF2 may function as an NES. We also confirmed that the N-NES is functional in other cell lines, including HEK 293T, LNCaP, and PC3 cells (supplemental Fig. 3). To determine that this atypical NES can be recognized by CRM1, we performed a co-IP assay to verify the interaction between CRM1 and ATF2(1–341). We coexpressed Myc-CRM1 and FLAG-Venus(A206K)-ATF2(1–341) or FLAG-Venus(A206K)-ATF2(1–341, N-NES4A) in COS-1 cells and then performed co-IP with anti-FLAG antibody. The insertion of Venus between FLAG and ATF2 is to avoid masking of the FLAG epitope when CRM1 binds to the NTD of ATF2. We found that Myc-CRM1 was efficiently co-immunoprecipitated with FLAG-Venus(A206K)-ATF2(1–341) but not FLAG-Venus(A206K)-ATF2(1–341, N-NES4A) (Fig. 4*C*), suggesting that the hydrophobic stretch ^{1}MKFKLHV^7 is recognized and bound by CRM1.

To examine the impact of N-NES on ATF2 subcellular localization, we introduced the mutations into ATF2 in the context of full-length ATF2 and determined the localization of ATF2. Mutation of N-NES significantly increased nuclear distribution of ATF2, indicating that N-NES does regulate the subcellular localization of ATF2 (Fig. 4*D*). Importantly, ATF2 was predominantly localized in the nucleus when both N-NES and LZ-NES were mutated. Moreover, LMB treatment did not further increase the nuclear localization of this mutant (supplemental Fig. 4), suggesting that no additional CRM1-dependent NES exists in ATF2. Function of N-NES in full-length ATF2 was also confirmed in HEK 293T and LNCaP cells, albeit N-NES seems to be a dominant export signal in both cell types (supplemental Figs. 5 and 6). Taken together, these results demonstrate that both NESs contribute to the nuclear export of ATF2 and suggest that a complete nuclear localization of ATF2 may require functional inactivation of both NESs.

Transcriptional Activity of ATF2 Is Negatively Regulated by N-NES—We previously demonstrated that the lack of transcriptional activity of exogenously expressed ATF2 is probably due to the predominant cytoplasmic localization of overexpressed ATF2 (19). The increase in nuclear localization of N-NES-disrupted ATF2 prompted us to examine if its transcriptional activity is enhanced. We similarly used the *jun2* luciferase reporter gene to examine the ATF2 transcriptional activity (9, 19, 41). Consistent with our previous observation (19), wild-type ATF2 barely activated the *jun2-luc* reporter (Fig. 5*A*). Interestingly, ~3-fold activation of *jun2-luc* by ATF2(N-NES4A) was observed. On the contrary, ATF2 with mutations in LZ-NES or both NESs did not activate the *jun2-luc* reporter. Because LZ-NES of ATF2 spans between the fourth and fifth heptad of the leucine zipper region and replacement of the leucine in the fourth heptad (corresponding to

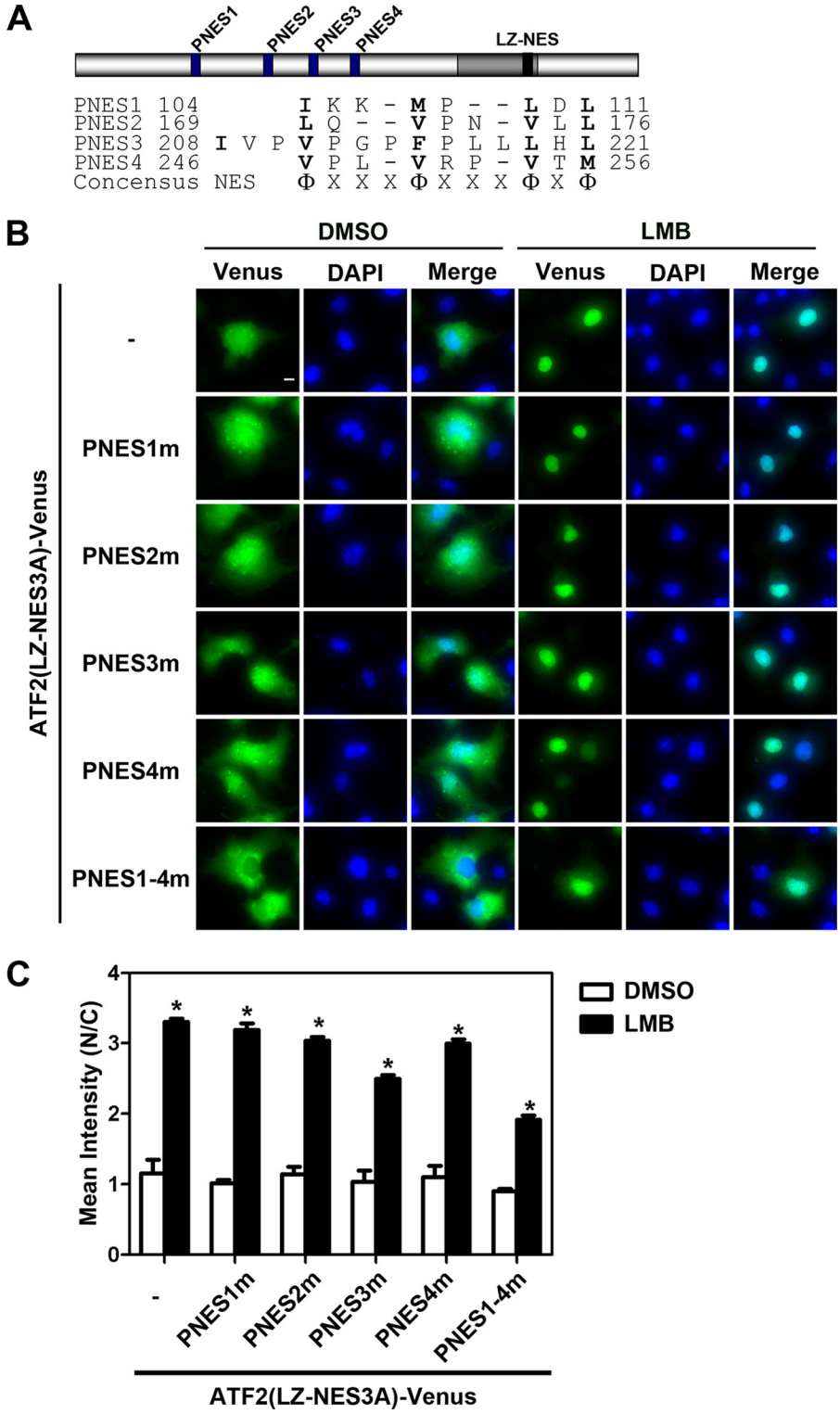

FIGURE 2. **ATF2 NTD does not contain a canonical NES.** *A*, schematic representation of four putative NESs identified in the ATF2 NTD. The amino acids shown in *boldface type* are hydrophobic residues that match the consensus NES. *B*, effects of LMB on subcellular localization of putative NES-mutated ATF2(LZ-NES3A)-Venus(A206K). The hydrophobic residues (shown in *boldface type* in *A*) of each (PNES1m, PNES2m, PNES3m, and PNES4m) or all putative NESs (PNES1–4m) were replaced with alanines in the context of ATF2(LZ-NES3A)-Venus(A206K). COS-1 cells were transfected with plasmids encoding the indicated C-terminal Venus(A206K)-fused proteins for 14 h, followed by LMB or DMSO treatment for 3.5 h. Shown are representative images. *Scale bar*, 10 μm. *C*, quantification of the results in *B*. Shown is the ratio of nuclear to cytoplasmic fluorescence intensity from three independent experiments. *Asterisks* indicate a significant difference ($p < 0.05$) when compared with the respective DMSO treatment group. *Error bars*, S.E.

the Leu-408 of ATF2) with alanine was shown to reduce the stability of leucine-zipper dimer (42, 43), we tested if LZ-NES3A mutation affects heterodimerization of ATF2 and c-Jun, the complex binding to the *jun2* response element (44). A co-IP was used to determine if this mutation affects the binding of exogenous ATF2 to endogenous c-Jun. HEK

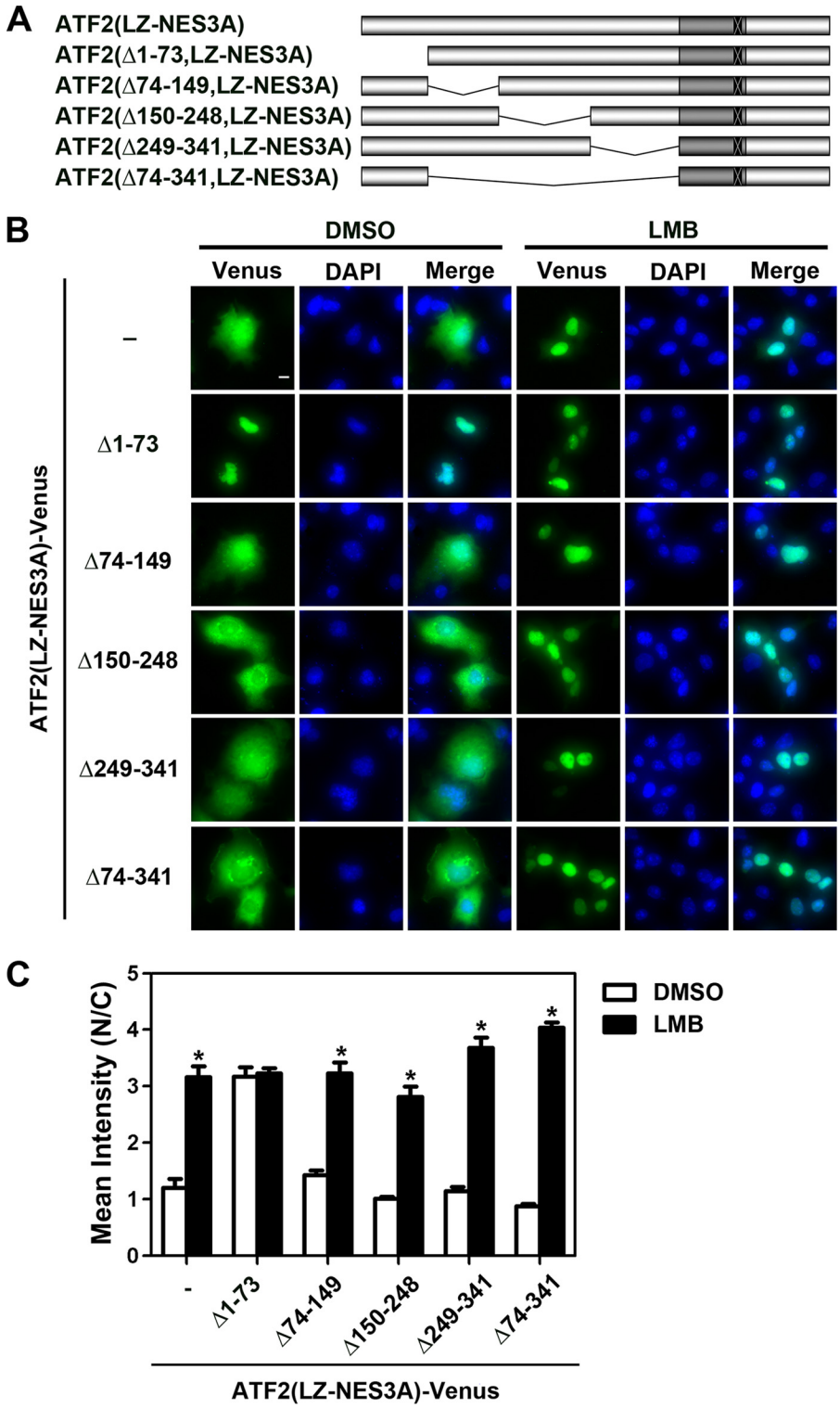

FIGURE 3. **N-terminal 73 residues of ATF2 confer the CRM1-dependent nuclear export activity.** *A*, schematic view of N-terminal truncation and various internal deletion mutants used for mapping the NES within the NTD of ATF2. *B*, effects of LMB on subcellular localization of ATF2(LZ-NES3A)-Venus(A206K) mutants in which various regions within NTD were deleted. COS-1 cells were transfected with plasmids encoding the indicated C-terminal Venus(A206K)-fusion proteins for 14 h, followed by LMB or DMSO treatment for 3.5 h. Shown are representative images. *Scale bar*, 10 μm. *C*, quantification of the results in *B*. Shown is the ratio of nuclear to cytoplasmic fluorescence intensity (*N/C*) from three independent experiments. *, significant difference ($p < 0.05$) when compared with the respective DMSO treatment group. *Error bars*, S.E.

293T cells were used due to the high transfection efficiency, which allowed us to efficiently co-immunoprecipitate endogenous c-Jun. As shown in Fig. 5*B*, LZ-NES3A mutation reduced the interaction between ATF2 and c-Jun, suggesting that the stability of ATF2·c-Jun complex is essential for its transcriptional activity.

We next sought to confirm that the subcellular localization of these ATF2 proteins is similar to that of Venus-fused ones.

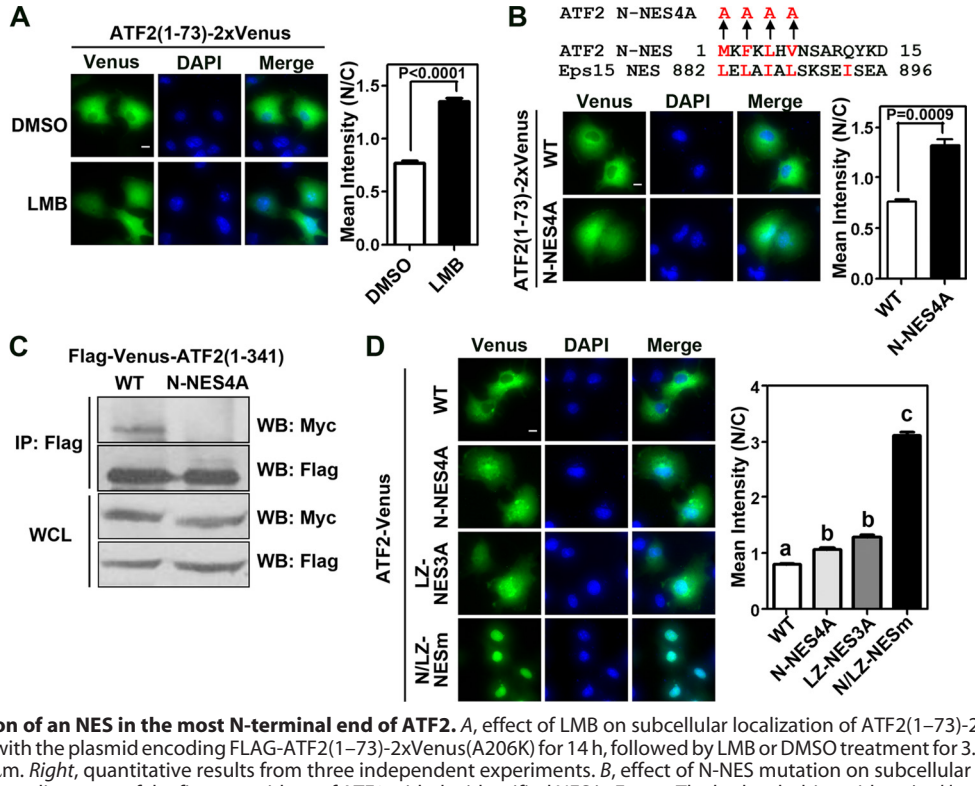

FIGURE 4. **Identification of an NES in the most N-terminal end of ATF2.** *A*, effect of LMB on subcellular localization of ATF2(1–73)-2xVenus(A206K). COS-1 cells were transfected with the plasmid encoding FLAG-ATF2(1–73)-2xVenus(A206K) for 14 h, followed by LMB or DMSO treatment for 3.5 h. *Left*, representative images. *Scale bar*, 10 μm. *Right*, quantitative results from three independent experiments. *B*, effect of N-NES mutation on subcellular localization of ATF2(1–73)-2xVenus(A206K). *Top*, alignment of the first 15 residues of ATF2 with the identified NES in Eps15. The hydrophobic residues (*red letters*) were replaced with alanines in ATF2 to make the N-NES4A mutant. COS-1 cells were transfected with plasmids encoding FLAG-ATF2(1–73)-2xVenus(A206K) or FLAG-ATF2(1–73, N-NES4A)-2xVenus(A206K) for 16 h. *Bottom left*, representative images. *Scale bar*, 10 μm. *Bottom right*, quantitative results from three independent experiments. *C*, interaction of CRM1 with ATF2 N-NES in COS-1 cells. COS-1 cells were co-transfected with plasmids encoding Myc-CRM1 and FLAG-Venus(A206K)-ATF2(1–341) or FLAG-Venus(A206K)-ATF2(1–341, N-NES4A). Whole cell lysate (*WCL*) was immunoprecipitated with anti-FLAG antibody. The immunoprecipitates were examined by Western blot (*WB*) using anti-Myc antibody. Similar levels of exogenous protein expression were confirmed by subjecting 4% of whole cell lysate to Western blot. Shown is a representative co-IP result from three independent experiments. *D*, effect of NES mutations on subcellular localization of full-length ATF2-Venus(A206K). COS-1 cells were transfected with plasmids encoding FLAG-ATF2(WT)-Venus(A206K), FLAG-ATF2(N-NES4A)-Venus(A206K), FLAG-ATF2(LZ-NES3A)-Venus(A206K), or FLAG-ATF2(N/LZ-NESm)-Venus(A206K) for 16 h. *Left*, representative images. *Scale bar*, 10 μm. *Right*, quantitative results from three independent experiments. *Different letters above* the *bars* indicate significant differences ($p < 0.05$) in the ratio of nuclear to cytoplasmic fluorescence intensity (one-way analysis of variance). *Error bars*, S.E.

To avoid the potential masking of FLAG epitope by the CRM1/N-NES interaction, we fused a Myc tag to the C-terminal end of each protein and determined the percentage of nucleus-localized ATF2 mutants by immunostaining with anti-Myc antibody. As shown in Fig. 5*C*, mutation of N-NES increased the nuclear distribution of ATF2 from 14 to 37%, whereas mutation of both NESs further brought the percentage of ATF2 in the nucleus up to 79%. We then performed the same reporter assay and found that mutation of N-NES also significantly enhanced transcriptional activity of the ATF2-Myc fusion protein, albeit to a lesser extent when compared with the counterpart without Myc tag (supplemental Fig. 7). In summary, these results suggest that N-NES negatively regulates ATF2 nuclear localization and the transcriptional activity.

N-NES Is Not Regulated by MAPK Phosphorylation—Transcriptional activity of ATF2 is regulated by MAPKs, which phosphorylate Thr-69/71 in the NTD. We previously demonstrated that MAPK phosphorylation did not affect the subcellular localization of full-length ATF2 with intact N-NES and LZ-NES (19). To determine whether MAPK-mediated phosphorylation has any impact on N-NES, we substituted Thr-69 and -71 with non-phosphorylatable alanine, phosphomimic aspartic acid, or glutamic acid in the background of ATF2(LZ-NES3A). As shown in Fig. 6*A*, none of the substitutions altered the subcellular localization of ATF2. We also found that the exogenous ATF2(LZ-NES3A)-Venus(A206K) but not the alanine mutant was readily phosphorylated at Thr-71 in cells (Fig. 6*B*). To further evaluate the effect of ATF2 Thr-69/Thr-71 phosphorylation on N-NES activity, COS-1 cells expressing ATF2(LZ-NES3A)-Venus(A206K) were subjected to UV irradiation, which induces ATF2 phosphorylation by activating JNK and p38 kinases (9, 12, 45). No significant change in subcellular localization of the exogenous ATF2 was observed (Fig. 6*C*), although UV irradiation indeed enhanced ATF2 phosphorylation (Fig. 6*D*). Taken together, these results indicate that the N-NES is unlikely to be regulated by MAPK-mediated phosphorylation.

DISCUSSION

We previously demonstrated that ATF2 possesses two NLS and one NES (LZ-NES) and constitutively shuttles between the cytoplasm and nucleus in a monomeric form (19). In the present study, we identified another NES (N-NES) in the most N-terminal end of ATF2, suggesting that the subcellular localization of ATF2 is modulated by multiple layers of regulations. Nuclear localization of ATF2 requires formation of a heterodimer with c-Jun, which masks the LZ-NES of ATF2 and anchors ATF2 in the nucleus. With limited c-Jun protein, ATF2

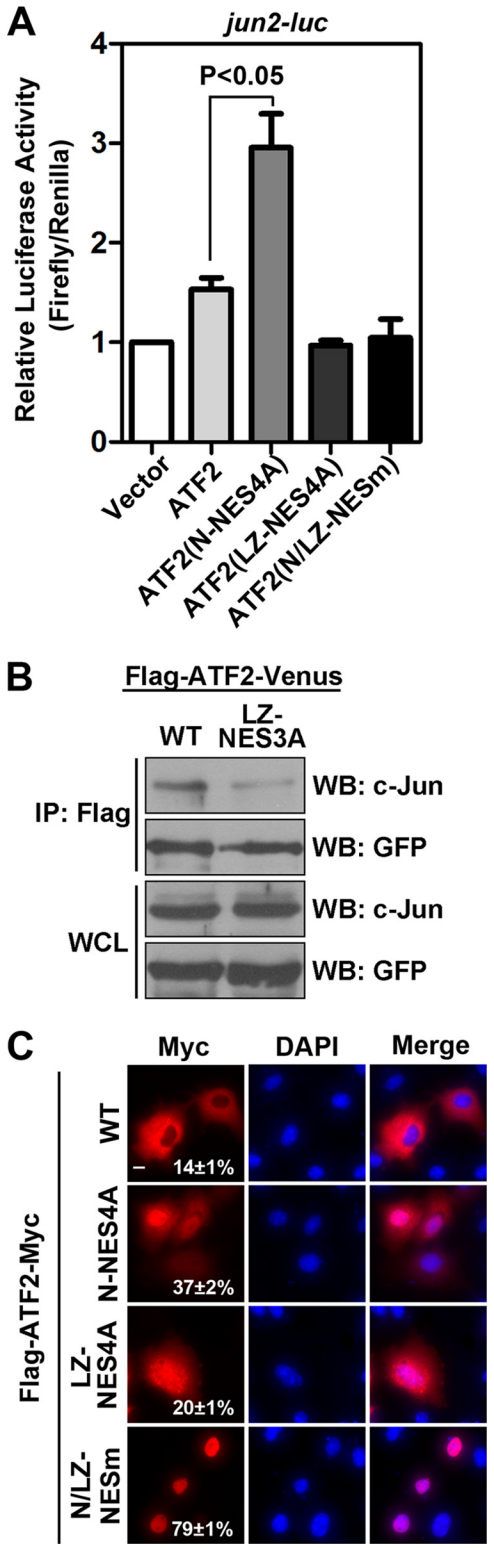

FIGURE 5. **Mutation of N-NES enhanced ATF2 transcriptional activity.** *A*, effect of NES mutations on transcriptional activity of ATF2. Serum-starved COS-1 cells were transfected with 0.5 μg of *jun2-luc*, 100 ng of pRL-TK along with 2 μg of pCMV-FLAG (vector), pFLAG-ATF2, pFLAG-ATF2(N-NES4A), pFLAG-ATF2(LZ-NES3A), or pFLAG-ATF2(N/LZ-NESm) for 24 h. Values of firefly/*Renilla* luciferase were presented as fold change over vector control. Results are shown as mean ± S.E. from three independent experiments done in duplicate. *B*, effect of LZ-NES mutation on ATF2·c-Jun heterodimerization. HEK 293T cells were transfected with plasmids encoding FLAG-ATF2-Venus(A206K) or FLAG-ATF2(LZ-NES3A)-Venus(A206K). Whole cell lysate (*WCL*) was immunoprecipitated with anti-FLAG antibody followed by Western blot (*WB*) analysis with anti-c-Jun antibody. Similar levels of exogenous protein expression were confirmed by subjecting 2% of whole cell lysate to Western blotting with anti-GFP antibody, which recognizes Venus. Shown is a representative co-IP result from two independent experiments. *C*, effect of NES mutations on subcellular localization of ATF2-Myc fusion proteins. COS-1 cells were transfected with pHA-Venus along with plasmids encoding FLAG-ATF2-Myc, FLAG-ATF2(N-NES4A)-Myc, FLAG-ATF2(LZ-NES3A)-Myc, or FLAG-ATF2(N/LZ-NESm)-Myc for 16 h. Cells were then fixed and subjected to immunostaining with anti-Myc antibody. *Scale bar*, 10 μm. The number indicates the percentage of nuclear distribution ± S.E. quantified from more than 60 cells. *Error bars*, S.E.

is predominantly located in the cytoplasm due to two mechanisms. First, ATF2 homodimerization in the cytoplasm can inhibit nuclear import (19). Second, localization of the ATF2 monomer is determined by the balance between N-NES, LZ-NES, and two NLSs. The nuclear export rate contributed by both N-NES and LZ-NES seems to outweigh the nuclear import rate conferred by the two NLSs because the homodimerization-deficient mutant ATF2(L4P) is predominantly located in the cytoplasm (19).

Since identification of the consensus NES motifs (36), many nucleocytoplasmic shuttling proteins have been demonstrated to possess the canonical NES motif. The NES motif is a hydrophobic-rich region, defined as $\Phi^1X_{2-3}\Phi^2X_{2-3}\Phi^3X\Phi^4$ (where Φ represents Leu, Ile, Val, Phe, or Met, and X is any amino acid) (35, 36). Interestingly, only 72% of reported NES motifs match this well defined consensus NES (35), and the remaining motifs have only partially conserved NESs. As presented in this study, the N-NES of ATF2, MKFKLHV, has only one amino acid residue between Φ^1/Φ^2 and Φ^2/Φ^3, respectively. Because similar sequence presented in Eps15 acts as a functional NES (40), we have provided several lines of evidence to demonstrate that the N-NES is also functional. First, the N-terminal 73 residues are sufficient to render a tandem Venus fusion to be localized in the cytoplasm (Fig. 4*A*). Second, this tandem Venus fusion is responsive to LMB treatment. Third, mutation of N-NES in the context of full-length ATF2 increased ATF2 nuclear localization (Fig. 4*D*). Finally, CRM1 can be coimmunoprecipitated with the wild-type N-terminal domain of ATF2 but not the mutant form (Fig. 4*C*). Thus, ATF2 has a canonical NES in its leucine zipper domain and a non-canonical NES in the most N-terminal end.

The N-terminal end localization of N-NES may allow it to be more accessible to CRM1 (46). Interestingly, due to its unique location, a careful experimental design is needed in order to determine ATF2 subcellular localization. We observed that an N-terminal FLAG tag immediately adjacent to the N-NES prevented us from staining the nucleus-localized FLAG-ATF2 (data not shown), which is probably due to the binding of CRM1 to the N-NES of FLAG-ATF2 in the nucleus. Similarly, we also observed a slight but significant increase in nuclear localization of ATF2 when Venus is fused to the N terminus of the protein (supplemental Fig. 8), which may be due to a steric hindrance for the CRM1/N-NES interaction. Therefore, C-terminal fluorescent protein or tag fusions are preferred when exogenous ATF2 fusion proteins are used for the analysis of ATF2 subcellular localization.

Nucleocytoplasmic shuttling of transcription factors has emerged as an important research area. Many transcription fac-

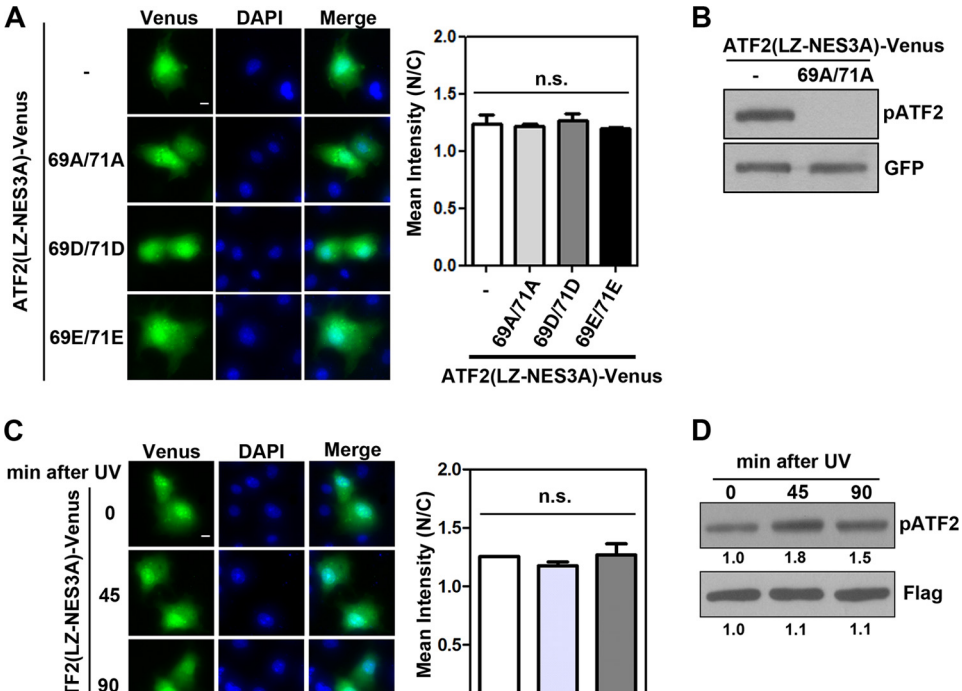

FIGURE 6. **N-NES of ATF2 is not regulated by MAPK phosphorylation.** *A*, effect of various Thr-69/Thr-71 mutants on subcellular localization of ATF2(LZ-NES3A)-Venus(A206K). COS-1 cells were transfected with plasmids encoding indicated mutant ATF2 fused to Venus for 16 h. *Left*, representative images. *Scale bar*, 10 μm. *Right*, quantitative results of the ratio of nuclear to cytoplasmic fluorescence intensity from three independent experiments. No significant difference was found (*n.s.*; one-way analysis of variance). *B*, effect of T69A/T71A mutation on Thr-71 phosphorylation status of ATF2(LZ-NES3A)-Venus(A206K). COS-1 cells were transfected with plasmids encoding FLAG-ATF2(LZ-NES3A)-Venus(A206K) or FLAG-ATF2(T69A,T71A,LZ-NES3A)-Venus(A206K) for 16 h. Thr-71 phosphorylation status was examined by Western blot. Comparable expression of both exogenous proteins was confirmed by immunoblotting with anti-GFP antibody. *C*, effect of UV irradiation on subcellular localization of ATF2(LZ-NES3A)-Venus(A206K). COS-1 cells were transfected with the plasmid encoding FLAG-ATF2(LZ-NES3A)-Venus(A206K) for 16 h followed by UV irradiation (120 J/m^2). Cells were fixed at 45 or 90 min after treatment. *Left*, representative images. *Scale bar*, 10 μm. *Right*, quantitative results of the ratio of nuclear to cytoplasmic fluorescence intensity from three independent experiments. No significant difference was found (one-way analysis of variance). *D*, effect of UV irradiation on Thr-71 phosphorylation status of ATF2(LZ-NES3A)-Venus(A206K). Thr-71 phosphorylation status of ATF2(LZ-NES3A)-Venus(A206K) at the indicated time point after UV treatment was determined by Western blot. The *number below* each *lane* is the quantified fold change when compared with the *first lane*. *Error bars*, S.E.

tors critical to cell fate determination are tightly regulated by multiple NLS and NES motifs. This may allow regulation of these transcription factors by multiple mechanisms. For example, p53 contains two NESs and three NLSs (47–50). The N-terminal NES is regulated by phosphorylation events in response to DNA damage (50), whereas the NES in the tetramerization domain is masked upon p53 oligomerization (49). In the case of ATF2, we have shown that the function of LZ-NES is inhibited when ATF2 heterodimerizes with the Jun family proteins. However, it is currently unknown whether and how the N-NES of ATF2 is regulated. Because phosphorylation at Thr-69 and Thr-71 by MAPKs is known to stimulate transactivation activity of ATF2, we initially thought that MAPK phosphorylation may regulate ATF2 subcellular localization. However, it does not appear to be the case because substitutions of these two residues to non-phosphorylatable alanines or phosphorylation-mimicking aspartic acid or glutamic acid residues did not affect the localization of ATF2(LZ-NES3A) (Fig. 6*A*). In addition, further induction of phosphorylation at these two residues by UV did not affect the localization of this mutant (Fig. 6*C*). Because ATF2 is also phosphorylated at other sites in the NTD (51, 52), it remains to be investigated whether phosphorylation of these additional sites regulates the activity of N-NES. Interestingly, mutation of LZ-NES increased nuclear localization of ATF2 in COS-1 cells but not in HEK 293T or LNCaP cells, suggesting that N-NES is a dominant export signal in the latter two cell types. One possible explanation is that N-NES activity is enhanced by signaling that is activated in these cell types. In this case, comparing the difference of cellular signaling between cell types with differential N-NES activity may help unravel mechanisms that regulate N-NES. Alternatively, activity of N-NES may be modulated by ATF2-interacting proteins, such as E1A and CREB-binding protein (21). Also, undifferentiated embryonic cell transcription factor 1 (UTF1) (53) and activating signal cointegrator-2 (ASC-2) (54) are reported to bind the NTD of ATF2 and function as coactivators. It will be interesting to test if these coactivators enhance ATF2 transcriptional activity by masking N-NES and anchoring ATF2 in the nucleus.

Our results showed that mutation of N-NES enhanced transcriptional activity of FLAG-ATF2 and FLAG-ATF2-Myc by ~90 and 30%, respectively (Fig. 5 and supplemental Fig. 7). Because C-terminal Myc tag does not appear to affect ATF2 stability (data not shown), it may reduce the transcriptional potential of ATF2 by causing a conformational change. Indeed, it has been reported that function of transcription factors can be affected by N- or C-terminal tags (55, 56). Nevertheless, the

enhanced reporter gene activation by ATF2 with mutations in the N-NES correlates with its increased nuclear localization, suggesting that regulation of N-NES by itself could increase the transcriptional activity of ATF2. In this sense, it is worth noting that there are multiple ATF2 alternative spliced variants that have been deposited to the NCBI database, although their functions remain largely uninvestigated. For example, ATF2-Var13 (GenBank™ number AAY17215.1) lacks the N-terminal 18 residues due to the loss of exon 3, where N-NES is located. Based on our finding here, it is very likely that the transcriptional activity of ATF2-Var13 may be less subject to the regulation by its subcellular localization. Therefore, a switch between spliced variants may be an alternative mechanism to regulate ATF2 subcellular localization and its activity. Consistent with this notion, alignment of full-length ATF2 with those from several species reveals that N-NES is only present in *Homo sapiens*, *Canis familiaris*, and *Bos taurus* ATF2 and not in *Gallus gallus*, *Mus musculus*, *Rattus norvegicus*, and *Xenopus laevis* (supplemental Fig. 9). It is therefore possible that this additional NES is evolutionarily acquired to deal with more complex regulatory mechanisms in higher organisms. Given that alteration of ATF2 subcellular localization has been observed in several human diseases (22–26), further analysis of the regulation of N-NES under these pathological conditions will probably provide exciting insight into the role of ATF2 in the pathogenesis of human diseases.

Acknowledgments—We thank Christopher Suarez for critically reading the manuscript. DNA sequencing was conducted in the Purdue University Center for Cancer Research Genomic Core Facility, supported by National Institutes of Health, NCI, Grant CCSG CA23168 (to the Purdue University Center for Cancer Research).

REFERENCES

1. Wagner, E. F. (2001) AP-1. Introductory remarks. *Oncogene* **20,** 2334–2335
2. Hai, T. W., Liu, F., Coukos, W. J., and Green, M. R. (1989) Transcription factor ATF cDNA clones. An extensive family of leucine zipper proteins able to selectively form DNA-binding heterodimers. *Genes Dev.* **3,** 2083–2090
3. Benbrook, D. M., and Jones, N. C. (1990) Heterodimer formation between CREB and JUN proteins. *Oncogene* **5,** 295–302
4. Hai, T., and Curran, T. (1991) Cross-family dimerization of transcription factors Fos/Jun and ATF/CREB alters DNA binding specificity. *Proc. Natl. Acad. Sci. U.S.A.* **88,** 3720–3724
5. Ma, Q., Li, X., Vale-Cruz, D., Brown, M. L., Beier, F., and LuValle, P. (2007) Activating transcription factor 2 controls Bcl-2 promoter activity in growth plate chondrocytes. *J. Cell Biochem.* **101,** 477–487
6. Salameh, A., Galvagni, F., Anselmi, F., De Clemente, C., Orlandini, M., and Oliviero, S. (2010) Growth factor stimulation induces cell survival by c-Jun. ATF2-dependent activation of Bcl-XL. *J. Biol. Chem.* **285,** 23096–23104
7. Shimizu, M., Nomura, Y., Suzuki, H., Ichikawa, E., Takeuchi, A., Suzuki, M., Nakamura, T., Nakajima, T., and Oda, K. (1998) Activation of the rat cyclin A promoter by ATF2 and Jun family members and its suppression by ATF4. *Exp. Cell Res.* **239,** 93–103
8. Beier, F., Lee, R. J., Taylor, A. C., Pestell, R. G., and LuValle, P. (1999) Identification of the cyclin D1 gene as a target of activating transcription factor 2 in chondrocytes. *Proc. Natl. Acad. Sci. U.S.A.* **96,** 1433–1438
9. van Dam, H., Wilhelm, D., Herr, I., Steffen, A., Herrlich, P., and Angel, P. (1995) ATF-2 is preferentially activated by stress-activated protein kinases to mediate c-jun induction in response to genotoxic agents. *EMBO J.* **14,** 1798–1811
10. Livingstone, C., Patel, G., and Jones, N. (1995) ATF-2 contains a phosphorylation-dependent transcriptional activation domain. *EMBO J.* **14,** 1785–1797
11. Ouwens, D. M., de Ruiter, N. D., van der Zon, G. C., Carter, A. P., Schouten, J., van der Burgt, C., Kooistra, K., Bos, J. L., Maassen, J. A., and van Dam, H. (2002) Growth factors can activate ATF2 via a two-step mechanism. Phosphorylation of Thr-71 through the Ras-MEK-ERK pathway and of Thr-69 through RalGDS-Src-p38. *EMBO J.* **21,** 3782–3793
12. Gupta, S., Campbell, D., Dérijard, B., and Davis, R. J. (1995) Transcription factor ATF2 regulation by the JNK signal transduction pathway. *Science* **267,** 389–393
13. Kawasaki, H., Schiltz, L., Chiu, R., Itakura, K., Taira, K., Nakatani, Y., and Yokoyama, K. K. (2000) ATF-2 has intrinsic histone acetyltransferase activity which is modulated by phosphorylation. *Nature* **405,** 195–200
14. Abdel-Hafiz, H. A., Heasley, L. E., Kyriakis, J. M., Avruch, J., Kroll, D. J., Johnson, G. L., and Hoeffler, J. P. (1992) Activating transcription factor-2 DNA-binding activity is stimulated by phosphorylation catalyzed by p42 and p54 microtubule-associated protein kinases. *Mol. Endocrinol.* **6,** 2079–2089
15. Fuchs, S. Y., Xie, B., Adler, V., Fried, V. A., Davis, R. J., and Ronai, Z. (1997) c-Jun NH_2-terminal kinases target the ubiquitination of their associated transcription factors. *J. Biol. Chem.* **272,** 32163–32168
16. Fuchs, S. Y., Fried, V. A., and Ronai, Z. (1998) Stress-activated kinases regulate protein stability. *Oncogene* **17,** 1483–1490
17. Li, X. Y., and Green, M. R. (1996) Intramolecular inhibition of activating transcription factor-2 function by its DNA-binding domain. *Genes Dev.* **10,** 517–527
18. Liu, F., and Green, M. R. (1990) A specific member of the ATF transcription factor family can mediate transcription activation by the adenovirus E1a protein. *Cell* **61,** 1217–1224
19. Liu, H., Deng, X., Shyu, Y. J., Li, J. J., Taparowsky, E. J., and Hu, C. D. (2006) Mutual regulation of c-Jun and ATF2 by transcriptional activation and subcellular localization. *EMBO J.* **25,** 1058–1069
20. Duyndam, M. C., van Dam, H., Smits, P. H., Verlaan, M., van der Eb, A. J., and Zantema, A. (1999) The N-terminal transactivation domain of ATF2 is a target for the co-operative activation of the c-jun promoter by p300 and 12S E1A. *Oncogene* **18,** 2311–2321
21. Sano, Y., Tokitou, F., Dai, P., Maekawa, T., Yamamoto, T., and Ishii, S. (1998) CBP alleviates the intramolecular inhibition of ATF-2 function. *J. Biol. Chem.* **273,** 29098–29105
22. Berger, A. J., Kluger, H. M., Li, N., Kielhorn, E., Halaban, R., Ronai, Z., and Rimm, D. L. (2003) Subcellular localization of activating transcription factor 2 in melanoma specimens predicts patient survival. *Cancer Res.* **63,** 8103–8107
23. Bhoumik, A., Fichtman, B., Derossi, C., Breitwieser, W., Kluger, H. M., Davis, S., Subtil, A., Meltzer, P., Krajewski, S., Jones, N., and Ronai, Z. (2008) Suppressor role of activating transcription factor 2 (ATF2) in skin cancer. *Proc. Natl. Acad. Sci. U.S.A.* **105,** 1674–1679
24. Yamada, T., Yoshiyama, Y., and Kawaguchi, N. (1997) Expression of activating transcription factor-2 (ATF-2), one of the cyclic AMP-response element (CRE)-binding proteins, in Alzheimer disease and non-neurological brain tissues. *Brain Res.* **749,** 329–334
25. Ricote, M., García-Tuñón, I., Bethencourt, F., Fraile, B., Onsurbe, P., Paniagua, R., and Royuela, M. (2006) The p38 transduction pathway in prostatic neoplasia. *J. Pathol.* **208,** 401–407
26. Deng, X., Liu, H., Huang, J., Cheng, L., Keller, E. T., Parsons, S. J., and Hu, C. D. (2008) Ionizing radiation induces prostate cancer neuroendocrine differentiation through interplay of CREB and ATF2. Implications for disease progression. *Cancer Res.* **68,** 9663–9670
27. Deng, X., Elzey, B. D., Poulson, J. M., Morrison, W. B., Ko, S. C., Hahn, N. M., Ratliff, T. L., and Hu, C. D. (2011) Ionizing radiation induces neuroendocrine differentiation of prostate cancer cells *in vitro*, *in vivo*, and in prostate cancer patients. *Am. J. Cancer Res.* **1,** 834–844
28. Zacharias, D. A., Violin, J. D., Newton, A. C., and Tsien, R. Y. (2002) Partitioning of lipid-modified monomeric GFPs into membrane microdomains of live cells. *Science* **296,** 913–916

29. Nagai, T., Ibata, K., Park, E. S., Kubota, M., Mikoshiba, K., and Miyawaki, A. (2002) A variant of yellow fluorescent protein with fast and efficient maturation for cell-biological applications. *Nat. Biotechnol.* **20,** 87–90
30. Shaner, N. C., Steinbach, P. A., and Tsien, R. Y. (2005) A guide to choosing fluorescent proteins. *Nat. Methods* **2,** 905–909
31. Ali, S. A., and Steinkasserer, A. (1995) PCR-ligation-PCR mutagenesis. A protocol for creating gene fusions and mutations. *BioTechniques* **18,** 746–750
32. Le, N. H., van der Bent, P., Huls, G., van de Wetering, M., Loghman-Adham, M., Ong, A. C., Calvet, J. P., Clevers, H., Breuning, M. H., van Dam, H., and Peters, D. J. (2004) Aberrant polycystin-1 expression results in modification of activator protein-1 activity, whereas Wnt signaling remains unaffected. *J. Biol. Chem.* **279,** 27472–27481
33. Hu, C. D., Chinenov, Y., and Kerppola, T. K. (2002) Visualization of interactions among bZIP and Rel family proteins in living cells using bimolecular fluorescence complementation. *Mol. Cell* **9,** 789–798
34. Kudo, N., Wolff, B., Sekimoto, T., Schreiner, E. P., Yoneda, Y., Yanagida, M., Horinouchi, S., and Yoshida, M. (1998) Leptomycin B inhibition of signal-mediated nuclear export by direct binding to CRM1. *Exp. Cell Res.* **242,** 540–547
35. la Cour, T., Kiemer, L., Molgaard, A., Gupta, R., Skriver, K., and Brunak, S. (2004) Analysis and prediction of leucine-rich nuclear export signals. *Protein Eng. Des. Sel.* **17,** 527–536
36. Bogerd, H. P., Fridell, R. A., Benson, R. E., Hua, J., and Cullen, B. R. (1996) Protein sequence requirements for function of the human T-cell leukemia virus type 1 Rex nuclear export signal delineated by a novel *in vivo* randomization-selection assay. *Mol. Cell Biol.* **16,** 4207–4214
37. Kazgan, N., Williams, T., Forsberg, L. J., and Brenman, J. E. (2010) Identification of a nuclear export signal in the catalytic subunit of AMP-activated protein kinase. *Mol. Biol. Cell* **21,** 3433–3442
38. Frederick, E. D., Ramos, S. B., and Blackshear, P. J. (2008) A unique C-terminal repeat domain maintains the cytosolic localization of the placenta-specific tristetraprolin family member ZFP36L3. *J. Biol. Chem.* **283,** 14792–14800
39. Murai, N., Murakami, Y., and Matsufuji, S. (2003) Identification of nuclear export signals in antizyme-1. *J. Biol. Chem.* **278,** 44791–44798
40. Poupon, V., Polo, S., Vecchi, M., Martin, G., Dautry-Varsat, A., Cerf-Bensussan, N., Di Fiore, P. P., and Benmerah, A. (2002) Differential nucleocytoplasmic trafficking between the related endocytic proteins Eps15 and Eps15R. *J. Biol. Chem.* **277,** 8941–8948
41. Devary, Y., Gottlieb, R. A., Lau, L. F., and Karin, M. (1991) Rapid and preferential activation of the c-*jun* gene during the mammalian UV response. *Mol. Cell Biol.* **11,** 2804–2811
42. Vinson, C., Myakishev, M., Acharya, A., Mir, A. A., Moll, J. R., and Bonovich, M. (2002) Classification of human B-ZIP proteins based on dimerization properties. *Mol. Cell Biol.* **22,** 6321–6335
43. Moitra, J., Szilák, L., Krylov, D., and Vinson, C. (1997) Leucine is the most stabilizing aliphatic amino acid in the d position of a dimeric leucine zipper coiled coil. *Biochemistry* **36,** 12567–12573
44. van Dam, H., Duyndam, M., Rottier, R., Bosch, A., de Vries-Smits, L., Herrlich, P., Zantema, A., Angel, P., and van der Eb, A. J. (1993) Heterodimer formation of cJun and ATF-2 is responsible for induction of c-jun by the 243-amino acid adenovirus E1A protein. *EMBO J.* **12,** 479–487
45. Raingeaud, J., Gupta, S., Rogers, J. S., Dickens, M., Han, J., Ulevitch, R. J., and Davis, R. J. (1995) Pro-inflammatory cytokines and environmental stress cause p38 mitogen-activated protein kinase activation by dual phosphorylation on tyrosine and threonine. *J. Biol. Chem.* **270,** 7420–7426
46. Xu, D., Farmer, A., and Chook, Y. M. (2010) Recognition of nuclear targeting signals by Karyopherin-β proteins. *Curr. Opin. Struct. Biol.* **20,** 782–790
47. Shaulsky, G., Goldfinger, N., Ben-Ze'ev, A., and Rotter, V. (1990) Nuclear accumulation of p53 protein is mediated by several nuclear localization signals and plays a role in tumorigenesis. *Mol. Cell Biol.* **10,** 6565–6577
48. Liang, S. H., and Clarke, M. F. (1999) A bipartite nuclear localization signal is required for p53 nuclear import regulated by a carboxyl-terminal domain. *J. Biol. Chem.* **274,** 32699–32703
49. Stommel, J. M., Marchenko, N. D., Jimenez, G. S., Moll, U. M., Hope, T. J., and Wahl, G. M. (1999) A leucine-rich nuclear export signal in the p53 tetramerization domain. Regulation of subcellular localization and p53 activity by NES masking. *EMBO J.* **18,** 1660–1672
50. Zhang, Y., and Xiong, Y. (2001) A p53 amino-terminal nuclear export signal inhibited by DNA damage-induced phosphorylation. *Science* **292,** 1910–1915
51. Sevilla, A., Santos, C. R., Vega, F. M., and Lazo, P. A. (2004) Human vaccinia-related kinase 1 (VRK1) activates the ATF2 transcriptional activity by novel phosphorylation on Thr-73 and Ser-62 and cooperates with JNK. *J. Biol. Chem.* **279,** 27458–27465
52. Yamasaki, T., Takahashi, A., Pan, J., Yamaguchi, N., and Yokoyama, K. K. (2009) Phosphorylation of activation transcription factor-2 at serine 121 by protein kinase C controls c-Jun-mediated activation of transcription. *J. Biol. Chem.* **284,** 8567–8581
53. Okuda, A., Fukushima, A., Nishimoto, M., Orimo, A., Yamagishi, T., Nabeshima, Y., Kuro-o, M., Nabeshima, Y., Boon, K., Keaveney, M., Stunnenberg, H. G., and Muramatsu, M. (1998) UTF1, a novel transcriptional coactivator expressed in pluripotent embryonic stem cells and extraembryonic cells. *EMBO J.* **17,** 2019–2032
54. Hong, S., Choi, H. M., Park, M. J., Kim, Y. H., Choi, Y. H., Kim, H. H., Choi, Y. H., and Cheong, J. (2004) Activation and interaction of ATF2 with the coactivator ASC-2 are responsive for granulocytic differentiation by retinoic acid. *J. Biol. Chem.* **279,** 16996–17003
55. Ishida, S., Yamashita, T., Nakaya, U., and Tokino, T. (2000) Adenovirus-mediated transfer of p53-related genes induces apoptosis of human cancer cells. *Jpn. J. Cancer Res.* **91,** 174–180
56. Lee, T. I., Rinaldi, N. J., Robert, F., Odom, D. T., Bar-Joseph, Z., Gerber, G. K., Hannett, N. M., Harbison, C. T., Thompson, C. M., Simon, I., Zeitlinger, J., Jennings, E. G., Murray, H. L., Gordon, D. B., Ren, B., Wyrick, J. J., Tagne, J. B., Volkert, T. L., Fraenkel, E., Gifford, D. K., and Young, R. A. (2002) Transcriptional regulatory networks in *Saccharomyces cerevisiae*. *Science* **298,** 799–804

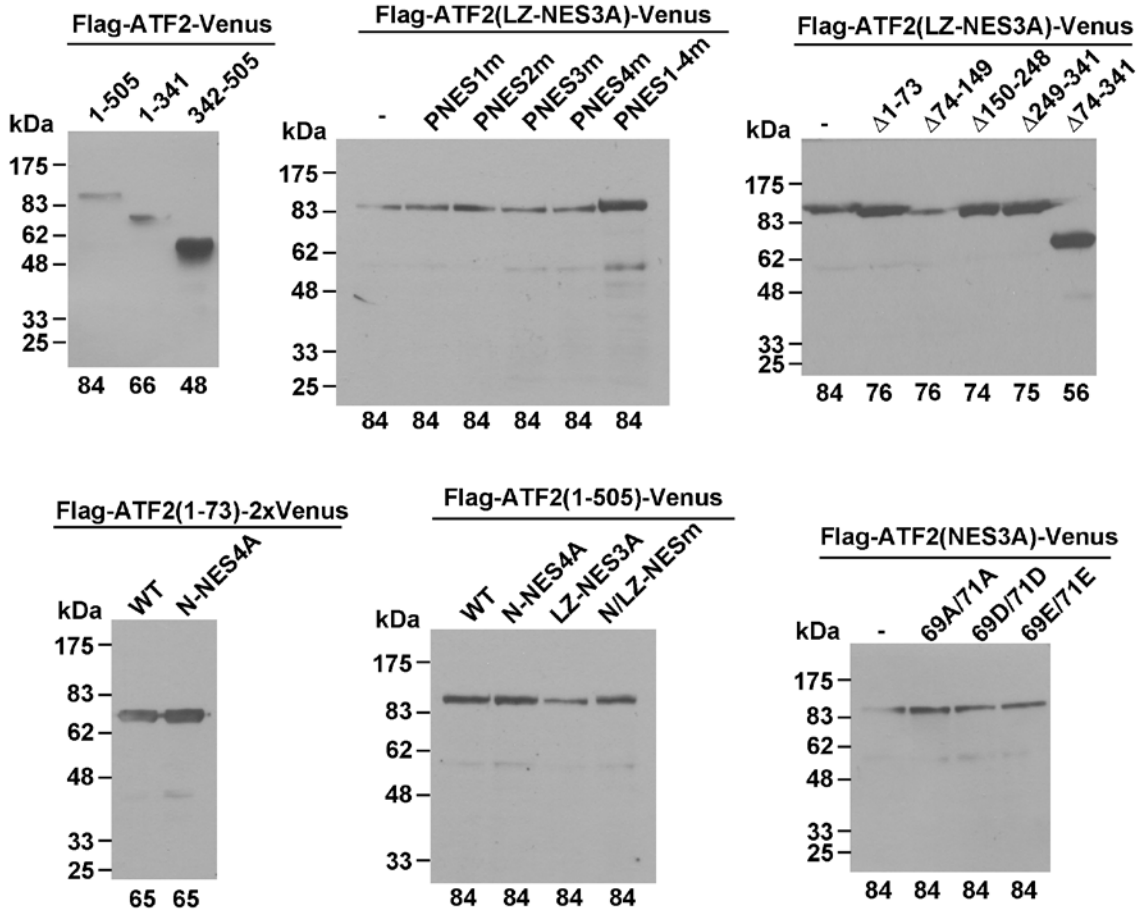

Supplementary Figure 1

Western blot analysis of ATF2-Venus fusion proteins. COS-1 cells transfected with plasmids encoding indicated proteins were lysed and subjected to Western blot with anti-Flag antibody. Number below each lane is the expected size (kDa) of the fusion protein. The "-" label indicates that no additional mutation or deletion was made in the indicated mutant ATF2-Venus fusion protein.

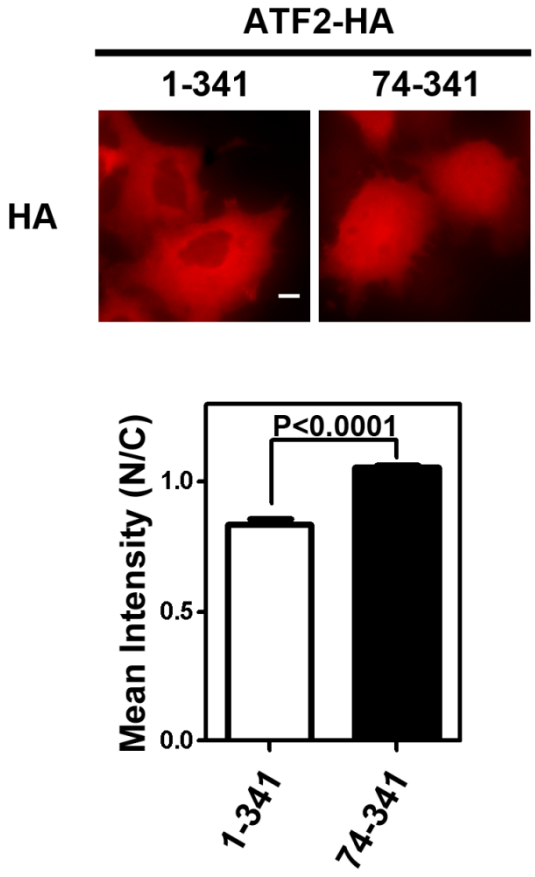

Supplementary Figure 2
Subcellular localization of ATF2(1-341) and ATF2 (74-149) fragments. COS-1 cells were transfected with plasmids encoding C-terminal HA tagged-ATF2(1-341) or ATF2(74-341) for 16 hr. Subcellular localization of ATF2 fragments was determined by immunostaining with anti-HA antibody. Top: Representative images. Scale bar represents 10 μm. Bottom: Quantitative results of the ratio of nuclear to cytoplasmic mean fluoresce intensity from more than 50 cells.

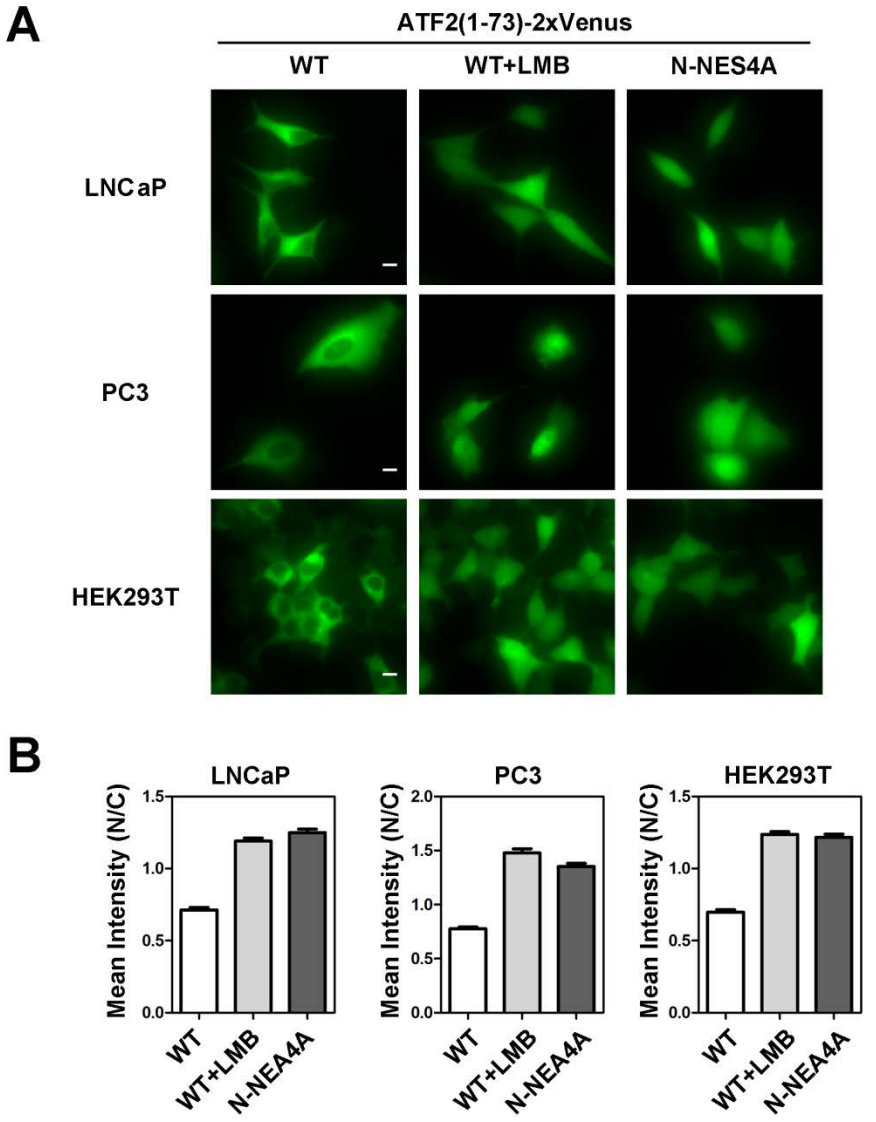

Supplementary Figure 3
Function of ATF2 N-NES in various cell lines. *A.* LNCaP, PC3 or HEK293T cells were transfected with plasmids encoding Flag-ATF2(1-73)-2xVenus(A206K) or Flag-ATF2(1-73,N-NES4A)-2xVenus(A206K). Cells expressing Flag-ATF2(1-73)-2xVenus(A206K) were then treated with or without LMB for 3.5 hr. Shown are representative images. Scale bar represents 10 μm. *B.* Quantitative results of ATF2 subcellular localization from more than 50 cells.

.

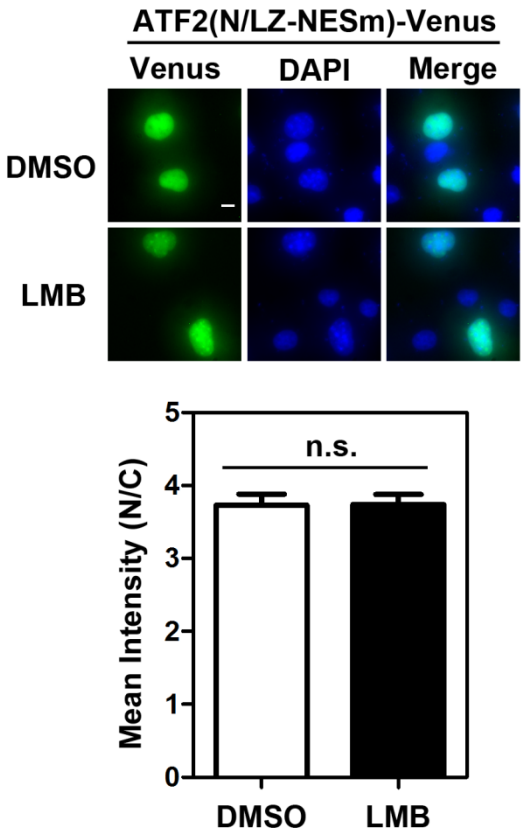

Supplementary Figure 4

Effect of LMB on subcellular localization of two NES-mutated ATF2. COS-1 cells were transfected with plasmid encoding Flag-ATF2(N/LZ-NESm)-Venus(A206K) for 16 hr, followed by DMSO or LMB treatment for 3.5 hr. Top: Representative images. Scale bar represents 10 μm. Bottom: Quantitative results of ATF2 subcellular localization from more than 50 cells. No significant difference was found.

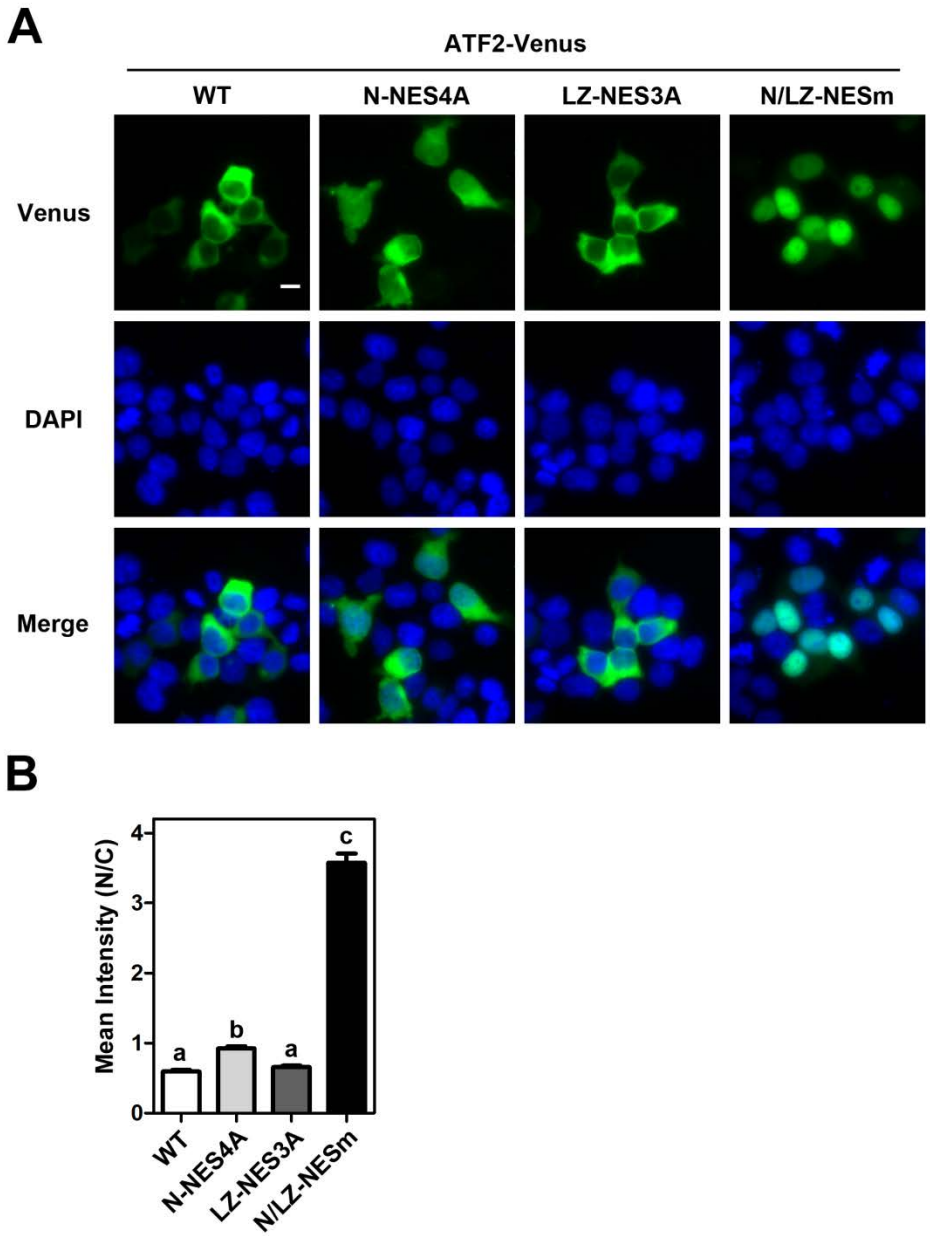

Supplementary Figure 5

Effect of NES mutations on subcellular localization of full-length ATF2-Venus(A206K) in HEK 293T cells. HEK 293T cells were transfected with plasmids encoding Flag-ATF2(WT)-Venus(A206K), Flag-ATF2(N-NES4A)-Venus(A206K), Flag-ATF2(LZ-NES3A)-Venus(A206K) or Flag-ATF2(N/LZ-NESm)-Venus(A206K). *A.* Representative images. Scale bar represents 10 μm. *B.* Quantitative results of ATF2 subcellular localization from more than 50 cells. Different letters above the bars indicate significant differences ($p < 0.05$) in the ratio of nuclear to cytoplasmic fluorescence intensity (One-way ANOVA).

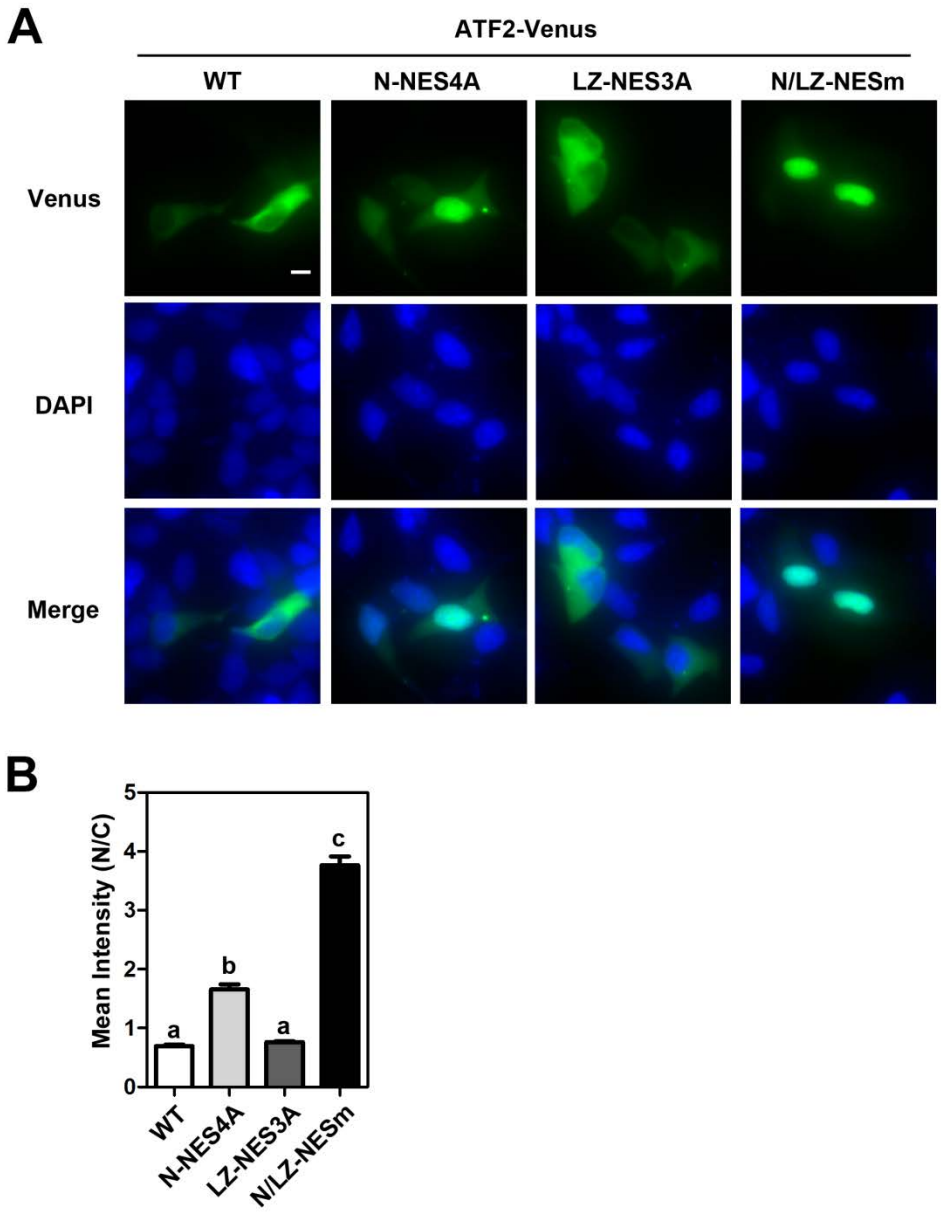

Supplementary Figure 6

Effect of NES mutations on subcellular localization of full-length ATF2-Venus(A206K) in LNCaP cells. LNCaP cells were transfected with plasmids encoding Flag-ATF2(WT)-Venus(A206K), Flag-ATF2(N-NES4A)-Venus(A206K), Flag-ATF2(LZ-NES3A)-Venus(A206K) or Flag-ATF2(N/LZ-NESm)-Venus(A206K). *A.* Representative images. Scale bar represents 10 μm. *B.* Quantitative results of ATF2 subcellular localization from more than 50 cells. Different letters above the bars indicate significant differences ($p < 0.05$) in the ratio of nuclear to cytoplasmic fluorescence intensity (One-way ANOVA).

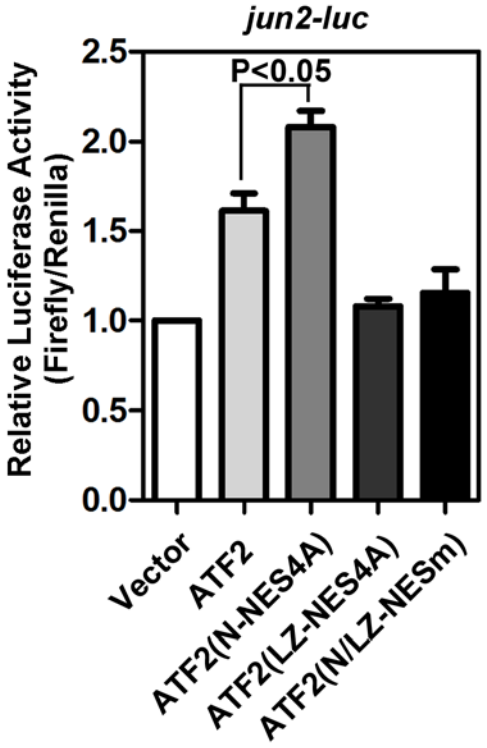

Supplementary Figure 7

Effect of NES mutations on transcriptional activity of ATF2-Myc fusion proteins. Serum starved COS-1 cells were transfected with 0.5 μg of *jun2-luc*, 100 ng pRL-TK, along with 2 μg of pCMV-Flag-Myc (vector), pFlag-ATF2-Myc, pFlag-ATF2(N-NES4A)-Myc, pFlag-ATF2(LZ-NES3A)-Myc or pFlag-ATF2(N/LZ-NESm)-Myc for 24 hr. Values of Firefly/Renilla luciferase were presented as fold over vector control. Results are shown as mean±S.E. from four independent experiments and each experiment was conducted in duplicate.

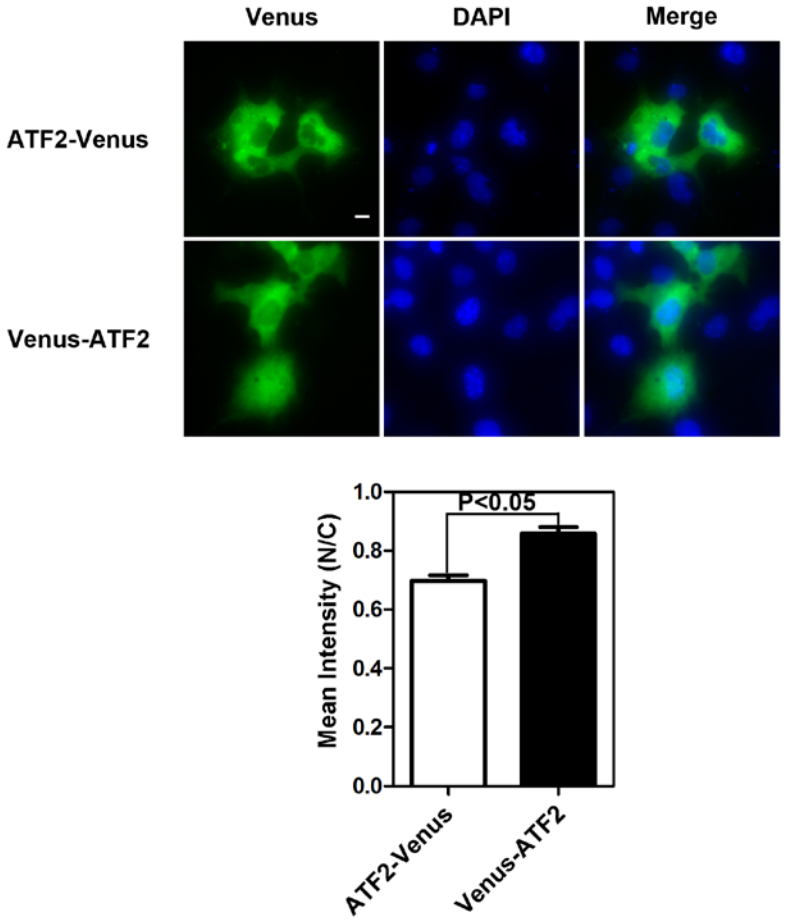

Supplementary Figure 8

Localization of ATF2 determined by N- or C-terminal Venus fusion. COS-1 cells were transfected with plasmids encoding Flag-ATF2-Venus(A206K) or Flag-Venus(A206K)-ATF2 for 16 hr. Top: Representative images. Scale bar represents 10 μm. Bottom: Quantitative results of ATF2 subcelluar localization from more than 50 cells.

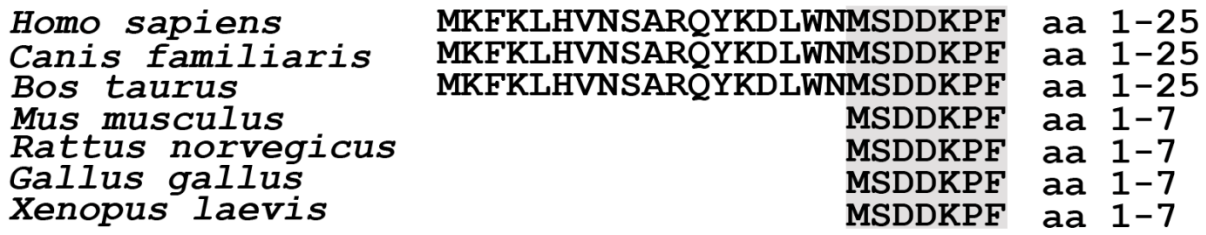

Supplementary Figure 9
Sequence alignment of the ATF2 N-terminus from various species.